Processing of laser speckle contrast images : study of mathematical models and use of nonlinear analyses to investigate the impact of aging on microvascular blood flow

Adil Khalil

UNIVERSITE BRETAGNE LOIRE

université angers

Thèse de Doctorat

Adil I. KHALIL

Mémoire présenté en vue de l'obtention du
grade de Docteur de l'Université d'Angers
sous le sceau de l'Université Bretagne Loire

École doctorale : Sciences et technologies de l'information, et mathématiques (STIM)

Discipline : Sciences, section CNU 26, 27, 61, 63
Spécialité : Traitement du Signal et de l'Image
Unité de recherche : Laboratoire Angevin de Recherche en Ingénierie des Systèmes (LARIS)

Soutenue le 5 avril 2017
Thèse n° : 108215

Processing of laser speckle contrast images:
Study from mathematical models and use of nonlinear analyses to investigate the impact of aging on microvascular blood flow

JURY

Rapporteurs :	**M. Walter BLONDEL**, Professeur des universités, Université de Lorraine **M. Jean-Marc GIRAULT**, Maître de conférences, Université François-Rabelais, Tours
Examinateurs :	**M. Jean-Luc CRACOWSKI**, Professeur des universités, Université Grenoble Alpes **M^{me} Emilie PERY**, Maître de conférences, Université de Clermont-Ferrand
Directrice de thèse :	**M^{me} Anne HUMEAU-HEURTIER**, Professeur des universités, Université d'Angers

Résumé

Selon l'Organisation mondiale de la santé, une augmentation de l'espérance de vie est observée (World Health Organization, 2015). En 2050, la population mondiale âgée de 60 ans et plus devrait atteindre 2 milliards, et a augmenté de 900 millions en 2015. Ainsi, 125 millions de personnes sont âgées de 80 ans ou plus (World Health Organization, 2015). Cependant, ces années supplémentaires sont dominées par la baisse des capacités physiques et mentales.

Le vieillissement est un facteur de risque des maladies cardiovasculaires. Il est associé à une réduction de l'activité microvasculaire, une augmentation de la rigidité des vaisseaux, une diminution de la densité vasculaire, et à une altération de l'organisation des vaisseaux (Tobin, 2017). Au fil du temps, ces modifications vasculaires conduisent à un risque accru de nombreuses maladies et à une diminution progressive de la capacité de l'individu à s'adapter aux conditions locales. À long terme, elles peuvent entraîner la mort. Par conséquent, le processus de vieillissement est l'un des domaines où la recherche et de nouvelles technologies doivent être appliquées. Néanmoins, des analyses chez des sujets sains sont d'abord importantes car elles sont la première étape avant une analyse chez des sujets pathologiques.

L'évaluation du flux sanguin microvasculaire est importante pour analyser l'impact du vieillissement (Li et al., 2006b; Tsuda et al., 2014). Pour cette raison, différentes techniques à base de lasers ont émergé pour surveiller le flux sanguin microvasculaire (Bi et al., 2015; Allen and Howell, 2014; Eriksson et al., 2014; Roustit and Cracowski, 2013). Parmi ces techniques, l'imagerie laser Doppler (LDI [1]) et l'imagerie de contraste par speckle laser (LSCI [2]) ont pris une place prépondérante en recherche clinique. Ces deux techniques offrent un temps de mesure de l'ordre de quelques millisecondes. En outre, pour effectuer des mesures de LSCI, un appareil photo bon marché - ayant une fréquence d'images de 200Hz - est suffisant pour fournir d'excellentes images de la circulation sanguine. Pour le LDI, une caméra possédant une fréquence d'acquisition élevée jusqu'à 25 kHz est nécessaire pour fournir des images de qualité comparable

1. Pour des raisons de cohérence, nous gardons l'acronyme LDI pour ce résumé en français.
2. Pour des raisons de cohérence, nous gardons l'acronyme LSCI pour ce résumé en français.

(Draijer et al., 2009).

Le LSCI fournit des images de la perfusion microvasculaire ayant de très bonnes résolutions spatiales et temporelles, et ceci avec du matériel à faible coût (Richards et al., 2013; Humeau-Heurtier et al., 2014a; Puissant et al., 2013). Le LSCI repose sur l'utilisation d'une lumière laser (Briers and Webster, 1996). Ainsi, un rayon laser est envoyé sur les tissus à étudier. Les photons de la lumière laser sont rétrodiffusés par des particules statiques et les globules rouges de la microcirculation sanguine. La lumière rétrodiffusée est imagée par une caméra. Puisque les globules rouges sont en mouvement, le "pattern" (de speckle) obtenu sur la caméra varie avec le temps. En raison du temps d'exposition de la caméra, un flou des "patterns" de speckle est obtenu. Le flou est quantifié à partir du contrast de speckle K défini par

$$K = \frac{\sigma}{\langle I \rangle} = \frac{\sqrt{\langle I^2 \rangle - \langle I \rangle^2}}{\langle I \rangle} \quad , \tag{1}$$

où σ est l'écart-type de l'intensité de speckle dans une région spatiale de l'image et $\langle I \rangle$ est l'intensité moyenne dans cette région spatiale.

Le contraste de speckle K est fonction du temps de corrélation de speckle τ_c et du temps d'exposition T de la caméra. Si la distribution de vitesse des éléments de diffusion est supposée suivre un profil statistique Lorentzien, le contraste K s'écrit alors (Boas and Dunn, 2010)

$$K^2_{Lorentzien} = \beta \left[\frac{\tau_c}{T} + \frac{\tau_c^2}{2T^2} \left(\exp\left(-\frac{2T}{\tau_c} \right) - 1 \right) \right] \quad , \tag{2}$$

où β est le facteur de cohérence.

À partir de cette expression, le temps de corrélation τ_c est calculé et utilisé pour déterminer la vitesse des érythrocytes de la microcirculation (Briers and Webster, 1996)

$$v_c = \frac{\lambda}{2\pi\tau_c} \quad , \tag{3}$$

où λ est la longueur d'onde du laser.

L'équation (2) est cependant insuffisante car elle ne prend pas en compte l'effet des particules statiques comme la peau. En prenant en compte les particules statiques, l'équation (2) devient (Boas and Dunn, 2010)

$$K^2_{Lorentzien} = \beta \left[\rho^2 \frac{\exp(-2x) - 1 + 2x}{2x^2} + 4\rho(1-\rho)\frac{\exp(-x) - 1 + x}{x^2} + (1-\rho)^2 \right] + C_{noise} \ , \tag{4}$$

où $x = T/\tau_c$, $\rho = I_f/(I_f + I_s)$ est la fraction de la lumière totale qui est diffusée dynamiquement avec I_f l'intensité de la lumière diffusée dynamiquement et I_s l'intensité de la lumière diffusée statiquement. De plus, C_{noise} correspond au bruit de la mesure (Boas and Dunn, 2010).

Il a été montré que si l'effet des diffuseurs statiques n'est pas considéré, alors il en résulte une sous-estimation des variations spatiales et temporelles de la dynamique de l'échantillon (Li et al., 2006a; Parthasarathy et al., 2008).

Pour évaluer la fonction microvasculaire, il nous faut extraire des informations physiologiques pertinentes à partir d'images médicales. Ainsi, de nombreuses méthodes de traitement de signal/d'image ont été proposées afin de permettre une meilleure compréhension des caractéristiques physiologiques sous-jacentes. Parmi ces méthodes, le calcul de la "sample entropy" (SampEn) a été particulièrement intéressant dans le domaine biomédical (Richman and Moorman, 2000). La SampEn a été utilisée pour mesurer la régularité de séries temporelles physiologiques (Chen et al., 2009; Humeau et al., 2008; Hornero et al., 2006). Toutefois, la SampEn effectue une analyse à une seule échelle. Cependant, le système cardiovasculaire se manifeste sur de multiples échelles temporelles pour augmenter sa capacité d'adaptation dans un environnement en constante évolution. Ainsi, la complexité du système cardiovasculaire doit être étudiée sur de multiples échelles temporelles. Pour pallier l'inconvénient de la SampEn (qui effectue une analyse à une seule échelle), l'entropie multi-échelle (MSE [3]) a été introduite comme un outil pratique pour traiter les signaux physiologiques sur des échelles de temps multiples (Costa et al., 2005, 2002). La MSE s'appuie sur la SampEn. Pour une série temporelle, $\{x_1, ..., x_i, ...x_N\}$ donnée, des sous-séries temporelles appelées "coarse-grained" sont construites. Ces séries temporelles "coarse-grained" sont obtenues en moyennant un ensemble de points se trouvant dans des fenêtres de taille τ qui ne se chevauchent pas.

Chaque élément $y_j^{(\tau)}$ de ces séries "coarse-grained" est calculé selon l'équation

3. Pour des raisons de cohérence, nous gardons l'acronyme MSE pour ce résumé en français.

$$y_j^{(\tau)} = \frac{1}{\tau} \sum_{i=(j-1)\tau+1}^{j\tau} x_i, \qquad 1 \leq j \leq N/\tau. \tag{5}$$

Une fois les sous-séries temporelles (ou “coarse-grained”) extraites de la série originale, une valeur de SampEn est calculée pour chacune d’entre elles, ce qui permet d’avoir une mesure d’entropie à chaque échelle τ.

À travers l’analyse d’images de contraste par speckle laser, l’objectif de cette thèse est d’étudier l’influence de l’âge sur la microcirculation. Pour ce faire, des données LSCI ont été acquises sur l’avant-bras de sujets sains jeunes et âgés. A partir de modèles mathématiques, nous avons déterminé la vitesse des érythrocytes de la microcirculation chez les deux groupes de sujets. Par ailleurs, nous avons également mené une étude de la complexité de séries temporelles de LSCI s’appuyant sur des mesures d’entropie multi-échelle.

En outre, dans cette thèse, nous avons aussi étudié l’impact possible des diffuseurs statiques sur les valeurs de la vitesse des érythrocytes. Les résultats ont été obtenus par des processus expérimentaux et des simulations. De plus, nous avons étudié l’effet du vieillissement simultanément sur les paramètres microvasculaires (perfusion et vitesse des érythrocytes) et macrovasculaires (vitesse de l’onde de pouls, PWV [4]). La relation entre ces paramètres est analysée.

Dans ce manuscrit, un aperçu de l’organisation du système cardiovasculaire, les différentes techniques pour surveiller le flux sanguin microvasculaire et l’état actuel de la recherche sur l’impact du vieillissement sur la microcirculation sont donnés dans le **chapitre** 2.

Dans le **chapitre** 3, le contexte théorique du LSCI et la façon de calculer la vitesse des érythrocytes de la microcirculation et la perfusion à partir de données LSCI sont exposés. En outre, plusieurs exigences de mesure sont discutées, y compris celles qui affectent l’estimation du flux sanguin à partir des données LSCI. Ensuite, les applications du LSCI et une comparaison avec des techniques de laser Doppler sont proposées. Enfin, les tendances futures du LSCI sont présentées.

Nos principaux résultats sont exposés dans les chapitres 4 et 5. Dans le chapitre 4, deux points principaux sont abordés :

— l’impact possible des diffuseurs statiques sur la vitesse des érythrocytes calculée

4. Pour des raisons de cohérence, nous gardons l’acronyme PWV pour ce résumé en français.

à partir de l'expression de contraste K. A cet effet, deux méthodes ont été utilisées. La première simule l'expression du contraste K mathématiquement. La deuxième consiste à calculer une valeur expérimentale de la fraction de la lumière diffusée statiquement. Pour ces deux méthodes, la vitesse des érythrocytes a été calculée à partir de l'expression du contraste K et comparée (comparaison entre l'état où l'effet des diffuseurs statiques est pris en compte et lorsqu'il ne l'est pas). L'analyse de l'effet des diffuseurs statiques sur la vitesse des érythrocytes à partir des données de LSCI montre que les particules statiques (par exemple la peau) jouent un rôle important dans la valeur de la vitesse des érythrocytes. Plus la quantité de diffuseurs statiques est importante, plus élevée est la valeur de la vitesse des érythrocytes. Les diffuseurs statiques comme la peau ont donc une influence sur les valeurs de la vitesse des globules rouges calculées à partir des images de contraste par speckle laser.

— l'impact du vieillissement sur les données de LSCI. A cet effet, nous avons analysé les paramètres de la microcirculation (perfusion et vitesse des érythrocytes) et paramètres de la macrocirculation (PWV) chez des sujets sains, répartis en deux groupes (jeunes et âgés). La relation possible entre ces paramètres a également été étudiée. Nos résultats montrent que l'impact de l'âge sur la vitesse des globules rouges peut être étudiée à partir des données de LSCI. Le groupe de sujets plus âgés présente des valeurs de vitesse de globules rouges significativement plus élevées que celles des sujets jeunes pendant l'hyperémie réactive post-occlusive. Cela peut être dû à la rigidité des vaisseaux qui augmente avec l'âge. La PWV est une mesure de la rigidité artérielle (Wilkinson et al., 1998) et elle augmente avec l'âge. La rigidité artérielle étant plus élevée pour les personnes âgées, la re-vascularisation des vaisseaux après l'occlusion vasculaire (hyperémie réactive post-occlusive) peut conduire à des valeurs de vitesse des globules rouges plus élevées.

D'autre part, la perfusion et la vitesse des érythrocytes, deux paramètres corrélés et liés à l'âge des sujets, sont corrélées à la PWV, un marqueur de la rigidité artérielle au niveau macrovasculaire.

Dans le chapitre 5, nous avons mené une étude de la complexité de séries temporelles de LSCI s'appuyant sur des mesures d'entropie multiéchelle. Trois mesures de complexité basées sur l'entropie ont été appliquées à des séries temporelles de LSCI : la MSE, l'entropie multi-échelle composite (CMSE [5]), et l'entropie multi-échelle composite améliorée (RCMSE [6]). Nous montrons que la RCMSE est capable de différencier

5. Pour des raisons de cohérence, nous gardons l'acronyme CMSE pour ce résumé en français.
6. Pour des raisons de cohérence, nous gardons l'acronyme RCMSE pour ce résumé en français.

le groupe de sujets jeunes du groupe de sujets plus âgés. La RCMSE est une méthode simple pour évaluer la complexité des signaux physiologiques de séries courtes. Nous avons constaté que les fluctuations des séries temporelles de LSCI dans le groupe des sujets jeunes ont une complexité supérieure à celle du groupe de sujets âgés. Ces modifications observées sur la microcirculation pourraient être attribuées à des modifications du système vasculaire dans son ensemble. Nous avons déjà mentionné (et ceci a été confirmé dans la littérature) que la macro et la microcirculation sont des systèmes corrélés (Khalil et al., 2015). De plus et au niveau central cette fois-ci, il a été montré par d'autres équipes que les fluctuations cardiaques des sujets sains jeunes sont complexes, mais cette complexité diminue avec l'âge (Lin et al., 2014; Beckers et al., 2006; Goldberger et al., 2002; Voss et al., 2009).

Enfin, un résumé et les perspectives de cette thèse sont donnés dans le **chapitre** 6.

Du point de vue clinique, nos résultats montrent que chez des sujets sains : 1) il est possible de révéler l'influence de l'âge sur le flux sanguin microvasculaire à travers une approche de traitement du signal sur les données de contraste laser; 2) la micro et la macrocirculation sont des systèmes corrélés.

Du point de vue scientifique, notre travail a permis : 1) d'étudier théoriquement et expérimentalement l'impact possible des diffuseurs statiques sur l'estimation de la vitesse des érythrocytes à partir de l'expression du contraste K; 2) d'analyser la fiabilité de trois algorithmes basés sur la "sample entropy".

L'étude chez des sujets sains nous a permis de révéler l'utilité des données LSCI pour évaluer l'impact du vieillissement sur la microcirculation. Les modifications de la microcirculation de la peau liées à l'âge peuvent être attribuées à des modifications du système circulatoire dans son ensemble. La compréhension de ces modifications peut donner de nouvelles perspectives en matière de prévention et de traitement des pathologies liées à l'âge.

Acknowledgments

Foremost, I would like to express my special appreciation and thanks to my supervisor, Prof. Anne Humeau-Heurtier, for guiding and accompanying me in accomplishing this work, for her patience, motivation, and immense knowledge. I could not have imagined having a better advisor and mentor than her for my PhD study.

Besides my supervisor, I would like to thank Prof. Jean-Luc Cracowski (University of Grenoble Alpes) and Asst. Prof. Emilie Pery (University of Clermont-Ferrand) for serving as my thesis monitoring committee. I want to thank them for their brilliant comments and suggestions.

Many thanks to the members of the jury, formed by Prof. Walter Blondel, Prof. Jean-Luc Cracowki, Asst. Prof. Jean-Marc Girault and Asst. Prof. Emilie Pery for accepting to participate at the thesis and for the patience to read it.

I would especially like to thank Prof. Pierre Abraham (University of Angers), Asst. Prof. Guillaume Mahé (CHU of Rennes), and Lydie Gascoin (CHU of Angers) for their support and assistance in my research and collecting data for my PhD study.

I gratefully acknowledge the support provided by the ministry of higher education and scientific research in Iraq (Baghdad), the university of Diyala in Iraq (Diyala), the Embassy of France in Iraq (service of cooperation and cultural action in Baghdad), and Campus France Paris, France.

I am also thankful to:
— staff of ISTIA for their partial financial support and administrative assistance.
— staff of LARIS for their various forms of support during my PhD study.
— group ISISV for welcoming me during these three years.

A special thank goes to my family. Words can not express how grateful I am to my mother, and father for all of the sacrifices they made on my behalf. Their prayer for me was what sustained me thus far. I would like to thank my brothers and sister for

supporting me spiritually throughout writing this thesis and my life in general.

Last but not the least, I take this opportunity to express my profound thanks to my beloved wife, Mareb Al-khalidi. Thank you for supporting me for everything, and especially I can not thank you enough for encouraging me throughout this experience.

Scientific contributions

Articles in refereed journals

1. A. Khalil, A. Humeau-Heurtier, G. Mahé, and P. Abraham, Laser speckle contrast imaging: age-related changes in microvascular blood flow and correlation with pulse-wave velocity in healthy subjects, *J. Biomed. Opt.*, 20(5):051010–1–8, 2015.

2. A. Khalil, A. Humeau-Heurtier, L. Gascoin, G. Mahé, and P. Abraham, Aging effect on microcirculation: A multiscale entropy approach on laser speckle contrast images, *Med. Phys.*, 43(7), 4008-4016, 2016.

International Communications

1. A. Khalil, A. Humeau-Heurtier, P. Abraham and G. Mahé, Processing of laser speckle contrast images to analyze the impact of aging on moving blood cells velocity when a Lorentzian velocity profile is assumed, in: EUSIPCO'2014 (22nd European Signal Processing Conference), Lisbonne, Portugal, pp. 2035-2039. ***Poster session***.

2. A. Khalil, A. Humeau-Heurtier, P. Abraham and G. Mahé, Comparative study to analyze the effect of aging on microvascular blood flow by processing laser speckle contrast images when Lorentzian and Gaussian velocity Profiles are assumed for moving scatterers, in: Image Processing Theory, Tools and Applications (IPTA), Paris, France, 2014, pp. 1-6. ***Oral session***.

3. A. Khalil, A. Humeau-Heurtier, G. Mahé, P. Abraham, Microvascular blood flow with laser speckle contrast imaging: analysis of static scatterers effect through modelling and simulation, in: IEEE EMS2014 (8th European Modelling Symposium on Mathematical modelling and Computer Simulation), Pise, Italy, ISBN: 978-1-4799-7411-5. ***Oral session***.

National communication

1. A. Khalil, A. Humeau-Heurtier, P. Abraham and G. Mahé, Analysis of the effect of static scatterers on blood cells velocity values computed from laser speckle contrast images: preliminary study, in: OPT-DIAG, Paris, France, 2014, pp. 52. ***Oral session***.

Other Communication

1. A. Khalil, Analysis of the effects of aging on microvasculature through the processing of laser speckle contrast images, Journée des doctorants de l'École Doctorale STIM, JDOC2015, 9 avril 2015, Angers.

Contents

List of Tables

List of Figures

Abbreviations

BZ ..... Biological Zero
CBF ..... Cerebral Blood Flow
CCD ..... Charge Coupled Device
CMSE ..... Composite Multiscale Entropy
CVS ..... Cardiovascular System
EDRF ..... Endothelium Derived Relaxing Factor
HSI ..... Hyperspectral Imaging
LASCA ..... Laser Speckle Contrast Analysis
LDV ..... Laser Doppler Velocimetry
LDI ..... Laser Doppler Imaging
LDF ..... Laser Doppler Flowmetry
LSFG ..... Laser Speckle Flowgraphy
LSCI ..... Laser Speckle Contrast Imaging
MBCV ..... Moving Blood Cells Velocity
MSE ..... Multiscale Entropy
MESI ..... Multi Exposure Speckle Imaging
MRI ..... Magnetic Resonance Imaging
NO ..... Nitric Oxide
NOS ..... Nitric Oxide Synthase
OPS ..... Orthogonal Polarization Spectral
OCT ..... Optical Coherence Tomography
PORH ..... Post Occlusive Reactive Hyperaemia
PWV ..... Pulse Wave Velocity
RBC ..... Red Blood Cells
RCMSE ..... Refined Composite Multiscale Entropy

ROI . . . . . Regions Of Interest
SampEn . . . . . Sample Entropy
SNR . . . . . Signal to Noise Ratio

1

Introduction

In this chapter, an introduction to the research areas of aging process and laser speckle contrast imaging is given. Furthermore, the aim of this PhD work will be introduced. Finally, the outline of this manuscript is presented.

Contents

1.1 General introduction

According to the world health organization, people around the world are living longer (World Health Organization, 2015). With the development of the health care system, most people can expect to live into their sixties and beyond. By 2050, the world population aged 60 years and older is expected to total 2 billion, and was up from 900 million in 2015. About 125 million of people are aged 80 years or older (World Health Organization, 2015). If people can experience these extra years of life in good health and if they live in a supportive environment, their ability to do the things they value will be little different from that of a younger person. These added years are dominated by declines in physical and mental capacity.

Aging is a primary risk factor for cardiovascular diseases. It is associated with a reduction in microvascular activity, increased vascular stiffness, decreased vascular density, and impaired vascular organization (see Tobin, 2017, for review). Over time, these damaged activities lead to an increased risk of many diseases, and a gradual decrease in the capacity of the individual to adapt to local conditions. In the long run, it will result in death. Therefore, aging process is one of the fields where the research and new technology have to be applied. Focused research, new metrics and methods could give an obviously better understanding of healthy aging and are essential for evidence-informed policy and evaluation. Therefore, analyses in healthy subjects are important as they are the first step before an analysis in pathological subjects.

The assessment of microvascular blood flow has been recognized as important to analyze the impact of aging (Li et al., 2006b; Tsuda et al., 2014). Therefore, different laser-based techniques have emerged to monitor microvascular blood flow (Bi et al., 2015; Allen and Howell, 2014; Eriksson et al., 2014; Roustit and Cracowski, 2013). Most of these techniques that are now being developed and become portable, make microvascular measurement techniques easily accessible at the bedside. Among these laser-based techniques, laser Doppler perfusion imaging (LDPI) and laser speckle contrast imaging (LSCI) have taken an emerging and more and more preponderant place in clinical and research applications imaging. Both of these techniques provide a measurement time in the millisecond range. Furthermore, to perform LSCI measurements,

an inexpensive camera – with frame-rate of 200Hz – is sufficient to provide excellent images of blood flow. For LDPI, a state-of-the-art high-speed camera that can achieve a frame-rate of about 25 kHz is needed to provide the same quality images (Draijer et al., 2009).

Laser speckle contrast imaging (LSCI) provides high temporal and spatial resolution images of the microvascular blood perfusion with low-cost devices (Richards et al., 2013; Humeau-Heurtier et al., 2014a; Puissant et al., 2013). This technique is based on the random interference pattern – known as speckle pattern – generated from diffused backscattered light when an area of interest is illuminated by a laser light. LSCI exploits the fluctuations in the speckle pattern to provide information about blood flow in the superficial tissue. These fluctuations in speckle pattern are recorded with a camera and due to the exposure time of the camera, the intensity fluctuations cause blurring of the recorded images. To quantify the degree of blurring, the expression of the speckle contrast is computed. Moreover, when assumptions are made on moving scatterers velocity profile, LSCI data provide information on red blood cells velocity values (Briers and Webster, 1996).

To assess the microcirculation function, a critical task is to obtain relevant physiological information from medical images. Therefore, the application of information theory analysis (in particular entropy measures, see below chap. 5) has been introduced as a supportive tool for the investigation of physiological signals (see Blokh and Stambler, 2016, for review). Consequently, many signal and image processing methods have been proposed in order to allow a better understanding of the underlying physiological characteristics. Multiscale entropy (MSE) has been introduced as a useful tool to process physiological signals in multiple time scales (Costa et al., 2005, 2002). MSE analyses are widely used on data recorded from the macrocirculation for the diagnosis of different kinds of pathologies, but also to analyze the impact of aging (Costa et al., 2005, 2008; Trunkvalterova et al., 2008; Escudero et al., 2006). On the other hand, the LSCI technique has recently been commercialized, and hence, few works discuss the postacquisition processing of laser speckle contrast images recorded *in vivo*. For instance, MSE algorithm has been applied by Humeau-Heurtier *et al.* (Humeau-Heurtier et al., 2013b, 2014b) to LSCI data obtained from the microvascular system. In their studies, the efforts were made to better understand the perfusion time series given by LSCI. However, no study related to aging was performed. The aging processes are multiparametric with nonlinear relations between these parameters (Blokh and Stambler, 2016). In this way, the application of nonlinear analyses to LSCI data might be reasonable for the investigation of such issues.

From another point of view, the studies have shown that aging generates changes in

the arterial network that constitutes the cardiovascular system. This network consists of two coupled systems, macrocirculation and microcirculation, which interact to enable an optimum adaptation of the organism to various physiologic disturbances. Studying the relationship between macro- and microcirculation may lead to an early estimation of many disorders in the cardiovascular system. Several authors emphasized that the two subsystems, macrocirculation and microcirculation, must be taken into account simultaneously (Feihl et al., 2009).

1.2 Scope of the thesis

Using image and signal processing algorithms, this PhD work aims at studying the influence of age on microcirculation, by processing LSCI data. For this purpose, two different ways are followed: 1) the study and analysis of microvascular parameters (perfusion and moving blood cells velocity, MBCV) when assumptions on moving scatterers velocity are made; 2) the processing of LSCI data with nonlinear analyses, more precisely with multiscale entropy. In our work, LSCI data are acquired from the forearm skin of healthy subjects, subdivided into two age groups. The first group includes young subjects whereas the second group includes older subjects.

Moreover, in this thesis we also study the possible impact of the static scatterers on MBCV values. The results are obtained through simulations and experimental processes. Furthermore, we study simultaneously the aging effect over microvascular parameters (perfusion and MBCV) and macrocirculation parameter (pulse wave velocity, PWV). The relationship between theses parameters is analyzed.

1.3 Outline of the thesis

An overview of the organization of the cardiovascular system, the different techniques to monitor microvascular blood flow, and the current state of research on the impact of aging on the microcirculation are given in **chapter** 2.

In **chapter** 3, LSCI theoretical background and the way to compute moving blood cells velocity and the perfusion from LSCI data are exposed. Furthermore, several measurement requirements are discussed, including those affecting blood flow estimation from LSCI data. Then, applications of LSCI and a trade-off with laser Doppler techniques are proposed. Finally, future trends of LSCI are presented.

Chapter 4 is subdivided into two main sections. The first section aims at studying the impact of aging on moving blood cells velocity extracted from LSCI data. For

this purpose, two age groups are studied, younger and older. Red blood cells velocity is computed from the microcirculation when a Lorentzian profile and when a Gaussian profile are assumed for moving scatterers. Furthermore, the possible impact of the static scatterers like skin on MBCV values is determined through simulations and experimental processes. The goals of the second section are: (i) to assess aging effect over microvascular parameters (perfusion and MBCV) and macrocirculation parameter (PWV); (ii) to study the relationship between these parameters.

By applying entropy-based complexity measures to LSCI time series, the objective of **chapter** 5 is to present our study on the impact of aging on the microcirculation, by measuring the complexity of microvascular signals over multiple time scales. For this purpose, forearm skin microvascular blood flow was studied with LSCI in two age groups (younger and older). To estimate age-dependent changes in microvascular blood flow, we applied three entropy-based complexity algorithms to LSCI time series. Thus, MSE and its refined versions, composite MSE (CMSE), and refined CMSE (RCMSE), are applied to LSCI time series. Furthermore, a comparison of the results given by MSE, CMSE, and RCMSE algorithms is proposed.

Finally, a summary and the perspectives of this thesis will be given in **chapter** 6.

2

Cardiovascular system and cutaneous microcirculation

The main objective of this chapter is to provide an overview of the organization of the cardiovascular system, the different techniques to monitor microvascular blood flow, and the current state of research on the impact of aging on the microcirculation.

Contents

2.1 Introduction

Skin is usually a barrier for mechanical and sensory protection in the body. It has been shown that age changes the morphology and quantification of the cutaneous microvasculature (Li et al., 2006b,a). With age, modifications in both structure and function of the skin microcirculation may occur. This is due to a reduction of the epidermal thickness, an alteration of elastic fibers, and to a decreased number of vessels (Calleja-Agius et al., 2013; Mizukoshi et al., 2015; Biniek et al., 2015; Puschmann et al., 2012; Kelly et al., 1995). These modifications caused by aging make the skin thinner and cutaneous connective tissue less elastic (Fenske and Conard, 1988). Therefore, the assessment of microvascular blood flow has been recognized as important to analyze the impact of aging (Li et al., 2006b; Tsuda et al., 2014). Moreover, age is a primary risk factor for cardiovascular disease (Najjar et al., 2005).

2.2 Physiological background

In the human organ, the individual cells evolve into complex systems. Therefore, these cells are not capable of being self-sustained (Obradovic et al., 1999). The arterial network of the cardiovascular system (CVS) – which consists of the heart and the blood vessels – provides a transport way (Porth, 2011) to distribute oxygen (O_2) and nutrients to each cell and takes away carbon dioxide (CO_2) and waste products. Furthermore, it also plays a vital role in temperature regulation and transport of various

immune substances that contribute to the defense mechanisms. Human cardiovascular or circulatory system plays an essential role in the maintenance of a constant internal body environment (Berne and Levy, 1998).

2.2.1 Organization of the cardiovascular system

The cardiovascular system is an organ system that can be divided into two parts: the pulmonary circuit is a short loop that transports deoxygenated blood from the right side of the heart to the lungs, where the blood picks up oxygen and returns to the left side of the heart; systemic circuit, a loop through the rest of the body that carries highly oxygenated blood from the left side of the heart for all other tissues.

The cardiovascular system is therefore composed of a pump, the heart, arteries, arterioles, capillaries, venules, and veins (Fig. 2.1). Arteries and arterioles carry blood away from the heart. Capillaries serve to exchange diffusible substances between blood and tissue (Shore, 2000). Venules and veins serve as storage vessels, those carrying blood back to the heart. Both sides of the heart are subdivided into two chambers, an atrium and a ventricle. The pumping chambers of the heart that support the pulmonary circulation loop are the right atrium and right ventricle. In contrast, the left atrium and left ventricle of the heart are the pumping chambers for the systemic circulation loop. The cardiovascular system is a closed system with the right and the left sides of the heart connected in series. Heart (left side) pumps the highly oxygenated blood through the arteries. Arteries are connected to smaller arterioles and then to smaller capillaries. Capillaries provide oxygen and nutrients to the tissues before traveling away from tissue and organs, carrying deoxygenated blood, flowing into venules and then to the larger veins carrying blood back to the heart, thus completing the cycle. In normal situation, the total volume of blood in the body is around 4-6 liters. Under baseline condition, heart beats from 60 to 70 times per minute and pumps on average 5.5 liters of blood per minute (Schmidt et al., 1989).

2.2.2 Function of the heart and blood vessels

Blood flow through the heart is shown in Fig. 2.2. The right atrium receives blood from the systemic venous system (the superior vena cava and inferior vena cava). Due to the atrial contraction around the blood within the cardiac chambers, blood is ejected and fills the right ventricle. Right ventricular contraction ejects blood – at high pressure that is so-called systolic pressure – from the right ventricle into pulmonary artery, which delivers it to the lungs. As the blood passes through the pulmonary circulation, the blood pressure falls to the minimum value (diastolic blood pressure). The left atrium receives the pulmonary venous blood, the blood passes into the left ventricle due to the atrial contraction. At relatively high systolic pressure compared to the right ventricle (Klabunde,

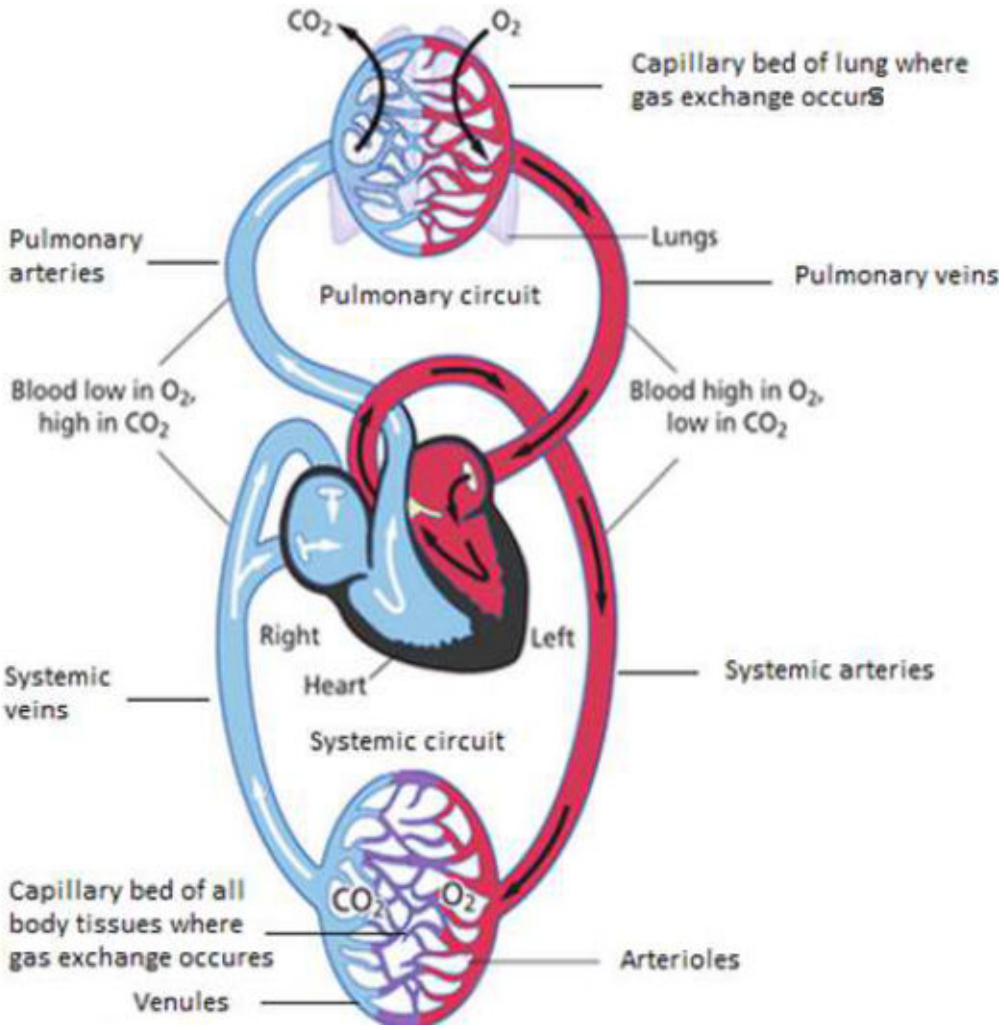

Figure 2.1 – Human circulatory system (adapted from Whittemore, 2009).

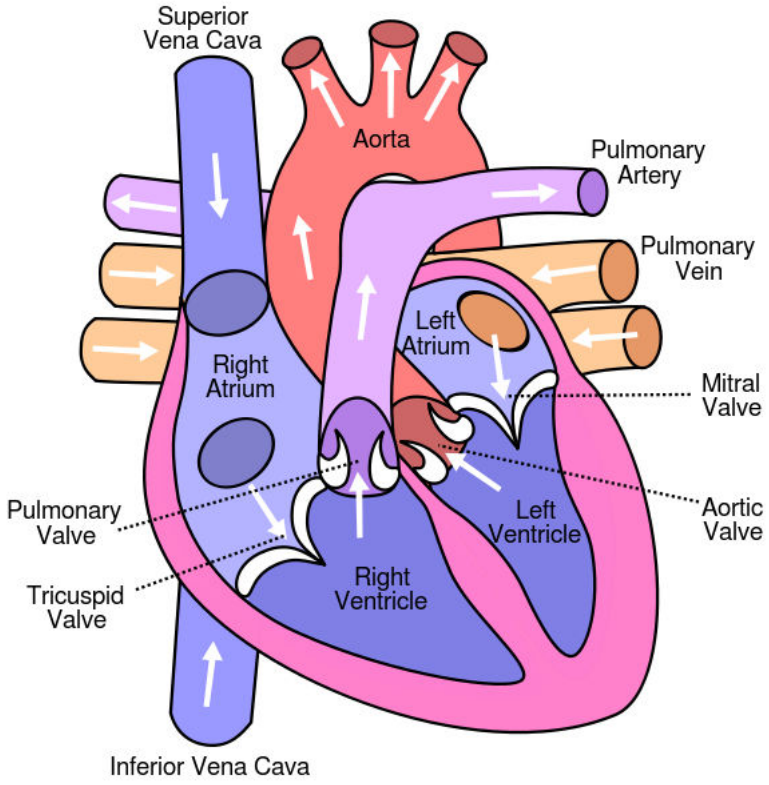

Figure 2.2 – Blood flow through the heart (from Balaji et al., 2014)

2011), left ventricle pumps blood to the rest of the body through the systemic arterial system (the aorta and its branches). In addition to pumping blood function, heart has other important functions, such as regulation of blood volume and blood pressure.

As mentioned above, the human vascular system consists of arteries, arterioles, capillaries, venules, and veins. All vessels except true capillaries comprise three layers; from the lumen to the outer part of the vessel: intima, media, and adventitia layers (Fig. 2.3). The endothelial lining, which usually consists of a single layer of flat cells is found in the intima. The media contains elastic fibers, collagen fibers and smooth muscle cells. The number of elastic and collagen fibers and the ratio between them determine the degree to which the vessels can be stretched. The adventitia contains collagen, fibroblasts, lymphatic vessels and autonomic nerves, as well as a network of small blood vessels, the vasa vasorum. True capillaries do not have media and adventitia, they are only lined by the endothelium.

Arteries are thick-walled vessels with large amounts of elastic fibers. The elasticity of these vessels allows them to stretch during systolic pressure and recoil during dias-

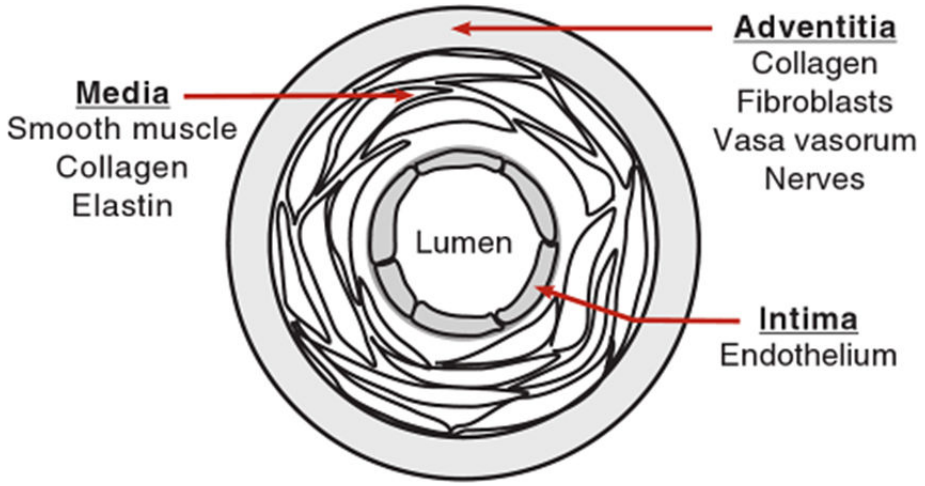

Figure 2.3 – Anatomical structure of blood vessel wall (from Klabunde, 2011)

tolic pressure. The arterioles branch out from the arteries, ending in more thinner blood vessels those so-called the capillaries. Venules and veins are thin-walled, distensible and collapsible vessels. The walls of the veins are less elastic than arteries, but veins are more compliant and function as capacitance vessels (Kheong and Cheng, 2015).

Blood vessels constrict and expand to: control arterial and capillary blood pressure, regulate blood flow within organs, and distribute blood volume within the body. Changes in vascular diameters are possible by activation of vascular smooth muscles within the vascular wall by autonomic nerves, metabolic and biochemical signals from outside of the blood vessels, and vasoactive substances released by endothelial cells that line the blood vessels.

The role of vascular endothelium Endothelium plays a crucial role in the regulation of blood flow and smooth muscle tone (Klabunde, 2011). The endothelium is a thin layer of endothelial cells that lies between the circulating blood and vascular smooth muscles. It serves as a physical barrier for vasoactive substances that circulate in the blood. Vascular endothelial cells line the entire circulatory system, from the heart to the smallest capillaries. The endothelium plays an important role in controlling vascular function, including blood fluidity, blood vessel tone, neutrophil recruitment, hormone trafficking, and hence is considered as a major mediator of cardiovascular system.

The intact endothelium is able to produce a factor that causes relaxation of vascular smooth muscle. This factor was originally named endothelium-derived relaxing factor (EDRF) and is now known to be nitric oxide (NO) (Kelm et al., 1988). The normal endothelium maintains a continuous release of NO which is formed from arginine by

the action of the enzyme NO synthase. The production of NO can be stimulated by a variety of endothelial agonists, including acetylcholine, as well as by shear stress resulting from an increase of blood.

In addition to exchange, regulation of blood flow, production of NO, the endothelium produces substances that regulate hemostasis (blood clotting) and inflammatory responses (Klabunde, 2011).

Vascular smooth muscle The smooth muscle cells are arranged in helical or circular layers around larger blood vessels and in a single circular layer around arterioles. Vascular smooth muscles provide active tension in the vessel wall and regulate the diameter of the vessels (Lotrič, 1999).

The vascular smooth muscle cells contain a large number of thin filaments and a comparatively small number of thick filaments. They are aligned in the long axis of the cell and the contraction is achieved via sliding filament mechanisms (Herrera et al., 2004). The interaction between filaments leads to the contraction of the smooth muscle cells. Therefore, vascular smooth muscle contracts or relaxes to control both the volume of blood vessels and the local blood pressure. This mechanism is responsible for the redistribution of the blood to the organs where it is needed. Thus the main function of vascular smooth muscle tonus is to regulate the caliber of the blood vessels in the body.

Arteries have more vascular smooth muscles within their walls than veins, thus their wall thickness is greater. The thickness of the arteries and its important smooth muscle layer is mainly due to the fact that the heart is a pulsatile system and the blood flow has to be continuous with a low pulsatile to avoid cell damage (Ganong and Barrett, 2005). This is the Windkessel effect (Frank, 1990).

In many vessels there are smooth muscle cells that undergo spontaneous depolarization. These cells act as pacemakers and excite neighboring cells, thus providing a background tension, the so-called myogenic basal tone. The vascular smooth muscle is innervated mainly by the adrenergic postganglionic fibers of the sympathetic nervous system.

2.2.3 Microcirculation

Microcirculation corresponds to the smallest blood vessels, which permits to deliver the oxygen and nutrients to the tissue and single cells. Therefore, microcirculation is the vascular network including arterioles, capillaries, and venules, as well as the flow of

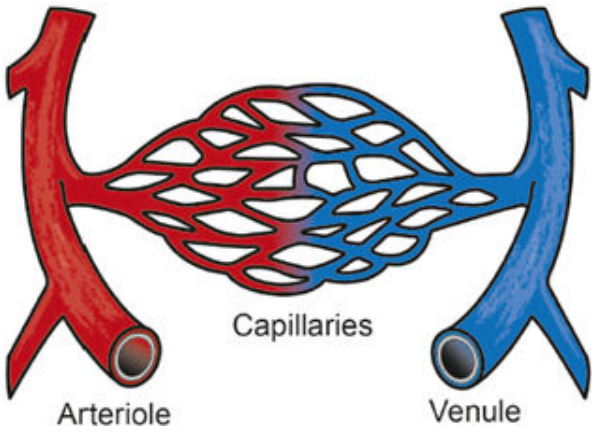

Figure 2.4 – Vascular network of the microvascular unit (from Olausson, 2015).

blood through this network (Fishman and Richards, 2013) (see Fig. 2.4).

A microcirculatory unit corresponds to a microvascular network, in which a mean diameter of 100 μm was usually considered as the upper limit for blood microvessels (Tuma et al., 2011). This includes the arterioles, capillaries, and venules. The microcirculations are found in the form of microcirculatory units in all body organs.

Arterioles An arteriole is defined as a small diameter blood vessel in the microcirculation, that branches out from an artery and leads to capillaries (Maton, 1997). Arterioles are defined as the primary resistance vessels that have a diameter of 10–100 μm. Their wall comprises three layers (Rhodin, 1967), the intima (lining endothelial cells), media (an internal elastic lamina apposed by one or two layers of smooth muscles) and the adventitia (tunica consisting of a few collagen fibers). Arterioles respond to a wide variety of chemical, physical, and electrical messages. The smooth muscle cells can contract and relax, varying the size of the arterioles, and as a result of that, regulate blood flow and blood pressure. Therefore, primary function of arterioles is flow regulation (Klabunde, 2011).

Arterioles respond to metabolic stimuli that are generated in the tissues. When tissue metabolism increases, catabolic products accumulate leading to vasodilation. The endothelium begins to control muscle tone and arteriolar blood flow tissue. Endothelial function in the circulation includes the activation and inactivation of circulating hormones and other plasma constituents. In addition, as mentioned above, there are also synthesis and secretion of vasodilator and vasoconstrictor substances for modifying the width as necessary.

Capillaries Capillaries are the smallest of a body's blood vessels, measuring around 5 to 8 μm in diameter and 0.5 to 1 mm in length. They connect arterioles and venules. Their endothelial linings are only one cell layer thick. They help to enable the exchange of oxygen and nutrients and waste chemical substances between blood and the tissues (Maton, 1997). Capillaries do not function on their own, but instead in a capillary bed. Capillary beds consist of two types of vessels: true capillaries, which branch from arterioles, are considered as a medium environment at the microcirculatory level between blood and tissues (Tortora and Derrickson, 2008), and metarterioles, which are short vessels that directly connect the arterioles and venules at opposite ends of the bed (Krstic, 1991).

Venules Venules connect the capillary beds to the veins. The diameter of the venous vessels is greater than the arteriole at the same level of the network (Tuma et al., 2011). The transitional factor between the capillary and venule is the appearance of smooth muscle cells in the wall. Venules are rich in connective tissue and elastic fibers, which gives them a remarkable distensibility property. The venular network is a reservoir of variable capacity for adjusting every moment of microcirculatory blood volume (Tortora and Derrickson, 2008).

2.3 Cutaneous microcirculation

2.3.1 Skin physiology

The skin is the heaviest (approximately 5 kg), and the largest (1.25 to 2 m^2) organ in the human body (Potts, 1997; Hadgraft, 2001; Kanitakis, 2001). It is the outer protective barrier of the body, and is considered as an active immune system (Bos and Kapsenberg, 1993). Thickness of skin is 2 mm in average. The latter varies according to the gender (thinner in women), age (thinner in the elderly), and according to the abundance of skin appendages (hair, sebaceous glands). Temperature of skin also varies by region, it is between 32 °C and 36 °C. The skin consists of three main layers (Tortora and Derrickson, 2008), from outside to inside the body: the epidermis, dermis, and hypodermis or subcutaneous tissue (see Fig. 2.5).

1. **Epidermis** is the outermost layer of cells in the skin (James et al., 2015). It forms a thin protective barrier against excessive water loss and for the conservation of vital fluids within the body. This layer is impermeable to air and substantially impermeable to water, also opposes to the entry of foreign particles in the body.

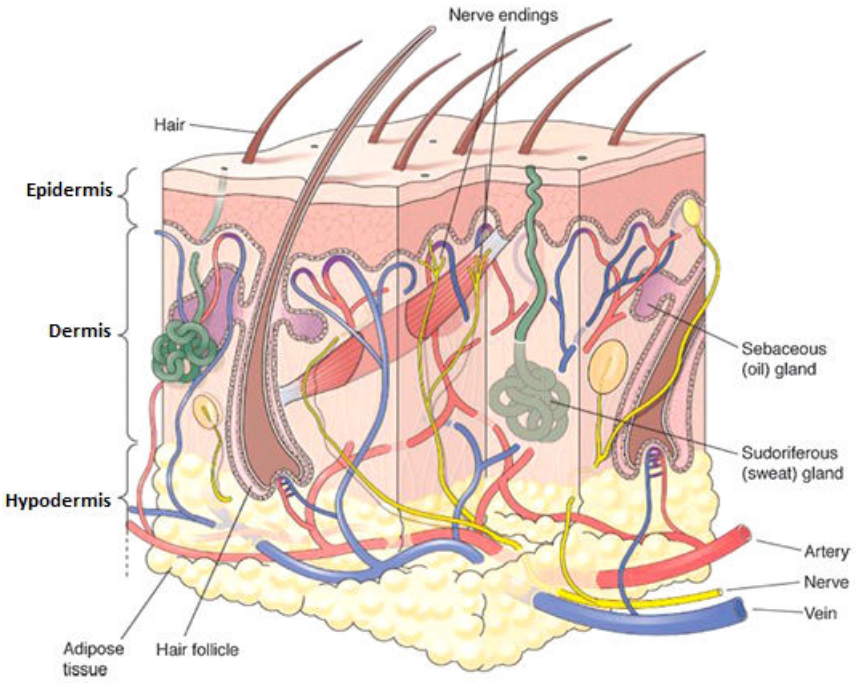

Figure 2.5 – Schematic representation of the microvascular organization in the human skin (adapted from Stelton et al., 2015).

The epidermis is not vascularized. Its cells are supplied by diffusion through the interstitial fluid from the blood vessels of the dermis.

2. **Dermis** is the inner layer of the skin. It contains fibroblasts, elastin and ground substance that give the support and elasticity of the skin. Dermis is rich in blood vessels and nerve endings that allow the perception of pressure, pain, and temperature.

   The dermis also contains sebaceous glands (sebum secretion that lubricates the skin and makes it impermeable to water), and sweat (sweat secretion to cool the skin).

3. **Hypodermis** is a loose connective tissue highly vascularized, which contains more or less fat, depending on the regions of the skin. It consists of lobules filled with fat cells (adipocytes) and separated by connective elastic walls enclosing the vessels and nerves of the skin. It sets the skin on the body and organs. It contains up to half of the reserves fat of the body. These reserves insulate the body and prevent heat loss and serve as mechanical protection (Dahan, 2008).

2.3.2 Skin functions

The skin has four main functions:

1. **Protection** Skin acts as the first physical barrier to mechanical and chemical impacts, variations in temperature, micro-organisms, infection and radiation (Odland and Ross, 1968).
2. **Thermal regulation** Skin is the primary interface by which the body controls its internal temperature. Temperature regulation is controlled by the skin through the sweat glands and blood vessels in the dermis. Vasodilation (relaxing of small blood vessels) in the dermis helps the body to release some heat and diminish the body temperature through skin. In contrast, with vasoconstriction (contracting small blood vessels), the dermis preserves the internal body temperature (Venus et al., 2011).
3. **Sensation** Skin is the organ of the widest sense of the body and contains different types of receptors for sensitivity to pressure, pain, and temperature. Sensation is detected through the nerve endings in the dermis which are easily affected by wounds. Impairment of these nerve cells is known as neuropathy, which results in a loss of sensation in the affected areas. Patients with neuropathy may not feel pain when they suffer injury, increasing the risk of acute wounding (Venus et al., 2011).
4. **Endocrine function** The hypodermis is an important energy reserve mainly in the form of triglycerides. Vitamin D is synthesized in the skin by photoreaction in the presence of ultraviolet light (Holick, 2007). This vitamin plays a critical role in bone metabolism and many cellular and immunological processes (Holick, 2003).

2.3.3 Cutaneous microcirculation

The epidermis, the pilosebaceous follicles, sweat glands and their excretory ducts, being avascular like all epitheliums, need a close nutritious network. This is the dermis, which is the main feeder structure of the skin. Dermis contains small blood vessels network which is called plexus. The subcutaneous tissue is rich in blood vessels. Like every organ, the skin has a circulatory system. Because of its size (2 mm thick in average), this system belongs only to the microcirculation.

The cutaneous microcirculation is arranged as two horizontal plexuses of arterioles and venules in the dermis (Yen and Braverman, 1976): one is situated around 1 to 1.5 mm below the skin surface and the other is at the dermal-subcutaneous junction. The two plexuses are connected through the ascending arterioles and descending venules. An upper horizontal network – arterial capillaries – rises to form the dermal papillary

loops that represent the nutritive component of the skin circulation (Braverman, 1989). There are sphincter-like smooth muscle cells at the point where the ascending arterioles divide to form the arteriolar component of the upper horizontal plexus. At the dermal-subcutaneous junction, there are collecting veins with two cusped valves that are oriented to prevent the retrograde flow of blood. Most of the microvasculature is contained in the papillary dermis 1 ± 2 mm below the epidermal surface (Braverman, 2000).

2.4 Techniques to monitor microvascular perfusion

Microcirculation provides a vital environment to the physiological processes of tissue oxygenation and nutritional exchange. In recent years, assessment of microvascular blood flow has been recognized as important for the follow-up of pathologies such as diabetes, Raynaud's phenomenon, and hypertension (see Tsuda et al., 2014; De Ciuceis et al., 2007). Therefore, different optical techniques have emerged to monitor microvascular blood flow (Bi et al., 2015; Allen and Howell, 2014; Eriksson et al., 2014; Roustit and Cracowski, 2013). Most of those techniques, that have now become portable, make microvascular measurement techniques easily accessible at the bedside.

Microvascular assessment can be accomplished with both single-point measurements and imaging methods. The better reproducibility (Roustit et al., 2010), and the ability to measure large area, make imaging methods more desirable than single-point measurements.

This section aims at summarizing some of the most important optical-based, non-invasive techniques that are used to monitor microvascular blood flow.

Laser Doppler techniques Laser Doppler techniques are well-known to monitor microvascular blood perfusion in the tissue (Wardell et al., 1993; Essex and Byrne, 1991). The first introduction was in the 1970s after the development of laser technology and fiber-optic systems. Laser Doppler flowmetry (LDF) was thus proposed by Stern (Stern, 1975). LDF is a single point measurement technology. Skin perfusion is obtained by measuring the Doppler shift induced by coherent monochromatic light reflected by both static (such as the static tissue) and moving scatterers (such as red blood cells, RBC) (Stern, 1975). Reflected light from static tissue surrounding the RBC returns with unchanged frequency. Measuring the zeroth and first order moments of the power spectrum of the photoelectric current leads to the concentration of RBC and perfusion, respectively (Wardell et al., 1993).

LDPI is a further development of LDF. LDPI is based on the same principle as LDF. It is a scanning or full-field technique that provides a two-dimensional image of blood flow by combining several single measurements over an area of interest at the tissue surface (Essex and Byrne, 1991). The standard LDPI apparatus uses a movable mirror that directs the laser beam on different measurement points, providing 2D images mapping the cutaneous perfusion.

LDPI can provide maps of capillary blood flow over a surface up to 50×50 cm^2 (O'Doherty et al., 2009). The tissue sampling depth is typically from 1 to 2 mm (Briers, 2001), while this depth depends on the laser wavelength and on the properties of the tissue.

LDPI has proven to be useful in a wide variety of biomedical applications. It is of utility in burn wound depth assessment (Monstrey et al., 2011), measure of microvascular dysfunction in Raynaud's phenomenon, and diabetes (Anderson et al., 2004; Muris et al., 2013), assessment of microvascular perfusion in the skin (Payette et al., 2005), and many other applications including chronic pain (Grothusen and Schwartzman, 2011), cancer and angiogenesis (Kalka et al., 2000; Ferraro et al., 2010), and brain (Broderick and Kolodny, 2010).

Laser speckle contrast imaging LSCI is an emerging noninvasive optical technique that allows the monitoring of microvascular function (Humeau-Heurtier et al., 2013a). Background method, advantages, limitations, and applications will be detailed in Chap. 3. Briefly, this technique is based on the random interference pattern – known as speckle pattern – generated from diffused backscattered light when an area of interest is illuminated by a laser light. LSCI is preferable to the scanning technique such as LDPI due to its full-field property and to its high performance-to-cost ratio: LSCI is a noninvasive, contactless, and highly reproducible technique (Puissant et al., 2013; Humeau-Heurtier et al., 2014a; Roustit et al., 2010). Moreover, LSCI provides high quality images of the microvascular blood flow at low cost (Richards et al., 2013).

Orthogonal polarization spectral imaging Orthogonal polarization spectral imaging (OPS) is a videomicroscopy technique that can be used for direct visualization of microcirculation. The physical concept behind OPS imaging has been described in detail by Groner *et al.* (Groner et al., 1999). Briefly, in OPS imaging, the area of interest is illuminated with a polarized light. An orthogonal polarizer is used to permit only reflected depolarized light to contribute to the image and preventing direct reflections. The reflected light is recorded with a CCD videocamera. This method permits direct

visualization of the microcirculation, and RBC velocity can be measured as well.

OPS imaging is widely used to monitor microcirculation in sublingual mucosa in patients with sepsis (see De Backer et al., 2002), and several other organs including skin (Lupi et al., 2008), gingiva (Lindeboom et al., 2005), brain (Pennings et al., 2006), liver (Puhl et al., 2003).

Thermography The amount of radiation emitted by an object increases with temperature. Thus, the underlying technique of thermography depends on the changes in tissue temperature. Using an infrared thermal imaging camera, one can determine the warm objects against cooler backgrounds. As a result, thermography is of utility during clinical diagnosis, and thus several studies, using thermography, have investigated skin temperature across the body surface (Zaproudina et al., 2008). Furthermore, other studies have compared skin blood flow in human measured by thermography, LDPI (Seifalian et al., 1994), or LSCI (Pauling et al., 2012).

Thermography is widely used to quantify the re-warming rate of the fingers in vasospastic conditions in Raynaud's syndrome patients after a cold challenge to the hand (Ring et al., 1981). Thermography is able to provide a real-time, two dimensional image for blood perfusion in skin (Szabó et al., 2013).

Nailfold capillaroscopy Capillaroscopy is a non-invasive technique for imaging and assessing the microvasculature *in vivo* (Bollinger and Fagrell, 1990). It is a microscope technique that allows to investigate the morphology of capillary loops over a few millimeters. It is considered as the most well-known tool to investigate nailfold capillary. However, depending on the microscope design, this technique can be used to examine other areas of the body as the lips, tongue, and mouth (see Scardina et al., 2013).

Optical coherence tomography Optical coherence tomography (OCT) is an imaging technique that uses a low-coherence light source to capture cross-sectional images in micrometer-resolution (typically from 1 to 15 μm) (Fujimoto et al., 2000; Fujimoto, 2003).

In this technique, a low-coherence light is focused into the sample being imaged. Hence, images of the tissue structure are acquired by measuring the delay time and the intensity of back-scattered light from the sample (Fujimoto, 2003). OCT is capable of providing information about the tissues depth (Zysk et al., 2007). OCT is used in a wide

range of clinical applications, including ophthalmology (Hahn et al., 2011), histology (Jung and Boppart, 2012), cardiology (Nammas et al., 2013), and several other applications reviewed by Mahmud *et al.* (Mahmud et al., 2013).

Hyperspectral imaging Hyperspectral imaging (HSI) is a new non-invasive, and optical imaging modality that can be used in biomedical applications. For example, HSI can provide perfusion map in superficial blood vessels as the skin (Lu and Fei, 2014).

The principle of this technique is based on a spectroscopic technique, acquiring two-dimensional images across a wide range of wavelengths of the electromagnetic spectrum. HSI achieves both spectral (identifying surface features) and spatial information (characterization of complex heterogeneous samples) from an object. Tissue is illuminated with near-infrared light, and due to the fact that scattering characteristics of tissue change during the progression of disease, the reflected light from tissue captured by HSI sensor, which is a camera (see Gowen et al., 2009) carries quantitative diagnostic information about tissue pathology (Tuchin and Tuchin, 2007).

There are many potential applications for HSI in assessing the microcirculation and associated perfusion (see Rodmell, 2005). Furthermore, the utility of HSI has been reported in the assessment of retinal blood vessels (Shahidi et al., 2013), assessment of allergic dermatitis (Nishino et al., 2013), monitoring temporal changes in epidermal thickness and oxyhaemoglobin concentration in diabetic feet at pre-ulcerative sites (Yudovsky et al., 2011).

Choosing a suitable imaging technique for the study of a specific organ or a pathology is of importance. While the question that has to be considered depends on the differences among the optical properties of tissues, interpretation of the measurements output and its relation to physiological and pathological processes is also of challenge (Eriksson et al., 2014). Furthermore, imaging rate, field of view and tissue penetration depth, cost, availability and ease-of-use of the device have also to be considered when choosing a technique to monitor microvascular perfusion (Allen and Howell, 2014).

2.5 Impact of aging on microcirculation

Skin cutaneous microcirculation can be considered as an accessible and a representative vascular bed to examine the mechanisms of microcirculatory function and dysfunction (Hellmann et al., 2015; Holowatz et al., 2008; Abularrage et al., 2005). Accordingly, skin is used as a model for age-related changes in the microcirculation (Bentov and Reed, 2015). It is well accepted that blood flow in skin is remarkably

reduced with age (Tsuchida, 1993). This probably reflects the modifications in the microcirculation. Aging is associated with a reduction in microvascular activity, increased vascular stiffness, decreased vascular density and impaired vascular organization (see Tobin, 2017, for review). This section highlights these age-related implications in microvascular function and structure.

2.5.1 Impaired microvascular function

It has been reported that, with age, the responses of the microvasculature to a variety of stimuli are decreased. For example, cutaneous vasodilation in response to heat decreases with age (Rooke and Brengelmann, 1994; Richardson, 1989; Weiss et al., 1992; Evans et al., 1993) and the maximum skin blood flow also decreases exponentially with age (Martin et al., 1995). In addition to changes in the structure of peripheral nervous system (Cowen, 1993) and vascular smooth muscle cells (Marín, 1995), the alteration of the cutaneous reactivity with age is thought to be the result of endothelial dysfunction (Gates et al., 2009). It is therefore assumed that aging is associated with endothelial dysfunction (Matz and Andriantsitohaina, 2003). This endothelial dysfunction is secondary to several mechanisms. With age, there is an imbalance between endothelial factors relaxation and contraction (Matz et al., 2000). Aging is also associated with impairment of nitric oxide (NO) and prostanoid dilator pathways (Singh et al., 2002; Holowatz et al., 2005; Kellogg et al., 2005). Thus, several hypotheses have been advanced to explain age-related endothelial dysfunction. On one hand, the production of NO may decrease with age due to altered expression and/or activity of endothelial nitric oxide synthase (NOS) (Feher et al., 2014; Cernadas et al., 1998). On the other hand, the bioavailability of NO decreases with age because NO has an anti-oxidant role: it is trapped by oxygen free radicals, the output increases due to mitochondrial dysfunction related to age (Bratz and Kanagy, 2004; Brandes et al., 2005). Moreover, it has been reported that by administering an antioxidant (vitamin C), vasodilation to acetylcholine increases in subjects aged over 60 years (Taddei et al., 2001). It has also been shown that the diffusion of NO in the endothelium into the vascular smooth muscle is decreased with age due to the increase in the thickness of the vascular wall, especially in the intima and media (Marín, 1995). Moreover, it has been reported that aging may involve alterations in nitric oxide, prostanoid, endothelium derived hyperpolarizing factor(s) and endothelin-1 pathways (Gates et al., 2009).

Concerning prostaglandins: (i) the activity of cyclo-oxygenase (COX) decreases with age (Heymes et al., 2000); (ii) the balance between vasoconstrictor and vasodilators products of COX favors vasoconstrictor products with age (Matz et al., 2000; Holowatz et al., 2005). Furthermore, several studies have reported an attenuated vasodilator response of skin microcirculation to a variety of stimuli, with age (Hagisawa et al., 1991; Minson et al., 2002; Holowatz et al., 2003; James et al., 2006). This attenuation is

thought to be the result of endothelial dysfunction (Gates et al., 2009). Thus, Tikhonova *et al.* recently reported a higher increase of perfusion in young people compared to aged subjects after an occlusion removal (Tikhonova et al., 2013). Hagisawa *et al.* reported the same conclusion some years before (Hagisawa et al., 1991).

On the other hand, age-related changes play an important role in the pathogenesis of many diseases (Ajmani and Rifkind, 1998; Lüscher and Noll, 1996; Makrantonaki and Zouboulis, 2007; Tanaka et al., 2000). Previous studies in elderly subjects suggested impairments of microvascular reactivity upon aging. For example, Yvonne *et al.* (Yvonne-Tee et al., 2008) found that the occlusion duration for absolute maximal increase in hyperaemia perfusion is affected by age. Furthermore, Tikhonova *et al.* (Tikhonova et al., 2013) pointed out that, during post-occlusive reactive hyperaemia (the case of increasing blood flow after its temporary interruption, PORH), a reduction in the activity of microvascular bed to transient ischemia appears with aging.

2.5.2 Alteration of microvascular structure

With aging, a number of hypoxia- and metabolism-related changes occur (Harris and Rumbaut, 2001; Konstantinova et al., 2004; Ogrin et al., 2005). These changes are due to alterations in the microcirculation, consequently, leading to a reduction in the number and density of cutaneous blood vessels. Moreover, as mentioned by Tikhonova *et al.* (Tikhonova et al., 2013), the number of functioning capillaries diminishes with age, and phenomena as vascular rarefaction, appearance of zones of complete vascular obliteration, irregular caliber of microvessels (Ryan, 2004; Kelly et al., 1995; Noon et al., 1997), inhibition of the processes of angiogenesis (Sadoun and Reed, 2003) may appear. As pointed out by Gates *et al.* (Gates et al., 2009), capillary rarefaction may be due to vessel destruction, impaired angiogenesis, impaired vasculogenesis. Oxidant stress may also contribute to capillary rarefaction by inducing endothelial cell apoptosis and/or reducing the nitric oxide needed for vascular budding and stimulation of vascular endothelial growth factor. Aging is accompanied by suppression of the endothelial function and cellular metabolism by degeneration of the sensor and sympathetic innervation (Bari et al., 2005; Kenney and Munce, 2003). It has been pointed out that a reduction in microvascular density has a crucial role in age-related nephropathy (Kang et al., 2001), and in neurodegeneration (Brown and Thore, 2011). Furthermore, disorganization in skin branching geometry of the arterioles and capillaries is observed with age (Li et al., 2006b). It is assumed that decreased vascular density and increased vessel disorganization contribute to age-related deficits in diffusive transport capacity of the skin vasculature (Bentov and Reed, 2015).

Aging also leads to a degradation of a number of extracellular matrix proteins, including collagen and elastic fibers (El-Domyati et al., 2002; Gilchrest, 1989). Aging

is one of the most common factors that leads to stiffening of the arteries. A deposition of fats, cholesterol that is referred to as arteriosclerosis could lead to stiffening of the arteries both structurally and functionally, and thus may lead to vessel wall damage (Tomiyama and Yamashina, 2010). Furthermore, we have to note that skin thickness could vary with age (Waller and Maibach, 2005). Thus, the stratum corneum is generally accepted to maintain its thickness during aging. However, dermal, epidermal, and whole skin thickness changes are controversial. Ultrasound reveals the appearance of a subepidermal low echogenic band that thickens with age (due to changes in collagen structure), especially in environmentally exposed areas (Shuster et al., 1975). Some studies also indicate the presence of an echogenic band in the lower dermis which thins with increased age. However, the whole dermis appears to become more echogenic in elderly people (Waller and Maibach, 2005).

From a general point of view and with regard to scientific researches, it is worth discussing a contradictory bibliography finding mentioned in this section, related to dermis density. Reduced dermis density with age has been shown by several authors (Li et al., 2006b), while others have found the opposite (Shuster et al., 1975). This can be explained by differences in the sensitivity of the method chosen, differences in the capillary density of the examined area in the skin, variations in baseline vascular tone, or by a combination of all of these (Vionnet et al., 2014). For instance, LDI is more sensitive to the blood flow of deeper plexuses than other techniques such as capillaroscopy. Furthermore, skin sites tested, methodology, and increased sample size have to be considered when studying the thickness changes with age (Waller and Maibach, 2005).

Finally, it is worth mentioning that the effects of stress conditions such as trauma, surgery, and shock states on microvascular function and structure are exacerbated by aging. However, an improvement of microvascular response to stress is possible via a wide range of interventions, including lifestyle modifications, clinical practice and experimental approaches (see Bentov and Reed, 2015, for review).

3

Laser speckle contrast imaging: theory, instrumentation, and applications

In this chapter, LSCI theoretical background and the way to compute moving blood cells velocity and the perfusion from LSCI data are exposed. Furthermore, several measurement requirements are discussed, including those affecting blood flow estimation from LSCI data. Then, applications of LSCI and a trade-off with laser Doppler techniques are proposed. Finally, future trends of LSCI are presented.

Contents

3.1 Introduction

The introduction of optical techniques in the medical imaging domain has offered exciting possibilities to obtain information about the tissue, noninvasively (see e.g., Vo-Dinh, 2014). Over the past few decades, several techniques have been developed to monitor microvascular blood flow (Essex and Byrne, 1991; Briers, 2001; Humeau-Heurtier et al., 2013a). Several of these techniques are based on the random interference pattern – known as speckle pattern – generated from diffused backscattered light. Besides LDPI which is considered as one of the most well known techniques to monitor microvascular blood flow, LSCI has recently been commercialized. It is considered as an alternative technique to monitor blood flow in the microcirculation. LSCI has the advantage of being full-field, contactless, highly reproducible, leading to high temporal and spatial resolution images of the microvascular blood perfusion, requiring low-cost devices, and simple setup (Humeau-Heurtier et al., 2014a; Puissant et al., 2013;

Richards et al., 2013; Yang and Choi, 2012; Roustit et al., 2010). This technique exploits the fluctuations in the speckle pattern to provide information about blood flow in the superficial tissue. These fluctuations in speckle pattern are recorded with a camera and due to the exposure time of the camera, the intensity fluctuations cause blurring of the recorded images. To quantify the degree of blurring, the expression of the speckle contrast is computed. Moreover, when assumptions are made on moving scatterers velocity profile, LSCI is able to extract moving blood cells velocity values (Briers and Webster, 1996).

3.2 Theoretical background

3.2.1 What are speckles?

During the developments of the laser in the early 1960s, researchers observed a new phenomenon which thereafter is called speckle (Pecora, 1972). Speckles are produced by the coherence of laser light: when a laser source diffuses a light over a rough object, the photons of the laser light are backscattered by both moving and static scatterers. The backscattered light forms an interference pattern of bright and dark pixels – called speckles – on the detector. Movements within the illuminated object lead to temporal fluctuations in the interference pattern. The pattern is therefore *dynamic*. Alternatively, if no movements occur within the illuminated object, and the laser light is stable, the interference pattern does not fluctuate over time. *Static* is therefore used to describe the pattern. Figure 3.1 shows a typical speckle pattern.

Laser speckle is a random phenomenon and can only be described statistically. Therefore, a statistical analysis in the temporal domain (Stern, 1975), or in the spatial domain (Fercher and Briers, 1981), provides essential information about the motion of scattering particles.

3.2.2 Time-varying speckle

For a small motion of a solid object, the speckles remain correlated and move with the object. In contrast, speckles are decorrelated quickly for large motions, and therefore, the pattern changes completely. Decorrelation also arises when the light is scattered from a large number of individual moving scatterers such as particles in a fluid. This phenomenon, which is called as “time-varying speckle”, can be observed when biological samples are illuminated by a laser light (Briers, 1975). The time-varying speckle is related to the temporal fluctuations which are caused inside the illuminated sample. It has been assumed that the frequency spectrum of the fluctuations is dependent on the velocity and velocity distribution of the scatterers (Bonner and Nossal,

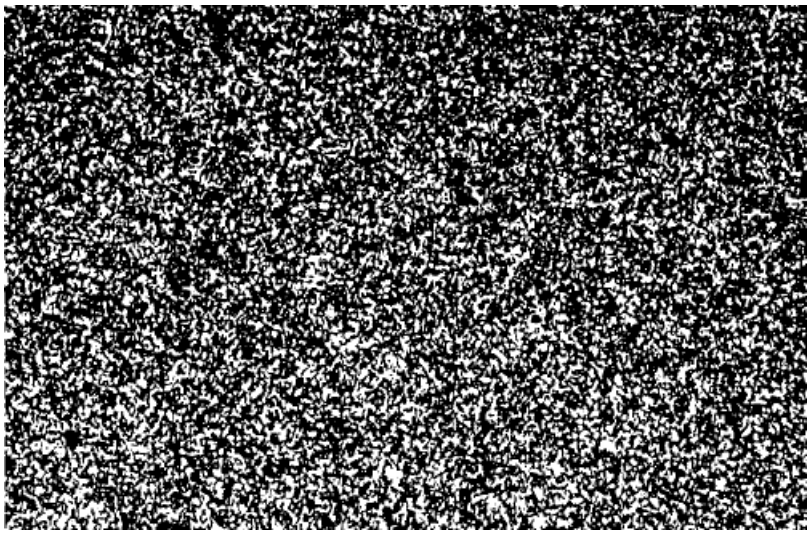

Figure 3.1 – Typical speckle pattern (from Briers, 2001).

1981). Information about the motion of the scatterers is therefore accessible from a study of temporal statistics of the speckle fluctuations. Nowadays, the applications of time-varying speckle techniques are numerous in the biomedical field for monitoring blood flow (Vo-Dinh, 2014).

3.2.3 What is speckle contrast?

When the speckle patterns are recorded using a detector, such as a CCD camera, and due to the movements of the scattering particles within the medium (such as the movements of red blood cells in the case of tissues), the speckle pattern changes over time. Dynamic speckled images are therefore obtained on the camera. The exposure time T of the camera (typically 1 to 10 ms) leads to a blurring of speckle patterns. To quantify the degree of blurring, the speckle contrast K is computed. The latter is defined as the ratio of the standard deviation σ to the mean intensity $\langle I \rangle$ (Briers and Webster, 1996):

$$K = \frac{\sigma}{\langle I \rangle} = \frac{\sqrt{\langle I^2 \rangle - \langle I \rangle^2}}{\langle I \rangle} \quad . \tag{3.1}$$

The standard deviation and mean of the pixels intensity in (3.1) are computed in a neighborhood N around the pixel P(x,y).

K values are between 0 and 1. If there is no or little motion to blur all the speckles, Goodman (Goodman, 1975) showed that assuming ideal conditions for producing a speckle pattern (i.e., perfectly diffusing surface, polarized light, and absence of noise),

the standard deviation and mean intensity will be same, and the speckle contrast is then equal to unity, which is the maximum value for the speckle contrast. Such types of speckle pattern are called "fully developed speckle". In contrast, a speckle contrast of 0 means that the scatterers are moving fast enough to blur all the speckles.

Yuan *et al.* (Yuan et al., 2005) found that the sensitivity of the measured changes in speckle contrast depends on the exposure time T. Furthermore, they reported that the sensitivity to relative changes in speckle contrast increases with longer exposure time, whereas the relative noise is also increased. However, they pointed out that at an exposure time greater than 2 ms, the sensitivity of the measured changes in the speckle contrast increases quickly, and then, remains near the same level for an increasing exposure time. As a result, they suggested $\sim$ 5 ms as an optimal exposure time for imaging stimulus-induced changes in cerebral blood flow in rodents (Yuan et al., 2005).

The speckle contrast K can be quantified either in the spatial domain (Dunn et al., 2001) or in the temporal domain (Li et al., 2006c). Each of these two methods will be covered in detail later in this chapter. Each of them has its advantages and disadvantages. In a few words, the temporal method has a better spatial resolution at the expense of temporal resolution, while the spatial method has a good temporal resolution, but lacks spatial resolution.

Speckle contrast values are considered as a marker of the level of motion in the specimen. However, those values are not directly proportional to speed or flow. The accurate quantitative relationship between speckle contrast and the underlying blood flow or speed is a complex function that is not completely understood for complex biological tissues (Duncan and Kirkpatrick, 2008a; Nadort et al., 2016). In their first work, Fercher and Briers (Fercher and Briers, 1981) presented a model that links speckle contrast to the speckle correlation time τ_c, and then to speed scattering particles. The objective of this model was to clarify the relation between time-integrated speckle and classical techniques based on dynamic light scattering such as laser Doppler (Briers, 2001). Therefore, this model has been widely used in biomedical applications to predict relative change in blood flow. The attempts are being continued for improving the interpretation of τ_c as a measure of speed scattering particles. Recently, Nadort *et al.* (Nadort et al., 2016) succeeded in presenting an independent quantitative measurement of τ_c and velocity of moving scatterers *in vitro* and *in vivo*. In this study, the efforts were made to demonstrate the feasibility of LSCI for quantitative mapping of blood flow velocities. Their model $1/\tau_c = \alpha_1 A(N) \times V$ takes into account the optical properties and experimental geometry of the examined area where α is the proportionality constant for single scattering and $A(N)$ scales for the average number of dynamic scattering events N (Nadort et al., 2016).

3.2.4 Determination of the moving scatterers velocity

From contrast K values, moving particles velocity values can be extracted provided assumptions are made on the velocity profile of the moving scatterers. This is due to the fact that the variance $\sigma_s^2(T)$ of the spatial intensity distribution in a time-averaged speckle pattern with an integration time T is linked to the autocovariance $C_t(\tau)$ of the temporal fluctuations in the intensity fluctuations of a single speckle (Fercher and Briers, 1981):

$$\sigma_s^2(T) = \frac{2}{T}\int_0^T \left(1 - \frac{\tau}{T}\right) C_t(\tau)\, d\tau \quad . \tag{3.2}$$

The autocovariance $C_t(\tau)$ of the temporal fluctuations in the intensity fluctuations of a single speckle is defined as:

$$C_t(\tau) = \langle [I(t) - \langle I\rangle_t][I(t+\tau) - \langle I\rangle_t]\rangle_t \quad , \tag{3.3}$$

where $\langle .....\rangle_t$ indicates a time-averaged quantity. We also have

$$g_2(\tau) = 1 + \frac{C_t(\tau)}{\langle I\rangle_t^2} \quad , \tag{3.4}$$

where $g_2(\tau)$ is the intensity temporal autocorrelation function. We can also write (Siegert relation)

$$g_2(\tau) = 1 + \beta|g_1(\tau)|^2 \quad , \tag{3.5}$$

where $g_1(\tau)$ is the electric field temporal autocorrelation function and β accounts for loss of correlation related to the ratio of the detector (or pixel) size to the speckle size and to polarization. From Eqs. 3.2, 3.4, and 3.5, and assuming ergodicity (Fercher and Briers, 1981) (we can in this case replace the time average by the ensemble average) we thus have

$$K^2 = \frac{2\beta}{T}\int_0^T (1 - \frac{\tau}{T})|g_1(\tau)|^2 d\tau \quad . \tag{3.6}$$

Integrating speckle contrast K over a short exposure time T and upon a small spatial area allows an estimate of the speckle correlation time τ_c. Assuming various flow distributions, different contrast equations have been proposed (Ramirez-San-Juan et al., 2008; Duncan and Kirkpatrick, 2008a). Although a Lorentzian profile is the most commonly used profile to determine the theoretical expression of contrast K (Briers and Webster, 1996; Fercher and Briers, 1981; Duncan and Kirkpatrick, 2008a; Duncan et al., 2008a; Ramirez-San-Juan et al., 2008), a Gaussian profile also has been the subject of research

(Parthasarathy et al., 2008; Nadort et al., 2013). If the moving scatterers are assumed to follow a Lorentzian distribution, we have (Duncan et al., 2008a)

$$g_1^L(\tau) = \exp(-\frac{|\tau|}{\tau_c}) \ , \tag{3.7}$$

where τ_c is the correlation time of intensity fluctuations. Inserting Eq. 3.7 in Eq. 3.6, the contrast K for a Lorentzian distribution can be written as

$$K^2_{Lorentzian} = \beta \left[\frac{1}{x} + \frac{1}{x^2} \left(\exp\left(-2x\right) - 1 \right) \right] \ , \tag{3.8}$$

where $x = T/\tau_c$.

Alternatively, for the Gaussian distribution, we have (Duncan and Kirkpatrick, 2008a)

$$g_1^G(\tau) = \exp(-\tau^2/\tau_c^2) \ . \tag{3.9}$$

Thus, using Eq. 3.9, for the electric field temporal autocorrelation function, we have (Duncan and Kirkpatrick, 2008a)

$$K^2_{Gaussian} = \frac{\tau_c \beta}{2T} \left[\sqrt{2\pi} erf\left(\frac{\sqrt{2}T}{\tau_c} \right) + \frac{\tau_c}{T} \left(\exp\left(-\frac{2T^2}{\tau_c^2} \right) - 1 \right) \right] \ . \tag{3.10}$$

The relationship between the correlation time τ_c and moving blood cells in the microcirculation is assumed to be inversely related (Briers and Webster, 1996). Therefore, from the experimental values of contrast K, velocity ν_c of moving blood cells can be calculated as (Fercher and Briers, 1981; Briers and Webster, 1996)

$$v_c = \frac{\lambda}{2\pi\tau_c} \ , \tag{3.11}$$

where λ is the laser wavelength.

3.2.5 Determination of perfusion through speckle contrast

If the moving scatterers are assumed to follow a Lorentzian distribution as in Eq. 3.8, and using Eq. 3.11, moving blood cells velocity can be computed. Moreover, in the laser speckle contrast imager used for the experimental acquisition (see below, Sec. 3.6), we have (from Perimed documentation)

$$Perfusion \sim \frac{1}{K} - 1 \ . \tag{3.12}$$

Thus, using Eq. 3.8, the perfusion can be written as

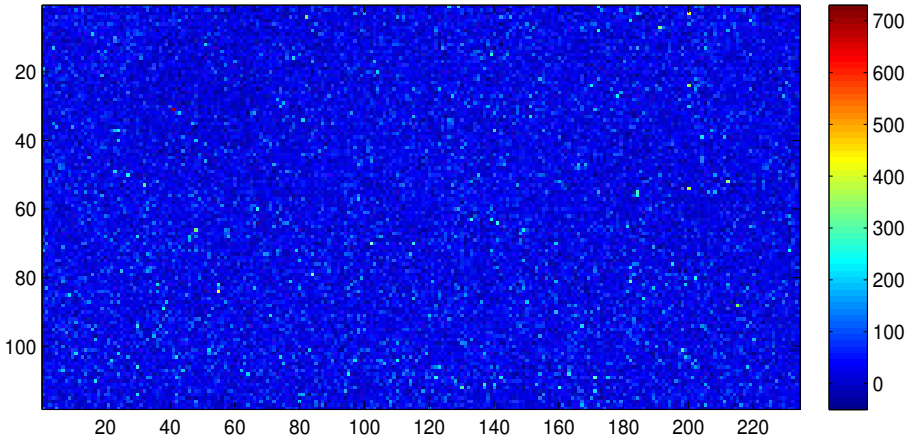

Figure 3.2 – Experimental perfusion image (118×234 pixels) of the forearm at rest in a healthy subject obtained with LSCI technique.

$$Perfusion \sim \left(\beta^{-1/2} \left[\frac{1}{x} + \frac{1}{x^2} \left(\exp\left(-2x\right) - 1 \right) \right]^{-1/2} \right) - 1 \ . \tag{3.13}$$

An example of a perfusion image is shown in Fig. 3.2.

3.3 Single-exposure speckle photography

Using the time-varying speckle technique, Fercher and Briers (Fercher and Briers, 1981) have noted that the speckle contrast reduces when photography is taken under laser illumination. This is the fundamental concept of single-exposure photography. The principle is the following: when a photography is taken with an exposure time that is of the same order as the correlation time of the intensity fluctuations, the speckle pattern is blurred to an extend that depends on the exposure time of the photodetector, and the velocity of flow. Therefore, the study of the temporal statistics of the speckle fluctuations reveals information about the motion of the scatterers. Later, this method was developed and used to monitor blood flow in the retina (Briers and Fercher, 1982).

Single-exposure speckle photography was limited by the digital processing techniques that were not sufficiently developed in the early of 1980s. In practice, it was difficult for the human eye to detect the contrast variation. Therefore, some methods of enhancements – a simple optical filtering such as a high-pass spatial filter – were used to improve the contrast maps. This process worked quite well to convert the contrast variation to intensity variation. Although single-exposure speckle photography has succeeded in biomedical applications, it suffered from the requirement of a two stage

process: 1) the use of optical filter for enhancing the results; 2) the need for a large number of photos for detecting small signal.

3.4 Laser speckle contrast imaging

With the accelerated development of digital processing tools in the last decades, the road to the real-time operation became easier. Hence, in single-exposure speckle imaging, the photography stage to enhance the photographs was removed by using digital processing tools (Fercher et al., 1986). However, single-exposure speckle imaging still required to take and process a photograph, that made it a non real-time technique. Later, a digital version of single-exposure speckle photography was introduced (Webster and Briers, 1994). This method removed the photographic stage. Local speckle contrast was computed, converted to a false-color map of contrast, and flow speed was then estimated from local speckle contrast (Briers and Webster, 1995). The new digital technique was called laser speckle contrast analysis (LASCA) (Briers and Webster, 1996). Nowadays, the more general term, that is used for this technique, is laser speckle contrast imaging (LSCI) or even laser speckle imaging (LSI).

A significant limitation of the first LASCA instruments was the lack of processing of image stream instantaneously. Images were recorded on film, and processed later (Fercher and Briers, 1981), which resulted in low temporal resolution and large doubt in the speckle contrast values. The introduction of CCD camera and modern computers in the 1990s, enabled acquisition with excellent temporal and spatial resolution images (Dunn et al., 2001). The processing of speckle images was improved remarkably (Bandyopadhyay et al., 2005; Parthasarathy et al., 2008; Yuan, 2008; Li et al., 2006d; Tom et al., 2008). Imaging of blood flow in superficial tissues became possible and easier (Dunn et al., 2003; Luo et al., 2009).

In LSCI, as mentioned above, the temporal and spatial statistics of the speckle pattern provide information about the motion of the scattering particles. The motion can be estimated by measuring and analyzing either the spatial speckle contrast (Fercher and Briers, 1981; Briers and Webster, 1995; Parthasarathy et al., 2008) or the temporal speckle contrast (Cheng et al., 2003; Forrester et al., 2004; Li et al., 2006c). It is important to note that the spatial statistics are used everywhere in this PhD manuscript to compute the speckle contrast K. Therefore, in what follows, several measurement requirements, those having an impact on the calculation of the speckle contrast K from the spatial statistics, are presented. These requirements include spatial sampling of the speckle pattern, velocity distribution assumptions, speckle size, and scattering from static tissues. Then, a comparison view between the temporal and spatial statistics is shown.

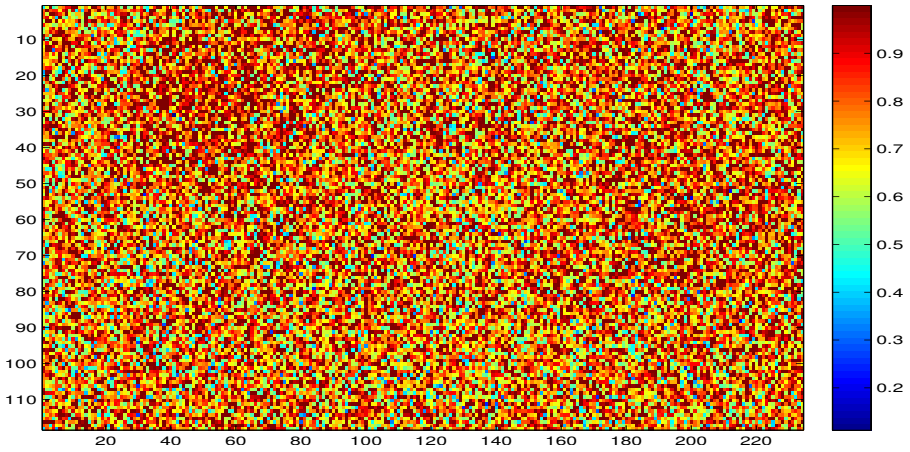

Figure 3.3 – Contrast image (118×234 pixels) of the forearm skin at rest in a healthy subject obtained with LSCI technique.

3.4.1 Measurement requirements

Effect of window size

In the spatial sampling of the speckle pattern, it is necessary to take into account the number of pixels which are used to determine the speckle contrast. To compute the speckle contrast K, a spatial square window of N_{pixels} is used in which the standard deviation σ and the mean intensity $\langle I \rangle$ are computed. The size of the window over which the speckle contrast is computed is critical (Briers, 2007): the statistics are compromise with too few pixels; by opposition, the spatial resolution is sacrificed with too many pixels. It has been reported that a square window of size 5×5 pixels or 7×7 pixels would be adequate (Briers, 2007), but all this be conditional on other determinants as the camera resolution, speckle size, and required contrast resolution. To obtain $2D$ contrast images (see an example of a contrast image in Fig. 3.3) reflecting the local motion due to blood flow, a sliding window is used to move along the raw speckle image.

Effect of velocity distribution

In Eq. 3.2, $C_t(\tau)$ depends, among others, on the velocity distribution of the scattering particles (Fercher and Briers, 1981; Goodman, 1985). Figure 3.4 shows the theoretical relationship between speckle contrast K and the ratio of the speckle correlation time τ_c to camera exposure time T, when a Lorentzian profile and when a Gaussian profile are assumed for velocity of moving scattering particles. From this figure we can observe that the choice of velocity profile has a major effect on the relation between the speckle contrast K and velocity values (Ramirez-San-Juan et al., 2008; Briers et al., 2013). Between unordered motion (i.e., Lorentzian velocity profile) and ordered motion

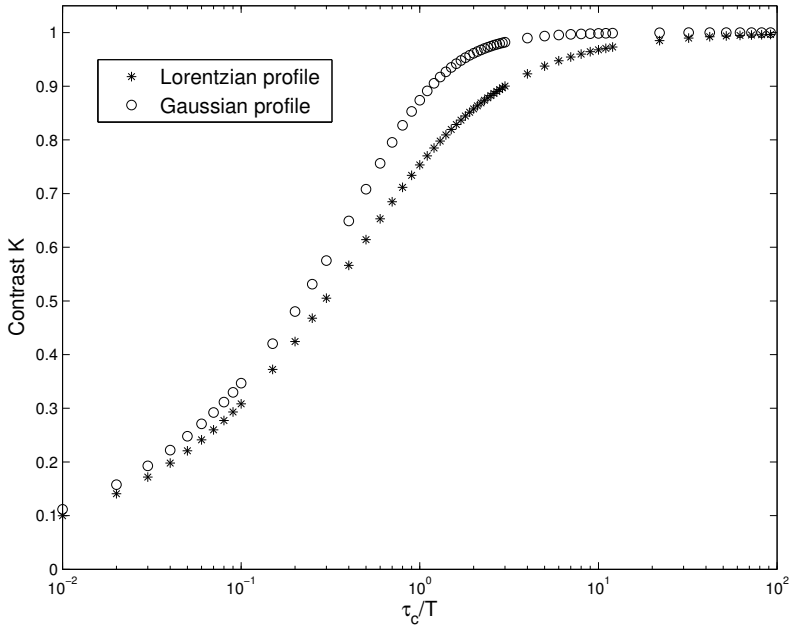

Figure 3.4 – Theoretical relationship between speckle contrast K and the ratio of the speckle correlation time τ_c to camera exposure time T, when a Gaussian profile, and when a Lorentzian profile are assumed for moving scattering. β is equal to 1 for each curve.

(i.e., Gaussian velocity profile) Duncan *et al.* (Duncan et al., 2008a) proposed a Voigt velocity profile as a compromise. The latter is the result of a convolution of Lorentzian and Gaussian profiles. However, the latter profile can not be used for single-exposure LSCI, because it has a single value of τ_c/T. Accordingly, by using single-exposure LSCI and regarding to Fig. 3.4, we can not determine which velocity profile is the correct one. As the correlation time τ_c is thought to be inversely proportional to the local velocity of the scatterers (Briers and Webster, 1996), changing the shape of the velocity distribution affects the shape of the curve representing the contrast K as a function of τ_c/T. Therefore, the question remains as to whether the actual velocity profile can be determined by other methods and then used to quantify LSCI measurements (Briers et al., 2013).

Effect of speckle size

The spatial sampling of the speckle pattern is closely related to several experimental parameters. In addition to window size, and speckle intensity distribution, the ratio of speckle size to the camera pixel size must be considered (Kirkpatrick et al., 2008). When a camera is used to image the speckle pattern, and in order to acquire good statistics, the

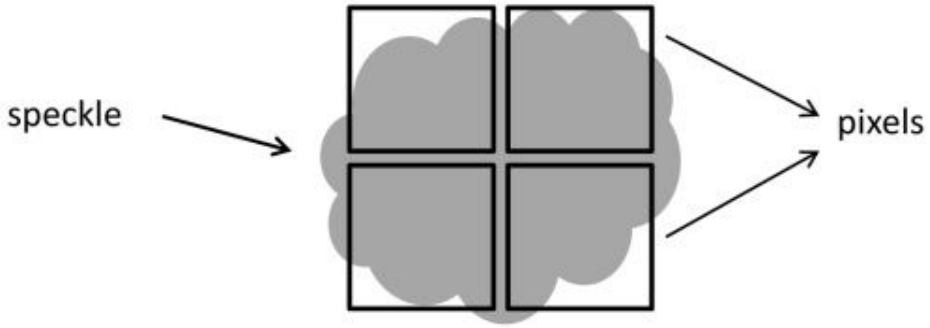

Figure 3.5 – Spatial sampling of a speckle pattern on a CCD camera. Several pixels are employed for sampling one speckle (from Ramirez-San-Juan et al., 2013).

speckle size should be carefully controlled. In LSCI systems the size of the speckles is determined by the wavelength of the laser (λ), the f-number of the lens system (F), and the imaging system magnification (M) as (Thompson et al., 2011)

$$d_{min} \approx 1.2(1+M)\lambda F \quad , \tag{3.14}$$

where d_{min} is the minimum speckle diameter in the same unit as the one used to express the wavelength.

Figure 3.5 shows the spatial sampling of one speckle, where several pixels are used to sample one speckle. Thus, by controlling the F number of the system, the optimal speckle size can be determined (see below). However, this reduces the ability to control the amount of light reaching the camera. This problem was solved by using neutral density filters to control the amount of light falling on the camera (Briers et al., 1999).

In the literature, it was frequently mentioned that the speckle size should match the pixel size, but Kirkpatrick *et al.* (Kirkpatrick et al., 2008) have demonstrated that the criterion of matching speckle/pixel size in LSCI leads to reduction in the speckle contrast, and as a result, decreases the variation in the laser speckle contrast image. Furthermore, they found that in order to maximize the contrast of the speckle patterns, the minimum speckle size must be two times larger than the pixel size (Kirkpatrick et al., 2008). This finding was supported using computer simulation of time-integrated dynamic speckle (Thompson et al., 2011).

In the past few years, Ramirez *et al.* (Ramirez-San-Juan et al., 2013) using experimental data, studied the effect of speckle-pixel size ratio on the dynamic speckle contrast value. They found that the speckle contrast value depends on the spatial sampling of the speckle pattern for both temporal and spatial speckle contrast analysis: the more the

ratio of pixel to speckle size, the higher the value of the speckle contrast, even at values beyond the Nyquist sampling criterion of $N_s = 2$, where N_s is the ratio of speckle area to pixel area which is employed in the operation of spatial sampling of speckle pattern. However, they concluded that during the study of the relative changes in blood flow, speckle flow index is minimally affected by both N_s values and flow speed (Ramirez-San-Juan et al., 2013).

All the works mentioned above in this section (Ramirez-San-Juan et al., 2013; Thompson et al., 2011; Kirkpatrick et al., 2008) agree with definition that the smallest speckle size is at least twice the size of a pixel. However, several recent papers (Basak et al., 2012; Valdes et al., 2014) continue to use 1 pixel/speckle which could be an unwise decision (Vaz et al., 2016). The validated results show that the contrast K is directly proportional to the number of pixels/speckle (up to 4 pixels/speckle). While each pixel in a CCD camera has a finite size, using an excessive number of pixels to represent the speckle leads to a reduction in the spatial resolution. This is because, since each speckle is the source of information, there are fewer speckles in the same area.

Other works reported an opposite conclusion. For examples, Qui *et al.* (Qiu et al., 2013) suggested that a speckle size under the pixel size can improve the SNR and the spatial resolution. They demonstrated that the local speckle contrast, even at speckle size much smaller than one pixel size, can be corrected through dividing the original speckle contrast by the static speckle contrast (Qiu et al., 2013). This process, when the speckle size is smaller than the pixel size, is like a general two dimensional low-pass filter. This filter produces an intensity increase in darker zones and an intensity decrease in brighter zones. The intensity mean is maintained but its standard deviation is reduced, leading to a reduction in the mean contrast and, more important, to the homogenization of the contrast values. This homogenization causes a reduction in the contrast standard deviation (σ) which results in the increase of the SNR in the proposed metric (Vaz et al., 2016).

Finally, it has been proposed that the spatial sampling of the speckle pattern has to be considered in two dimensional mapping, and at least two pixels should be sampled in each dimension (see Fig. 4 from Vaz et al., 2016).

Effect of static scattering

The expression of speckle contrast K is used to determine the velocity of the moving blood cells in the microcirculation. Nevertheless, Eqs. (3.8) and (3.10) do not take into account the presence of static scatterers (such as bones, skin, and skull). It has been reported that if the static scatterers effect is not considered, then it results in an underestimation of the spatial and temporal variations in the sample dynamics (Li et al., 2006a;

Parthasarathy et al., 2008). Moreover, some authors mentioned that the computation of blood flow velocity from LSCI data leads to erroneous values when the presence of static scatterers is not taken into account (Zakharov et al., 2006). In presence of static scatterers, the detected light is composed of photons scattered by dynamic and static components:

$$E(t) = E_d(t) + E_s \ , \tag{3.15}$$

where $E_d(t)$ is the light electrical field scattered by dynamic components and E_s the light electrical field scattered by static components. The new intensity autocorrelation function can be written as:

$$g_2(\tau) = 1 + \beta \left[(1-\rho)^2 \mid g_{1d}(\tau) \mid^2 + 2\rho(1-\rho) \mid g_{1d}(\tau) \mid + \rho^2 \right] \ , \tag{3.16}$$

where $g_{1d}(\tau)$ corresponds to the field autocorrelation function and $\rho = I_f/(I_f + I_s)$ is the fraction of total light that is dynamically scattered, with I_f the time-averaged intensity of the fluctuating dynamically scattered light, and I_s the intensity of the statically scattered light (Nadort et al., 2013).

The application of the Siegert relation, Eq. 3.5, to the intensity autocorrelation function yields to the modified field autocorrelation function (Zakharov et al., 2009).

$$g_{1m} = (1-\rho) \mid g_{1d}(\tau) \mid + \rho \ . \tag{3.17}$$

Only a few authors studied the effect of static scatterers on the estimation of moving blood cells velocity from the expression of speckle contrast K (see Boas and Dunn, 2010). In what follows, we present some of the most important studies to determine the expression of speckle contrast K when the effect of static scatterers is taken into account.

Expressions of speckle contrast K for a Lorentzian profile In the literature, a Lorentzian profile is the most commonly used profile to determine the theoretical expression for the speckle contrast K. As mentioned above, when a Lorentzian velocity profile is assumed for moving scatterers, and when the effect of static scatterers is not taken into account, the theoretical expression for the speckle contrast K is the one mentioned in Eq. (3.8). A few studies proposed a theoretical expression for the speckle contrast K in the presence of static scatterers. Thus, Parthasarathy *et al.* (Parthasarathy et al., 2008) suggested the following equation for the spatial contrast:

$$K^2 = \Bigg[\beta\rho^2 \frac{\exp(-2x) - 1 + 2x}{2x^2} + 4\beta\rho\,(1-\rho)\,\frac{\exp(-x) - 1 + x}{x^2} + v_{ne} + v_{noise}\Bigg] \quad , \tag{3.18}$$

where $x = T/\tau_c$, T is the integration time of the camera, τ_c is the correlation time of intensity fluctuations, and $\rho = I_f/(I_f + I_s)$ is the fraction of total light that is dynamically scattered with I_f the time-averaged intensity of the fluctuating dynamically scattered light, and I_s the intensity of the statically scattered light. Moreover, β is a normalization factor to account for speckle averaging effects. Furthermore, v_{ne} is the constant variance due to nonergodic light, and v_{noise} is the constant variance due to experimental noise (Parthasarathy et al., 2008).

Zakharov *et al.* (Zakharov et al., 2009) introduced another theoretical expression that takes into account the effect of static scatterers in the case of a Lorentzian velocity profile for the moving scatterers. The fraction of static scatterers to the total intensity is mentioned as ρ (as above). The expression of contrast is in this case written as

$$K^2 = \frac{2\beta}{T}\int_0^T \left[(1-\rho) \mid g_{1d}(\tau) \mid +\rho\right]^2 (1 - \tau/T)\, d\tau \quad , \tag{3.19}$$

where β is the coherence factor of the detection optics, and $g_{1d}(\tau)$ is the correlation function of the pure dynamic part.

Boas *et al.* (Boas and Dunn, 2010) proposed another formulation for the expression of the speckle contrast K that takes into account the effect of static scatterers when a Lorentzian velocity profile is assumed for the moving scatterers. They suggested the following expression:

$$K^2 = \beta\Bigg[\rho^2 \frac{\exp(-2x) - 1 + 2x}{2x^2} + 4\rho(1-\rho)\frac{\exp(-x) - 1 + x}{x^2} + (1-\rho)^2\Bigg] + C_{noise} \quad , \tag{3.20}$$

where $x = T/\tau_c$, $\rho = I_f/(I_f + I_s)$ with I_f the time-averaged intensity of the fluctuating dynamically scattered light, I_s the intensity of the statically scattered light and C_{noise} a measurement noise such as shot noise or camera readout noise (Boas and Dunn, 2010).

Expressions of speckle contrast K for a Gaussian profile A Gaussian profile has also been proposed by other authors to determine the speckle contrast K in the presence of dynamic and static scatterers. Thus, Parthasarathy *et al.* (Parthasarathy et al., 2010) suggested the following equation for the spatial contrast:

$$\begin{aligned} K^2 = & \Bigg[\beta\rho^2 \frac{\exp(-2x^2) - 1 + \sqrt{2\pi}x\text{erf}(\sqrt{2}x)}{2x^2} + \\ & 2\beta\rho(1-\rho)\frac{\exp(-x^2) - 1 + \sqrt{\pi}x\text{erf}(x)}{x^2} + \\ & v_{ne} + v_{noise} \Bigg] \ , \end{aligned} \tag{3.21}$$

where $x = T/\tau_c$, T is the camera exposure time, τ_c is the correlation time and $\rho = I_f/(I_f + I_s)$ is the fraction of total light that is dynamically scattered. Moreover, β is a normalization factor to account for speckle averaging effects, v_{noise} is the constant variance due to experimental noise and v_{ne} is the constant variance due to nonergodic light. erf is the Gaussian error function.

Nadort *et al.* (Nadort et al., 2013) presented another integrated quantitative measurement model to compute the speckle contrast K in the presence of static scatterers, when a Gaussian velocity profile is assumed for the moving scatterers

$$\begin{aligned} K^2 = & \beta \Bigg[\rho^2 \frac{\exp\left(-2x^2\right) - 1 + \sqrt{2\pi}x\text{erf}\left(\sqrt{2}x\right)}{2\left(x\right)^2} + \\ & 2\rho\left(1-\rho\right)\frac{\exp\left(-x^2\right) - 1 + \sqrt{\pi}x\text{erf}\left(x\right)}{\left(x\right)^2} + \\ & \left(1-\rho\right)^2 \Bigg] + C_{noise} \ , \end{aligned} \tag{3.22}$$

where $x = T/\tau_c$, T is the camera exposure time, τ_c is the correlation time and $\rho = I_f/(I_f + I_s)$ is the fraction of total light that is dynamically scattered, and C_{noise} an added noise term for measurement noise.

Ramirez *et al.* (Ramirez-San-Juan et al., 2014a) proposed another formulation to compute the speckle contrast K that takes into account the effect of static scatterers by assuming a Gaussian velocity profile for the moving scatterers. They suggested

$$K^2 = \alpha \left[\sqrt{\frac{1}{M}} \text{erf}\left(\sqrt{\pi M}\right) - \left(\frac{1}{\pi M}\right)\left(1 - \exp(-\pi M)\right) \right] \times \left[\rho^2 \frac{\exp(-2x) - 1 + 2x}{2x^2} + 4\rho\left(1-\rho\right)\frac{\exp(-x) - 1 + x}{x^2} + \left(1-\rho\right)^2 \right] + K_n \ , \tag{3.23}$$

where $M = A_D/A_C$, A_D is the sensitive area of the photodetector, A_C is the correlation area of the intensity (effectively, the speckle size) on the detector, α is a normalization parameter that accounts for effects (e.g., polarization) that reduce speckle contrast and that differ from spatial sampling of the speckle pattern, $x = T/\tau_c$, T is the camera exposure time, τ_c is the correlation time and $\rho = I_f/(I_f + I_s)$ is the fraction of total light that is dynamically scattered. Moreover, β is a correction factor to account for the speckle averaging effects, and K_n is a noise term.

These expressions will be studied more deeply later in this PhD manuscript.

3.4.2 Temporal versus spatial speckle contrast

The temporal speckle contrast method is based on the choice of a local contrast neighborhood only in the temporal domain (Li et al., 2006c). This means that the temporal speckle contrast K is obtained from the ratio of temporal standard deviation σ to the mean intensity. This method achieves a higher spatial resolution at the expense of temporal resolution. Furthermore, it has been shown that the temporal contrast K correlates well with the true speed, when estimated from a stream of 15 or more consecutive pixels in the time domain (Cheng et al., 2003). In contrast, the spatial statistics lead to higher temporal resolution at the expense of spatial resolution. This is due to the spatial speckle contrast computation that needs a large window of pixels in the calculations, and therefore, the signal-to-noise ratio (SNR) decreases consequently. A minimum of 25 pixels (5×5 pixels) are needed to quantify blood flow speed from the spatial speckle contrast (Duncan et al., 2008b). Therefore, this makes spatial speckle contrast more expensive due to the need for more computational time, and hence, may prevent real-time visualization of blood flow. Alternatively, temporal speckle contrast needs less computational time compared to spatial speckle contrast, which makes it less expensive and allows real-time visualization of blood flow (Le et al., 2007). Tom *et al.* (Tom et al., 2008) presented an algorithm that enables the image processing (calculations of speckle contrast and blood flow changes) at a time rate that exceeds the time rates of images

acquisition.

In spite of the utility of spatial speckle contrast to provide high temporal resolution, many hemodynamic patterns, including those examined in functional stimulation, and disease models such as stroke, tend to be slow in their dynamic flow ($\sim$ seconds). Thus, using temporal speckle contrast to quantify the dynamic flow will provide a sufficient temporal resolution. By opposition, for rapid dynamic flow patterns such as heartbeat, temporal speckle contrast may not be sufficient (Senarathna et al., 2013).

It is worth mentioning that the spatial resolution is of importance when the choice lies between spatial and temporal statistics. In fact, the difference between spatial and temporal statistics appears when static scatterers are taken into account. Static scatterers produce an additive offset to the spatial speckle contrast (Zakharov et al., 2009). In contrast, static scatterers do not produce an additive offset in the temporal speckle contrast (Ramirez-San-Juan et al., 2014b), but instead scale the speckle contrast by a factor related to the relative contribution of statically and dynamically scattered photons. While this confounds estimates of the absolute speckle contrast, the scale factor generally cancels when estimating relative changes in speckle contrast (Boas and Dunn, 2010).

In addition to these two methods of quantifying speckle contrast (temporal and spatial methods), one can use a spatiotemporal method to quantify the speckle contrast (Dunn et al., 2001; Duncan and Kirkpatrick, 2008b; Rege et al., 2012b; Le et al., 2007). A spatiotemporal method uses neighborhoods extending in both the spatial and temporal domains. Thus, local contrast in a spatial neighborhood is first calculated. The calculated contrast values over a temporal image stream are then averaged. This method, is a compromise between the spatial and temporal resolution.

Finally, there are several interesting reviews on different speckle contrast techniques, and the major advances in speckle contrast methods, including those leading towards a better efficiency of LSCI (Vaz et al., 2016; Briers, 2001, 2007; Draijer et al., 2009; Boas and Dunn, 2010; Basak et al., 2012; Briers et al., 2013).

3.5 Multi-exposure speckle imaging

Some recent progress have been made to improve the theory and instrumentation of LSCI (Zölei-Szénási et al., 2015; Sujatha and Banerjee, 2015; Miao et al., 2015; Lal et al., 2013; Kirkpatrick and Khaksariand, 2015; Kirby et al., 2015; Son et al., 2013; Liu et al., 2008; Yuan et al., 2005; Kirkpatrick et al., 2008). However, validation studies of speckle flowmetry thus far have failed to present an optimal choice of single-exposure LSCI duration to accurately map blood flow observable *in vivo* (Kazmi et al., 2013).

Furthermore, the estimation of flow dynamics from single-exposure LSCI is sensitive to a number of nonflow related parameters, such as duration of exposure time and the effect of static scatterers. These parameters, and others, have an impact on the ability to quantify accurately the baseline of flow dynamic (Ayata et al., 2004; Duncan and Kirkpatrick, 2008a).

As mentioned above, the speckle contrast values are strongly related to the exposure time T of the camera, and to flow (or speed). At long exposure times, the moving scatterers have sufficient time to blur all the speckles and therefore, speckle contrast values are close to zero. Alternatively, at very short exposure times, the speckle will be frozen and contrast values will be close to one. For instance, areas of low flow such as the small vessels generate speckle fluctuations that are slow compared to exposure time. Therefore, these small vessels will not appear in the speckle contrast image because no considerable blurring occurred in the speckle pattern. As exposure time increases, those small vessels will appear in the speckle contrast image. Therefore, there is a close relationship between the exposure time and flow or speed. As a result, an optimal detection of different flow rates can be achieved by selecting properly the exposure time (Yuan et al., 2005) to extract more accurate values of the speckle correlation times τ_c.

Multi-exposure speckle imaging (MESI) is an extension of LSCI. It uses an improved mathematical model and instrumentation to extract more precisely the flow related to contributions. In other words, MESI is thought to be able to improve the quantitative accuracy of flow dynamic. This is done by enabling better separation of related static scatterers contribution from flow dynamic. Briefly, this technique takes advantage of the dependence of the speckle contrast on camera exposure time T and addresses some important limitations of LSCI: 1) LSCI can produce good measures of relative flow but cannot measure baseline flows. Lack of baseline measures leads to difficult calibration (Strong et al., 2005); 2) the inability of traditional speckle models to predict the light reflected from the static tissue element such as intact or thinned skull (Parthasarathy et al., 2010).

Parthasarathy *et al.* (Parthasarathy et al., 2008) were the first to introduce MESI to improve the measuring accuracy of flow dynamics. They presented their new speckle imaging instrument and a new speckle expression that could overcome the limitations mentioned above. In this instrument, speckle images are acquired at different exposure durations (e.g., from 50μs to 80 ms (Parthasarathy et al., 2008)). They use the multi-exposure data (e.g., 15 different exposure durations (Parthasarathy et al., 2010)) to quantify correlation time τ_c of speckles more accurately than the traditional LSCI techniques. It is found that the flow measures computed using MESI are more accurate than traditional LSCI (Kazmi et al., 2013).

In addition to achieving varying exposure times, maintaining a constant intensity over a wide range of exposures, and ensuring that the noise variance is constant, are also of importance to obtain the correlation time τ_c (Parthasarathy et al., 2008). Therefore, to validate these considerations and in order to obtain speckle images at multiple exposure durations, Yuan *et al.* (Yuan et al., 2005) fixed the camera exposure time (such as 20 ms). Then, the effective exposure time has been varied by pulsing the laser diode in synchrony with the camera.

Thompson and Andrews (Thompson and Andrews, 2010) demonstrated that the problem of velocity distribution might be solved by using multiple exposures with different integration times. They showed that multiple-exposure laser speckle methods produce the same spectral information as laser Doppler methods when applied to targets with embedded moving scatterers. Furthermore, Kazmi *et al.* (Kazmi et al., 2015b), through *in vitro* microfluidic and *in vivo* neurovascular imaging experiments, provided evidence that the correlation times estimated by MESI agreed well with those obtained from direct temporal autocorrelation measurements, and provide a more accurate estimation of *both* blood flow and perfusion.

The MESI approach has been introduced to improve the quantitative accuracy of flow dynamics at the expense of acquisition and processing time. The additional time necessary for acquiring different exposure time series is the main drawback of MESI compared to traditional single-exposure speckle imaging. To overcome this drawback, many studies have attempted to optimize the choice of camera exposures used in MESI (see Kazmi et al., 2014; Schrandt et al., 2015). Recently, Dragojević et al. (Dragojević et al., 2015) presented a new MESI approach, known as single-shot acquisition MESI (sMESI) based on state-of-the-art high-speed complementary metaloxide-semiconductor (CMOS) single-photon avalanche diode (SPAD) array. This method takes advantage of the noise-free readout and the high-sensitivity of CMOS SPAD to compute the whole set of multi-exposure images from a single acquisition at shortest exposure time, and achieve real-time speckle contrast measurement with high temporal resolution and accuracy. sMESI is capable of acquiring thousands of frames rapidly with negligible dead time, and with postprocessing of the data, to simulate multi-exposure data. In phantom and *in vivo*, they reported that the sMESI can provide equivalent measures to standard MESI in a significantly shorter time.

3.6 Instrumentation

LSCI has become widely adopted in the biomedical field due to the simplicity of the instrumentation required to monitor blood flow (Richards et al., 2013). LSCI instru-

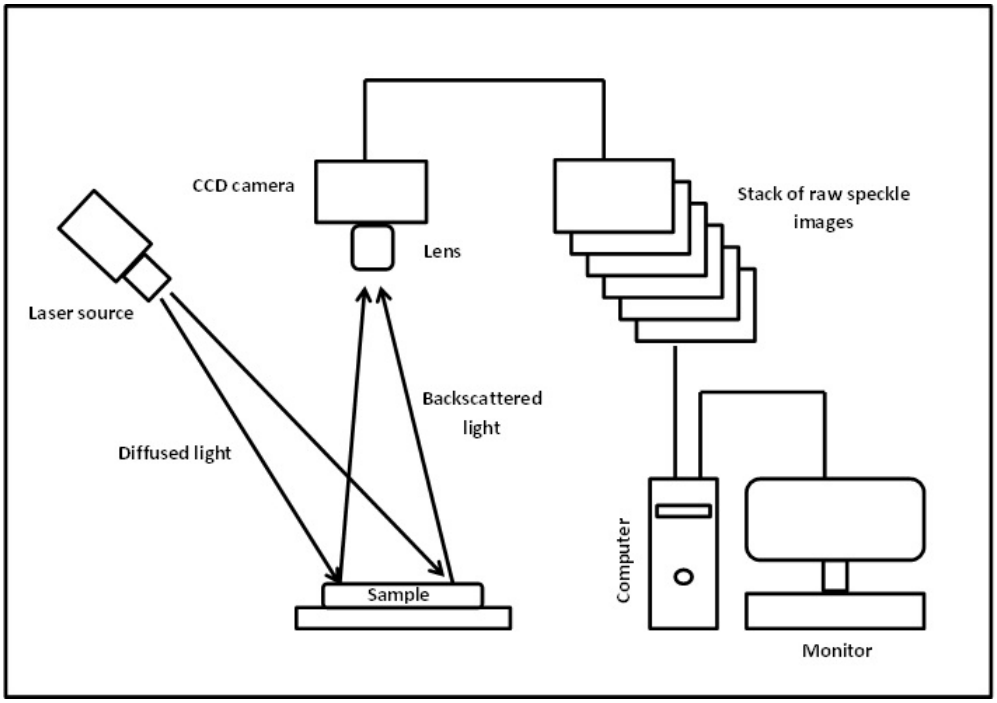

Figure 3.6 – Schematic diagram of LSCI setup.

ments consist of a laser source for illuminating the area of interest such as the tissues, a camera for sensing the backscattered light, and a lens to collect the light onto the camera sensor (see Senarathna et al., 2013). A schematic diagram of LSCI setup is shown in Fig. 3.6. The laser beam is extended and controlled to illuminate the area of interest, which may vary from a few millimeters to several centimeters, depending on the setting conditions. Laser light is typically in the red to close to the infrared region to reduce the impacts generated from hemoglobin absorption. In LSCI setup, an inexpensive standard CCD camera can be used to obtain excellent images of blood flow (Dunn et al., 2001). In addition, recent papers have demonstrated that LSCI can provide high quality blood perfusion maps even with simple imagers such as consumer-grade color cameras (Yang and Choi, 2012), webcams (Richards et al., 2013), and camera phones (Jakovels et al., 2014; Ragol et al., 2015).

An important advantage of LSCI is the ability to monitor microvascular blood flow continuously under different physiological conditions. Figure 3.7 illustrates an example of relative blood flow changes of microcirculation computed from LSCI data, acquired on the forearm skin of a healthy subject: at rest, during vascular occlusion, and during post-occlusive reactive hyperaemia. On the other hand, it has been reported that LSCI can be integrated simultaneously with other imaging modalities (Madsen, 2013; Jones

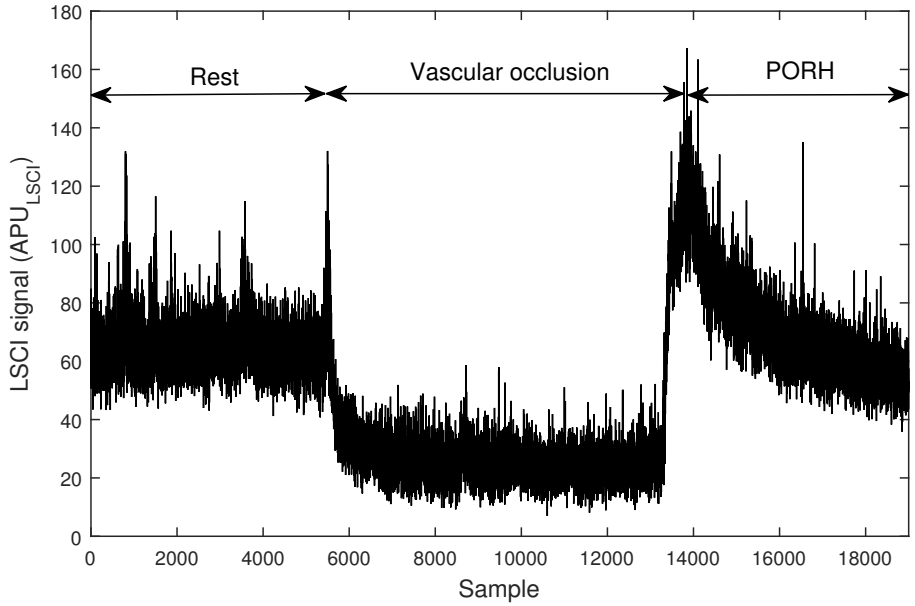

Figure 3.7 – Relative blood flow time course computed from LSCI data during three physiological conditions: rest, vascular occlusion, and PORH. LSCI signal computed from a region of interest of 7×7 pixels.

et al., 2004; Obrenovitch et al., 2009; Nadort et al., 2016).

Both internal and external conditions (e.g., the heavily scattering nature of skin tissue, air movement, among others) limit the spatial resolution of LSCI to the millimeter scale (Senarathna et al., 2013). Several studies have been published on the impact of some external conditions, such as skin movement (Mahe et al., 2011), influence of distance between laser head and the skin on the analysis of blood flow (Mahé et al., 2011b), and impact of air movement on the LSCI measurements (Mahé et al., 2011a). Furthermore, Mahe *et al.* (Mahe et al., 2012) published a topical review listing the major technical and environmental conditions, including those that have an influence on microvascular studies achieved by laser recordings.

3.7 Clinical applications of laser speckle contrast imaging

LSCI has been applied in a variety of biomedical applications, and several researchers have presented their results both *in vivo* and *in vitro*. In what follows, we mention sev-

eral of these applications.

3.7.1 Retinal imaging

Retinal imaging is considered as one of the earliest applications of LSCI. It is used widely to quantify blood flow in *both* humans and animal studies. The monitoring of retinal blood flow is of importance, because its deterioration is integral in a number of pathophysiologies such as diabetic retinopathy (Kempen et al., 2004), age-related macular degeneration (Rosenfeld et al., 2005). The first introduction of retinal imaging with LSCI was performed by Briers and Fercher (Briers and Fercher, 1982). They presented a preliminary study using single-exposure laser speckle photography to give an instant map of retinal blood flow instead of using laser Doppler, which measures the perfusion at only one point in time.

Tamaki *et al.* (Tamaki et al., 1994) developed a new measure called the normalized blur (NB), which uses the same principles as LSCI. In this method, the difference between the average of the speckle intensity (I_{mean}) and the speckle intensity for consecutive images is computed. The ratio of I_{mean} to this difference (defined as normalized blur, NB), corresponds to blood velocity. Using an animal model, they found that retinal microcirculation can be studied two dimensionally and noninvasively in the rabbits under various conditions. Their findings allowed for a high spatial resolution, because their measure quantified the speckle blur in the temporal domain.

Srienc *et al.* (Srienc et al., 2010) described experimentally a rat retina. LSCI was used in conjunction with confocal microscopy to monitor light-evoked changes in blood flow in retinal vessels. They visualized both the changes in vascular morphology as well as dynamic blood flow levels in retinal vasculature.

The majority of the earliest human retinal studies have reported average blood flow velocities (Briers and Fercher, 1982), without focusing on the spatial map of blood flow (Boas and Dunn, 2010). This could be due to the small camera sensor used in the earliest versions (100×100 pixels), which limited the spatial resolution (Konishi et al., 2002). After the invention of CCD camera, blood flow map of human retina with high spatial resolution became possible. Konishi *et al.* (Konishi et al., 2002) visualized the blood flow map of human retina using an ordinary CCD camera (400×400 pixels) with high spatial resolution. Also, Isono *et al.* (Isono et al., 2003) used laser speckle flowgraphy (LSFG) and indocyanine green (ICG) angiography to measure blood flow in retinal and choroidal vessels of 9 volunteers. They found that blood flow map achieved by LSFG is comparable with that of ICG angiography. Furthermore, Ponticorvo *et al.* (Ponticorvo et al., 2013) succeeded in overcoming the major difficulties in retinal imaging: i) the refractive error generated due to the curved cornea (Srienc et al., 2010); ii) the difficult

and time-consuming alignment of the camera to find the correct angle (Cheng et al., 2008). They used LSCI in conjunction with an endoscope to obtain high spatiotemporal blood flow images in rat retinas (Ponticorvo et al., 2013). Furthermore, recently, using a novel index of blood flow in the human retina derived from LSFG, Shiga *et al.* (Shiga et al., 2014) reported a good reproducibility of relative flow volume measured from the data of retinal vessels. Furthermore, they demonstrated that LSFG is correlated significantly with laser Doppler velocimetry (LDV) measurements.

In addition to all mentioned above works, several studies have been published in the same domain of ophthalmology (Nagahara et al., 2001; Flammer et al., 2002; Cheng et al., 2008; Watanabe et al., 2008; Sugiyama et al., 2010; Okamoto et al., 2014; Matsumoto et al., 2014). Nevertheless, several restrictions have limited LSCI from being fully exploited for retinal imaging. LSCI must be carefully controlled, as to not have a negative effect on the retinal tissue. Furthermore, any movement of the eye may lead to poor quality images.

3.7.2 Skin perfusion imaging

Perfusion is the local distribution of blood to the vascular bed of tissue. It is responsible for transferring the oxygen and nutrients for cell-life. Skin perfusion studies are gaining increased interest due to their wide clinical applications. The cutaneous circulation is an accessible vascular bed which allows for non invasive investigations of endothelial, neurovascular, cardiovascular, and vascular smooth muscle vasoreactivity *in vivo* (Acharya et al., 2014; Bruning et al., 2015; Minson, 2010; Holowatz et al., 2008; Hellmann et al., 2015). Skin perfusion can be studied using different techniques (Salgado et al., 2014; Sandberg et al., 2005; Turek et al., 2008; Roustit and Cracowski, 2012, 2013), but each one has some restrictions. LSCI has the advantage of not requiring scanning to observe a desired area, and it is able to directly give perfusion levels in real time (Briers and Webster, 1996).

Cracowski *et al.* (Cracowski et al., 2011, 2013) have successfully coupled LSCI with microdialysis (a technique used to introduce a small fiber with semipermeable membranes into the dermis) to assess microvascular reactivity. Moreover, Roustit *et al.* (Roustit et al., 2010) reported very good reproducibility of LSCI for assessing skin blood flow during PORH at the human forearm of volunteers.

Cordovil *et al.* (Cordovil et al., 2012) compared cutaneous microvascular function in 50 healthy subjects with 50 patients of cardiometabolic diseased using LSCI. They found that LSCI was able to evaluate systemic microvascular endothelial function. Moreover, they reported a reduced endothelium-dependent vasodilator responses during both acetylcholine administration and forearm post-occlusive reactive hyperaemia in the

cardiometabolic disease group.

Lindahl *et al.* (Lindahl et al., 2013) used LSCI to measure the perfusion in skin burns 0–14 days post-burn and compared it to 32 uninjured areas. They observed high perfusion values with the burns that healed within 14 days compared to those that healed after 14 days or underwent surgery. Recently, Ragol *et al.* (Ragol et al., 2015) extended LSCI, resulting in a new metric known as the processing scheme static laser speckle contrast analysis (stLASCA), demonstrating its use *in vivo*. This method depends on the ratio of static-to-dynamic scattering composition of the speckle contrast K over time in order to identify burns of different depth. They provided an accurate estimate of the relative static-to-dynamic scattering composition ratio, allowing their model to distinguish burns of different severity.

Qiu *et al.* (Qiu et al., 2012) used LSCI for monitoring microcirculatory changes of port wine stains (PWS) before and 5 min after vascular targeted photodynamic therapy (V-PDT). They proved an utility of LSCI for imaging PWS microvasculature and monitoring microvascular reactivity to V-PDT.

Recently, Souza *et al.* (Souza et al., 2014), using LSCI, evaluated cutaneous blood flow in the forearm of volunteers. They pointed out a reduction of the endothelium-dependent and endothelial-independent skin microvascular vasodilator responses in patients with premature coronary artery disease compared to healthy subjects. LSCI was also used in the assessment of peripheral blood perfusion in systemic sclerosis patients (Ruaro et al., 2015). In addition to the above studies, there are several other publications of LSCI (Mahe et al., 2013; Stanhewicz et al., 2014; Shih et al., 2014; Ren et al., 2014, to cite only a few).

3.7.3 Cerebral blood flow imaging

Although at first developed for retinal imaging, LSCI is now used in a wide variety of biomedical applications and research studies. Monitoring cerebral blood flow (CBF) was the main objective of many works.

Dunn *et al.* (Dunn et al., 2001) measured CBF in the rats by illuminating the cortex with a laser light and by imaging the resulting speckle pattern. They found that the use of the speckle technique provides high resolution images of the spatio-temporal dynamics of CBF.

Royl *et al.* (Royl et al., 2006) quantified blood flow in the rat somatosensory cortex with both LSCI and LDF. They found that the magnitude of changes in CBF measured

by the two techniques correlated well. Furthermore, LSCI localizes the highest relative changes of CBF in microcirculatory areas, with a smaller contribution of larger vessels.

Armitage *et al.* (Armitage et al., 2010) used LSCI to map dynamic changes in collateral blood flow after middle cerebral artery occlusion. In rats, they identified the anastomotic connections that developed between brain vessels after vessel occlusion which persist for 24 hours.

Zakharov *et al.* (Zakharov et al., 2009) measured blood flow in the rodent brain using a processing scheme that takes into account the effect of static scatterers to improve the results. Furthermore, by monitoring induced cortical ischemia in rats, an absolute flow velocity was established using LSCI with other oxygenation measurements (Levy et al., 2012).

LDPI and magnetic resonance imaging (MRI) have been widely used for many years to quantify blood flow changes in animal models of stroke. However, these techniques were not able to provide sufficient details about blood flow dynamics due to the lack of spatial and temporal resolutions. LSCI has the advantage to provide excellent temporal and spatial resolution images. Nowadays, LSCI is used extensively in animal models of stroke for quantifying both the spatial and temporal blood flow changes with high spatial and temporal resolutions (Strong et al., 2005; Shin et al., 2005, 2007).

A quantitative accuracy of the blood flow changes is of importance during the study of the stroke. Duncan and Kirkpatrick (Duncan and Kirkpatrick, 2008a) compared single exposure LSCI and MESI in stroke model. They found that MESI is more accurate in quantifying blood flow changes than traditional single exposure LSCI.

Using the LSCI technique, more recent paper, have attempted to measure the CBF in order to study both the normal and pathopshysiological brain (Kazmi et al., 2015a; Lu et al., 2015; Timoshina et al., 2015; Takeshima et al., 2015; Schrandt et al., 2015).

3.7.4 Other applications of laser speckle contrast imaging

The three sections above are just a few examples of medical applications of LSCI. LSCI is used in a lot of other medical applications. Fukuoka *et al.* (Fukuoka et al., 1999) measured blood flow during surgery for 100 cases of osteonecrosis of the femoral head. They demonstrated that LSCI is able to distinguish the ischaemic from normal tissue areas in 92 of the cases. LSCI was also used in an investigation of migraines (Bolay et al., 2002), and in the field of dentistry for the assessment of the pulp (Stoianovici et al., 2011). LSCI is also of utility beyond the medical field, such as in the study of

the velocity of vehicles (Aliverdiev et al., 2002), and for the assessment of drying paint (Romero and Rabal, 2000).

3.8 Laser speckle contrast imaging versus laser Doppler techniques

Laser Doppler techniques are well-known to monitor microvascular blood perfusion in the tissue (Wardell et al., 1993; Essex and Byrne, 1991). LDF was first introduced in the 1970s after the development of laser technology and fiber-obtic systems (Stern, 1975). The physical principle behind this method is the following: a laser beam is sent to the area of interest. Photons of the laser light penetrate into the tissue and are diffused by static particles (e.g., the skin) and moving red blood cells. The interaction with the moving red blood cells generates a change in the frequency of the photons due to the Doppler effect. Doppler-shifted and unshifted photons are backscattered, and collected on the photodetector. The moments (M_i) of the power spectrum $S(\omega)$ of the photocurrent are computed as (Bonner and Nossal, 1981):

$$M_i = \propto \int_0^\infty \omega^i S(\omega) d\omega \quad . \tag{3.24}$$

Therefore, computing the zeroth order moment ($i = 0$) corresponds to the volume of red blood cells, while the first order moment ($i = 1$) is equal to the flux or perfusion.

Bonner and Nossal (Bonner and Nossal, 1981) provided a widely accepted theoretical model of laser Doppler measurements. They have shown that for low blood volume, the first order moment ($i = 1$), in Eq. 3.24, is linearly proportional to the product of the root mean square (rms) velocity of moving red blood cells and their concentration.

In contrast, LSCI is considered as an alternative technique to provide perfusion map (Briers, 2001, 2007; Bezemer et al., 2010; Rege et al., 2012a). The principle of LSCI techniques is based on blurring of speckle pattern on the detector (see Sec. 3.4). Therefore, to link this blurring with an average velocity of moving scatterers (such as moving blood cells), an appropriate model of velocity distribution (e.g., Lorentzian, Gaussian), and other parameters (e.g., speckle size) should be chosen. So there is no proper model linking the speckle contrast to the velocity or perfusion. Hence, this is the major challenge for determining the velocity of moving blood cells with LSCI (Draijer, 2010). However, very recently, integrating the LSCI with sidestream dark field (SDF) microscopy demonstrated the feasibility of LSCI for quantitative measurement of the time integrating speckle and blood flow velocity (Nadort et al., 2016).

Furthermore, due to the spatial heterogeneity of skin perfusion (Braverman, 2000) and because LDF evaluates the perfusion in a small volume (O'Doherty et al., 2009), LDF signals present large spatial variability leading to poor reproducibility of the measures (Roustit et al., 2010). Nevertheless, LDF shows good temporal resolution (real-time recordings of the perfusion variations). On the other hand, LSCI has the advantage of showing good spatial and temporal resolutions, and excellent reproducibility (Roustit et al., 2010).

Tew *et al.* (Tew et al., 2011) studied the relationship between integrating-probe LDF values and LSCI, expressed in cutaneous vascular conductance (CVC), i.e., laser Doppler flow/mean arterial pressure. They found a nonlinear relation between the perfusion values. Similar conclusions have recently been found between LSCI and LDF (monopoint probes) perfusion values (Humeau-Heurtier et al., 2013c; Binzoni et al., 2013).

Laser Doppler perfusion imaging (LDPI) was less favorable for the clinical environment due to the need to scan. This scanning mode resulted in long measurement times, whereas LSCI has the advantage of being a full-field technique. However, recently LDPI became a full-field technique by introducing a high-speed CMOS camera for the detection of the Doppler-shifted light (Serov and Lasser, 2005; Serov et al., 2005, 2003). Since then, LDPI can be used to monitor blood perfusion in real time for clinical applications (Leutenegger et al., 2011). Both techniques now have a measurement time in the millisecond range. The introduction of the high-speed CMOS cameras in LDPI directly reveals another advantage of LSCI at the expense of LDPI. To perform LSCI measurements, an inexpensive camera – with frame-rate of 200Hz – is sufficient to provide excellent images of blood flow, whereas for LDPI, a state-of-the-art high-speed camera that can achieve a frame-rate of about 25 kHz is needed to provide the same quality images (Draijer et al., 2009).

Stewart *et al.* (Stewart et al., 2005) reported a very good linear correlation between LSCI and LDPI in burn scar perfusion assessment. Millet *et al.* (Millet et al., 2011) tested the linearity between skin blood flux recorded by LSCI and LDPI. They found an excellent correlation between both techniques for measuring blood flow on the forearm of healthy volunteers, when data are expressed as raw arbitrary perfusion units.

Because LDF, LDPI, and LSCI are very sensitive to movements (movements of the subjects, of the skin, etc.), the movement-induced artifacts are the main disadvantage when recordings are performed on people unable to remain still such as children or patients with tremors. Recently, this disadvantage has been overcome with LSCI by subtracting the signal backscattered from an opaque adhesive surface located near the

skin region of interest (Mahe et al., 2011, 2013). These results are very promising for a wide use of LSCI.

Another drawback of the traditional LSCI is the choice of the exposure time T. As it has been reported by many studies that there is a strong relationship between the speckle contrast K values and the exposure time T (Yuan et al., 2005). So, the choice of the integration time determines what can be seen in the image. The introduction of MESI overcame this disadvantage of the choice of an optimal exposure time. Other studies compared LSCI and laser Doppler techniques either experimentally or theoretically (Forrester et al., 2002; Serov and Lasser, 2006; Draijer et al., 2008; Thompson and Andrews, 2008).

In conclusion to all the above discussion, LSCI is still gaining interest in the field of tissue perfusion imaging due to its high spatial and temporal resolutions, and low cost compared to laser Doppler techniques. On the other hand, and with respect to laser Doppler techniques, theory behind laser Doppler is widely accepted. In contrast, the link between speckle contrast and perfusion still need to be studied.

3.9 Future trends of laser speckle contrast imaging

Since the first introduction of laser speckle techniques in the early 1980s, many enhancements have been done to improve results. LSCI is finally being well known as a promising tool for monitoring blood flow. Here we try to point out some of the current limitations, technical development, and future challenges.

1. Although the physical concept behind LSCI is well known, the link between microvascular blood perfusion values and speckle contrast is not well established yet. Therefore, the essential challenge is to model the link between the speckle contrast measure and the perfusion. One approach is to use multiple exposure times, thus giving rise to multiple autocorrelation functions, which allows one to easily model multiple dynamics, having different characteristic speeds. Recently, an integrating SDF-LSCI system has been proven to be an effective method for improving the reliability of LSCI (Nadort et al., 2016). SDF-LSCI videomicroscope enables consecutive multi-exposure laser speckle imaging and SDF-imaging of the same microcirculation area. Using fitting equation to the measured speckle contrast, this approach permits to independently estimate τ_c (by LSCI) and velocity (by SDF) of the same vessels, resulting in an excellent agreement between theory and experiment (Nadort et al., 2016). Their equation $1/\tau_c = \alpha_1 A(N) \times V$ takes into account the optical properties and experimental geometry of the examined area. In this model, α is the proportionality constant

for single scattering and $A(N)$ scales for the average number of dynamic scattering events N (Nadort et al., 2016).

2. Monitoring microvascular function in movements is of interest, because some of the vascular diseases are detected under exercise conditions (Sharma et al., 2012). Furthermore, in the special cases such as fever or Parkinson disease, the patients can suffer from trembling or shivering. Using a specific patch, LSCI can monitor microvascular function even when subjects are in movements (Mahe et al., 2011, 2013). This patch allows movement artifact removal on laser signal (Mahe et al., 2011). Recently, Omarjee *et al*. (Omarjee et al., 2015) succeeded in separating flow from movements during LSCI recording. Their adhesive opaque surface allowed an efficient movement artifact removal of LSCI measurements without the need for individual calibration. The development of an automatic movement artifact removal will be of interest to facilitate the procedure of processing (Humeau-Heurtier et al., 2013a). In addition, the development of sterile patchs is needed to allow microvascular function recordings of internal organs. Motion artifact problems can also be addressed using signal processing tools or interframe registration (Miao et al., 2010).

3. The use of signal processing tools may lead to better performances and improve the diagnoses. Humeau-Heurtier *et al.* (Humeau-Heurtier et al., 2013b) used multiscale entropy to analyze LSCI data. They found that the use of signal and image processing tools may reveal more physiological information. Furthermore, recently, Humeau-Heurtier *et al.* (Humeau-Heurtier et al., 2015b) proposed a new post-acquisition visual representation for LSCI perfusion data using an algorithm that is called generalized differences (GD). In addition, a method based on the complete ensemble empirical mode decomposition with adaptive noise (CEEMDAN) has been proposed as a promising tool to extract features from LSCI data in order to improve image understanding (Humeau-Heurtier et al., 2015c,a). An algorithm based on histogram analysis of the speckle contrast distribution has also been proposed recently to provide rapid differentiation of macro- and microcirculation (Abdurashitov et al., 2015).

4. It could be interesting to develop algorithms that combine data from LSCI with other optical techniques. This may enable better diagnosis, and the understanding of physiological biomarkers through multi-parameter imaging (Dunn, 2012; Nadort et al., 2016). Diffuse correlation spectroscopy (DCS) is a noninvasive technique to obtain the relative blood flow in deep tissue (Buckley et al., 2009). The disadvantage of this technique is that its setup is relatively expensive (Bi et al., 2013). Therefore, Bi *et al.* (Bi et al., 2013) combined LSCI and DCS to present diffuse speckle contrast analysis (DSCA). The latter was able to investigate the blood flow in deep tissue using an inexpensive instrument of LSCI, and a simplified analysis (Bi et al., 2013).

5. LSCI could become a predictive tool for monitoring patients at risk of cardiovascular disease. It would be interesting to demonstrate that a low endothelial response assessed by laser technology is predictive of an early coronary heart disease or other vascular diseases. Furthermore, it has recently been shown that LSCI can be used to measure depth of blood flow region, making it a useful tool for real-time diagnosis of various skin diseases (Yokoi and Aizu, 2015).
6. To date, no normal value exists for any vascular function tests using laser technology. It would be important to perform studies to determine these values for each microvascular test, but standardization of the procedure measurement is first needed (Mahe et al., 2012).
7. LSCI is a valuable real–time, semi–quantitative tool for monitoring flow dynamics. Its result is not directly related to the actual flow values (Duncan and Kirkpatrick, 2008a). Several issues such as optical properties of the fluid and surrounding tissue, the effects of different flow models on LSCI contrast values, the effects of static scatterers, among others, still remain a challenge and prevent LSCI from being an accurate quantitative tool, for example, in time course studies, or in population comparison. Therefore, several recent studies have been performed in order to improve LSCI as an imaging tool for the qualitative assessment of flow velocity (see Sujatha and Banerjee, 2015; Miao et al., 2015; Lal et al., 2013; Kirkpatrick and Khaksariand, 2015; Kirby et al., 2015). Furthermore, a numerical method to calculate an autocorrelation function flows of arbitrary geometries was recently introduced by Davis and Dunn (Davis and Dunn, 2015), requiring no assumptions regarding the number of scattering events, the final form of the autocorrelation function, or the degree of correlation between scattering events. Additionally, Nadort *et al.* (Nadort et al., 2016) presented a modified SDF-LSCI videomicroscopy enabling consecutive multi-exposure laser speckle imaging and SDF-imaging of the same microcirculation area. Their metric enables simultaneous, independent measurement of τ_c and velocity in microcircularity vessels or phantom flow channels.

   The introduction of MESI improved the quantitative accuracy of LSCI by incorporation of multi–exposures, and a better separation of the related static scatterers contribution. However, the number of exposures required to achieve the flow values have to be considered (Briers et al., 2013). It is worth mentioning that efforts have recently been made to identify an optimal subset of exposures (Kazmi et al., 2014).

   In order to improve the estimation of blood flow speed in LSCI, Li *et al.* (Li et al., 2014) presented a novel method, which is called frequency-domain laser speckle imaging (FDLSI) to analyze speckle variation in the frequency domain.

They demonstrated a blood flow model, that can obtain the autocovariance function without the influence of static scattering or illumination intensity. Their flow speed values found in phantom experiments agreed well with the preset real speed obtained from syringe pump (Li et al., 2014). FDLSI has the advantage of not requiring the control of the illumination intensity to fit exposure time, in consequence, leading to high robustness to imaging illumination (Parthasarathy et al., 2008; Dunn, 2012; Li et al., 2014). Furthermore, Lal *et al.* (Lal et al., 2013) found that blood flow speed and concentration of scatterers present in fluid could be measured simultaneously by analysis speckle contrast and fractality features of speckle pattern.

Further theoretical studies such as Monte Carlo simulations and blind deconvolution may improve the robustness of LSCI theory (Briers et al., 2013). For example, Monte Carlo simulations have been applied to address the problem of spatial resolution, blurring due to multiple scattering caused by the reflected light from the static structures surrounding the blood vessels, and the sampling depth of LSCI (Zakharov et al., 2006; Davis et al., 2014).

LSCI has suffered from being semi-quantitative (Briers and Webster, 1996). However, some recent efforts have been made to calibrate its results and move toward quantitative measures (see e.g., Rice et al., 2013). We believe that LSCI continues to be a valuable tool, and still offers some advantages at the expense of other techniques such as LDPI, especially when the maximum temporal resolution and real-time monitoring of blood flow are essential requirements. Finally, due to the rapid development of technology related to LSCI, it is thought that speckle contrast processing could eventually be executed by a smartphone application within several tens of milliseconds (Ragol et al., 2015; Remer and Bilenca, 2015).

4

Impact of aging on micro- and macrocirculation parameters

This chapter is subdivided into two main sections. The first section aims at studying the impact of aging on MBCV extracted from LSCI data. In addition, the possible impact of the static scatterers like skin on MBCV values is determined through a simulation and an experimental process. The goals of the second section are: (i) to assess aging effect over microvascular parameters (perfusion and MBCV) and macrocirculation parameter (PWV); (ii) to study the relationship between these parameters. The main findings show that moving scatterers velocities data vary with age: blood cells velocities increase with age. Moreover, the more the static scatterers, the higher the moving scatterers velocity values. Finally, the micro- and macrocirculation systems are correlated.

Contents

4.1 Introduction

In order to study the impact of aging on microvascular blood flow, experimental LSCI data were processed in two populations (young and older). From these data, red blood cells velocity and perfusion were computed and analyzed. Red blood cells velocity is computed from a model of velocity distribution.

As mentioned above in Chap. 3, several measurement requirements have to be considered when computing the expression of speckle contrast K. One of these requirements is the effect of static scatterers on the estimation of moving blood cells velocity from the speckle contrast K. Thus, several formula were introduced to address this issue as discussed in Sec. 3.4.1. We present herein our effort to evaluate the influence of the fraction of statically scattered light (ρ) on the computation of the speckle contrast K. Two ways are followed in order to determine the value of ρ. The first way is by simulating the expression of speckle contrast K mathematically. Therefore, different values of ρ are injected in the expression of speckle contrast K. The second way is by computing an experimental ρ value to be used in the speckle contrast K. For these two ways, moving blood cells velocity is computed from speckle contrast K and compared.

On the other hand, we present in this chapter our work to study the possible correlation between the macro- and microcirculation associated with age. Impact of aging on microvascular blood flow was analyzed when the static scatterers effect is taken into account and when it is not. Furthermore, the impact of aging was considered under the simulation and experimental processes of static scatterers effect.

In what follows, the general protocol of measurement, signal and image processing procedure, and the statistical analysis used in this manuscript are shown in Secs. 4.2, 4.3, and 4.4, respectively. Then, Sec. 4.5 focuses on the impact of aging on MBCV associated with a simulation process to take into account static scatterers, whereas Sec. 4.6 focuses on the impact of aging on the micro- and macrocirculation parameters associated with an experimental process to take into account static scatterers. A conclusion is finally proposed in Sec. 4.7.

4.2 General measurement procedure

All the subjects provided written, informed consent prior to participation and the studies were carried out in accordance with the Declaration of Helsinki. Subjects were supine in a quite room with controlled temperature (Abraham et al., 2013), without any air movement (Mahé et al., 2011a). For each subject, the ventral face of the forearm was studied. A pressure cuff was placed on the upper arm, ipsilateral to forearm LSCI recording site. A PeriCam PSI System (Perimed, Sweden) having a laser wavelength of 785 nm and an exposure time T of 6 ms has been used to acquire the contrast images. The distance between the laser head to forearm skin was set at 15 ± 1 cm (Mahé et al., 2011b) which gave images with a resolution around 0.45 mm. Contrast images were stored on a computer for off-line analysis.

The recording procedure was composed of three physiological states: 1) 2 min at rest; 2) 3 min of vascular occlusive (biological zero, BZ) (Tee et al., 2004), obtained by inflating an arm cuff to 220 mmHg; 3) 5 min of post-occlusive reactive hyperaemia.

4.3 General image and signal processing procedure

To compute moving blood cells velocity and perfusion values from the microcirculation, the following image processing procedure was used to process the speckle contrast images.

1. On the first contrast image of each image sequence, a pixel was chosen randomly and its contrast value was followed in time.

2. Around each pixel chosen in step 1, regions of interest (ROI) of different sizes of $N \times N$ pixels (see below) were chosen in order to get a reasonable signal and reduce the spatial variability of blood flow (Rousseau et al., 2011a). The mean of the contrast pixels values inside each ROI was computed. This operation has been carried out over all the images in the image sequence to obtain contrast

time evolution signals (Rousseau et al., 2011a).

3. LSCI data are – by definition – very sensitive to movements (Mahe et al., 2013). These artefacts appear as high and transient peaks in the data. To remove movement artifacts and get a reasonable LSCI signal, each contrast time evolution signal was passed through a low-pass sixth order Butterworth digital filter with a cutoff frequency of 3 Hz.

4. The value of the speckle correlation time τ_c for each ROI of the image sequence was determined assuming a velocity profile for moving scatterers. Two main profiles are taken into account in this manuscript, Lorentzian and Gaussian profiles. In the laser speckle contrast imager we used (PeriCam PSI System, Perimed, Sweden), the contrast is automatically corrected to ensure that it is equal to unity for static objects. A coherence factor, C_F, that is naturally instrument specific, is used in the computation of the contrast computation as

$$K_{measured} = C_F \frac{\sigma}{\langle I \rangle} \ . \tag{4.1}$$

Moreover, the coherence factor C_F is connected to β by

$$C_F = \frac{1}{\sqrt{\beta}} \ . \tag{4.2}$$

Therefore, in our work, there is no need to include β in the expression of the contrast within the distribution model to solve the equations mentioned in Chap. 3. Thus, we simply have

$$K^2_{measured} = f_D(\tau_c) \ . \tag{4.3}$$

with $f_D : \tau_c \longmapsto \frac{1}{\beta} K^2(\tau_c)$ where K stands for the contrast within the chosen distribution models. Therefore, for the Lorentzian model, the equation 3.20 becomes

$$\begin{aligned} K^2 = \Bigg[& \rho^2 \frac{\exp(-2x) - 1 + 2x}{2x^2} + \\ & 4\rho(1-\rho) \frac{\exp(-x) - 1 + x}{x^2} + \\ & (1-\rho)^2 \Bigg] + C_{noise} \ . \end{aligned} \tag{4.4}$$

In contrast, for the Gaussian model, the equation 3.22 becomes

$$K^2 = \left[\rho^2 \frac{\exp\left(-2x^2\right) - 1 + \sqrt{2\pi}x\mathrm{erf}\left(\sqrt{2}x\right)}{2\left(x\right)^2} + \right.$$
$$2\rho\left(1-\rho\right)\frac{\exp\left(-x^2\right) - 1 + \sqrt{\pi}x\mathrm{erf}\left(x\right)}{\left(x\right)^2} + \tag{4.5}$$
$$\left.\left(1-\rho\right)^2\right] + C_{noise} \ .$$

Therefore, Eq. 4.4 was used everywhere in this manuscript to determine moving blood cells velocity values when a Lorentzian velocity profile is assumed, whereas Eq. 4.5 was used to determine moving blood cells velocity values when a Gaussian velocity profile is assumed.

Intuitively, when a Lorentzian distribution is assumed for moving scatterers, the Eq. 3.13 to compute the perfusion can be written as

$$Perfusion \sim \left[\frac{1}{x} + \frac{1}{x^2}\left(\exp\left(-2x\right) - 1\right)\right]^{-1/2} - 1 \ . \tag{4.6}$$

5. To study the effect of static scatterers on red blood cells velocity values, two ways were considered in this manuscript. The first way is by simulating the expression of speckle contrast K through different values of ρ. Four cases have been considered mathematically to simulate static scatterers effect: $\rho = 1$, $\rho = 0.9$, $\rho = 0.8$, and $\rho = 0.7$. The case $\rho = 1$ therefore corresponds to the situation where static scatterers (skin for example) are not taken into account. The second way is by computing an experimental value of ρ, which corresponds to the fraction of statically scattered light. More details about this way will be discussed later in this chapter (see Sec. 4.6).

6. For the numerical determination of the correlation time τ_c from contrast values K, we used a combination of bisection, secant, and inverse quadratic interpolation method (Brent, 1973; Forsythe et al., 1976). From the values of τ_c, the velocity of the red blood cells has been determined from Eq. 3.11.

4.4 Statistical analysis

In order to compare velocity values obtained from younger and older groups, MedCalc for Windows, version 12.5 (MedCalc Software, Ostend, Belgium) was used. We compared velocity values using Friedman test (Conover, 1999). It takes into account the number of comparisons and there is no need to make a Bonferroni correction. For each statistical analysis, a p value < 0.05 was considered significant.

4.5 Results of aging effect on microcirculation when static scatterers influence is simulated

4.5.1 Static scatterers effect on red blood cells velocity

In this section we present our work to simulate red blood cells velocity values from the processing of laser speckle contrast data and analyze the possible impact of static scatterers (like skin). The experimental contrast values are obtained and injected in the mathematical expression of K mentioned in Eq. 4.4 when a Lorentzian velocity profile is assumed for the moving scatterers distribution (Duncan et al., 2008a). From the mathematical expression of the contrast K, the velocity of moving blood cells in the microcirculation is computed by using different values of ρ (1, 0.9, 0.8, 0.7) in Eq. 4.4. Moreover, the velocity values are computed for different ROI sizes: 1×1 pixels, 3×3 pixels, 5×5 pixels, and 7×7 pixels. The computations are performed for three physiological states: rest, vascular occlusion and post-occlusive reactive hyperaemia.

In this work, twenty healthy subjects have been studied (12 women and 8 men; 39.0 years $\pm$ 14.5; 65.2 kg $\pm$ 5.2 kg; 170.5 cm $\pm$ 12.8 cm).

Results and discussion The mean results for the velocity of the moving scatterers obtained from laser speckle contrast images for twenty healthy subjects at rest (mean value on 1 min), during the vascular occlusive (mean value on 1 min) and during reactive hyperaemia peak (mean value on 3 s at peak) are shown in Tables 4.1 to 4.3, respectively. From these three Tables, it is evident that, at rest, during vascular occlusion, and during reactive hyperaemia, the moving scatterers velocity values computed increase when ρ values decrease. Thus, this finding shows that static scatterers like skin have an influence on the moving scatterers velocity values computed from LSCI recordings performed on human forearm skin. Moreover, in Table 4.3 for a ROI size of 1×1 pixels, the values of velocity obtained for $\rho = 0.7$ are much higher than the values of velocity obtained from the other ρ values. This is due to some subjects who present higher values. The latter are the oldest ones in the population. As it will be presented later, age has an impact on

Table 4.1 – Average velocity (μm/s) for the moving blood cells during 1 min at rest for twenty healthy subjects. Moving blood cells velocity is computed from a Lorentzian velocity distribution. Four cases are considered to simulate the effect of static scatterers: $\rho = 1$, $\rho = 0.9$, $\rho = 0.8$, and $\rho = 0.7$.

ROI (pixels)	$\rho = 1$	$\rho = 0.9$	$\rho = 0.8$	$\rho = 0.7$
1×1	44.5	53.1	67.0	98.2
3×3	39.3	46.5	55.9	72.0
5×5	39.4	46.2	56.0	71.9
7×7	39.2	46.0	55.7	71.4

Table 4.2 – Same as Table 4.1, but during 1 min of recording at vascular occlusion.

ROI (pixels)	$\rho = 1$	$\rho = 0.9$	$\rho = 0.8$	$\rho = 0.7$
1×1	19.6	22.7	26.9	33.6
3×3	14.3	16.3	18.9	22.5
5×5	14.1	16.5	18.6	22.1
7×7	14.4	16.3	18.9	22.4

the velocity results (Khalil et al., 2014a,b).

Furthermore, the results obtained herein show that the moving scatterers velocity values at rest are higher than the ones obtained during biological zero. Moreover, the moving scatterers velocity values obtained during hyperaemia peak are higher than the ones obtained at rest. This is in accordance with what is expected. Furthermore, it is worth mentioning that the velocity values computed from single pixels are different from the velocity values found when ROI (3×3, 5×5, and 7×7 pixels) are performed; see Tables 4.1, 4.2 and 4.3. This could be due to the fact that the statistical properties of LSCI single pixels in time are similar to those of white noise. It has been shown that, the LSCI results for larger ROI sizes are different from the ones obtained from LSCI single pixels in time (Bricq et al., 2012; Humeau-Heurtier et al., 2012, 2013b). The signal-to-noise ratio increases for larger ROI sizes on LSCI data (Mahé et al., 2011b; Tee et al., 2004). Larger ROI sizes have not been tested due to the computational time needed to process the data.

Table 4.3 – Same as Table 4.1, but during 3 s of recording at reactive hyperaemia peak.

ROI (pixels)	$\rho = 1$	$\rho = 0.9$	$\rho = 0.8$	$\rho = 0.7$
1×1	106.0	135.4	209.9	560.5
3×3	91.3	112.7	153.1	256.7
5×5	91.3	112.5	151.9	255.3
7×7	92.0	113.1	152.4	254.4

4.5.2 Impact of aging on red blood cells velocity

Our goal herein is to analyze if alterations of microcirculation with age can be determined by processing experimental laser speckle contrast data. To compute moving blood cells velocity values, a Lorentzian velocity profile was assumed and the presence of static scatterers, like skin, was taken into account mathematically as discussed above.

In this study, we included 14 subjects subdivided into two groups. The first group was composed of 7 subjects (4 men and 3 women, 20–30 years old). The second group was composed of 7 subjects (2 men and 5 women, 45–58 years old).

Results and discussion The mean velocities of moving scatterers for $\rho = 1$, $\rho = 0.9$, $\rho = 0.8$, and $\rho = 0.7$ are shown in Tables 4.4 to 4.7, respectively. For each table, mean results for the three physiological states are shown: rest (mean value on 1 min), vascular occlusive (mean value on 1 min) and post-occlusive reactive hyperaemia (mean value on 3 s at peak). Moreover, values obtained for different ROI sizes (1×1 pixels, 3×3 pixels, 5×5 pixels, and 7×7 pixels) are detailed for the two populations: young and older subjects.

The results obtained herein (Tables 4.4 to 4.7) show that the moving scatterers velocity values at rest are higher than the ones obtained during biological zero. Moreover, the moving scatterers velocity values obtained during hyperaemia peak are higher than the ones obtained at rest. These findings confirm the results shown in the previous study mentioned in Sec. 4.5.1. Furthermore, our results show that, for a given ROI size and a given ρ value, at rest and during the biological zero, the velocities found for young subjects are lower than the ones obtained for older subjects (see Tables 4.4 to 4.7). Nevertheless, these differences are not statistically significant. From the literature, the value of basal blood flow (product of velocity by concentration of moving blood cells) for young and elderly subjects remains debatable (see e.g., Ogrin et al., 2005; Tew et al., 2010). However, during reactive hyperaemia, for a given ROI size and a given ρ value, we find statistically significant differences between the velocities obtained for young subjects and the ones obtained for older subjects (see Tables 4.4 to 4.7). The mean velocities obtained for the older subjects are higher than the ones obtained for the younger subjects. This may be due to the stiffness of vessels that increases with age. Stiffness being higher for aged people, the revasculatisation of vessels after the vascular occlusion (post-occlusive reactive hyperaemia) may lead to higher moving blood cells velocity values.

We also demonstrate that, for the two populations, the velocity of moving scatterers increases while the value of ρ decreases (see Tables 4.4 to 4.7). These results are in accordance with the ones presented above in Tables 4.1 to 4.3. Therefore, our results

Table 4.4 – Mean velocity results (μm/s) of moving scatterers computed from LSCI data over different ROI sizes and for $\boldsymbol{\rho = 1}$. Three physiological states are analyzed: 1 min at rest, 1 min during BZ and 3 s during PORH peak. The results are obtained from two groups (young and older) of seven subjects in each group, when a Lorentzian velocity profile is assumed. *means statistically significant with results obtained from the older group for the same ROI size.

ROI (pixels)	1×1		3×3		5×5		7×7	
group	young	elderly	young	elderly	young	elderly	young	elderly
Rest	43.7	47.8	39.0	42.4	38.7	42.0	37.9	42.0
BZ	20.0	20.7	14.1	15.7	14.0	15.5	14.8	15.5
PORH	89.6*	129.0	77.1*	109.0	76.7*	107.0	76.4*	107.0

Table 4.5 – Same as Table 4.4, but for $\boldsymbol{\rho = 0.9}$.

ROI (pixels)	1×1		3×3		5×5		7×7	
group	young	elderly	young	elderly	young	elderly	young	elderly
Rest	51.8	57.0	45.7	49.8	45.3	49.3	44.4	49.3
BZ	23.1	23.9	16.0	17.9	15.8	17.6	16.8	17.6
PORH	110.6*	167.3	93.5*	134.8	92.8*	133.2	92.5*	132.4

Table 4.6 – Same as Table 4.4, but for $\boldsymbol{\rho = 0.8}$.

ROI (pixels)	1×1		3×3		5×5		7×7	
group	young	elderly	young	elderly	young	elderly	young	elderly
Rest	65.1	72.6	55.5	60.7	53.7	60.1	53.7	59.9
BZ	27.4	28.4	18.6	20.7	18.4	20.5	19.4	20.4
PORH	156.1*	281.3	122.1*	185.9	120.8*	182.4	120.2*	181.1

Table 4.7 – Same as Table 4.4, but for $\boldsymbol{\rho = 0.7}$.

ROI (pixels)	1×1		3×3		5×5		7×7	
group	young	elderly	young	elderly	young	elderly	young	elderly
Rest	92.3	110.6	71.6	79.0	70.5	77.8	68.8	77.5
BZ	34.4	35.6	22.1	24.7	21.8	24.3	23.2	24.3
PORH	312.9*	942.3	187.7*	344.3	183.5*	323.6	181.7*	317.9

stress an effect of static scatterers (like skin) over the velocity of moving scatterers.

Furthermore, using the same LSCI experimental data presented in this section, we compared red blood cells velocity values from the microcirculation when a Lorentzian profile is assumed with the ones obtained when a Gaussian profile is assumed for moving scatterers.

Figures 4.1a and 4.1b present the theoretical relationship between the speckle contrast K and the ratio of the speckle correlation time τ_c to camera exposure time T for Lorentzian and Gaussian profiles, respectively, with different values of ρ. From these two figures we can observe that, for the lowest value τ_c/T shown, the contrast K becomes higher when the ρ value decreases: K goes from 0.1 (for $\rho = 1$) to more than 0.3 (for $\rho = 0.7$). These differences are due to the static scatterers that have an additive effect in the speckle contrast K for τ_c/T close to zero. Our results are in accordance with another study where it has been reported that, when using single-exposure LSCI (as in the present study), the perfusion values decrease when the thickness of the static scattering layer increases (Thompson et al., 2012). As perfusion is linked to the inverse of the contrast K, the present results are in accordance with the latter study. Moreover, it has also been shown that static scattering significantly affects the determination of relative $1/\tau_c$ in an *in vitro* system (Smausz et al., 2009). However, it has much less influence in the study of the cortical microcirculation of piglets (Domoki et al., 2012). Furthermore, the two figures show a S-shape but with a different slope. The Gaussian profile leads to a steeper slope than the Lorentzian profile. This result in accordance with other studies where it has been reported that a Gaussian curve has a steeper slope than a Lorentzian curve (Briers et al., 2013).

The mean velocity values obtained for a Lorentzian and for a Gaussian profile for $\rho = 1$, $\rho = 0.9$, $\rho = 0.8$, and $\rho = 0.7$ are shown in Tables 4.8 to 4.11, respectively.

It is worth mentioning that, for a given group of subjects (young subjects or older subjects), the velocity values of moving scatterers vary with the profile of moving scat-

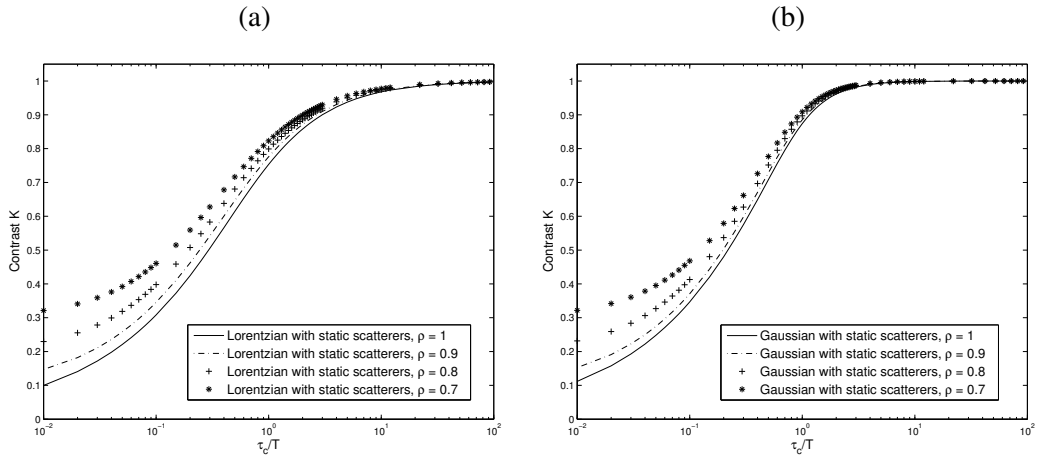

Figure 4.1 – Theoretical relationship between speckle contrast K and the ratio of the speckle correlation time τ_c to camera exposure time T for (a): a Lorentzian profile; (b) a Gaussian profile, with different values of ρ.

terers. By using the same experimental data, we found that the velocity values obtained when a Gaussian profile is assumed to compute the theoretical expression of speckle contrast are higher than the ones obtained when a Lorentzian profile is assumed. These differences in the velocity values are obvious in the presence or absence of static scatterers (Tables 4.8 to 4.11, respectively). However, a Gaussian profile presents the same behavior on the results as the one observed when a Lorentzian profile is assumed for moving scatterers, for both younger and older groups. This means that the velocity of moving scatterers at rest, during biological zero and during reactive hyperaemia vary with ρ values: the velocity of moving scatterers increases when the value of ρ decreases. Furthermore, at rest and during the biological zero, we can observe that the velocities found for young subjects are lower than the ones obtained for older subjects. Nevertheless, these differences are not statistically significant. Alternatively, during reactive hyperaemia there is an obvious difference in the mean velocity results between young and older people (Tables 4.8 to 4.11, respectively). The mean velocities obtained from the older group are statistically higher than the ones obtained from the young group.

Table 4.8 – Mean velocity results (μm/s) of moving scatterers computed from LSCI data over different ROI sizes and for $\boldsymbol{\rho = 1}$. Three physiological states are analyzed: 1 min at rest, 1 min during BZ and 3 s during PORH peak. The results are obtained from two groups (young and elderly) of seven subjects in each group, when Lorentzian and Gaussian velocity profiles are assumed for moving scatterers. *means statistically significant with results obtained from the elderly group for the same ROI size.

ROI (pixels)	1×1				3×3				5×5				7×7			
Type of Profile	Lorentzian		Gaussian		Lorentzian		Gaussian		Lorentzian		Gaussian		Lorentzian		Gaussian	
Group	young	elderly	young	elderly	young	elderly	young	elderly	young	elderly	young	elderly	young	elderly	young	elderly
Rest	43.7	47.8	62.2	67.2	39.0	42.4	56.3	61.2	38.7	42.0	56.4	56.0	37.9	42.0	55.1	55.1
BZ	20.0	20.7	33.7	34.5	14.1	15.7	27.5	28.8	14.0	15.5	28.3	26.8	14.8	15.5	27.1	28.8
PORH	89.6*	129.0	121.4*	167.8	77.1*	109.0	101.6*	141.9	76.7*	107.0	100.8*	140.6	76.4*	107.0	100.2*	140.0

Table 4.9 – Same as Table 4.8, but for $\boldsymbol{\rho = 0.9}$.

ROI (pixels)	1×1				3×3				5×5				7×7			
Type of Profile	Lorentzian		Gaussian		Lorentzian		Gaussian		Lorentzian		Gaussian		Lorentzian		Gaussian	
Group	young	elderly	young	elderly	young	elderly	young	elderly	young	elderly	young	elderly	young	elderly	young	elderly
Rest	51.8	57.0	68.5	74.2	45.7	49.8	61.6	66.5	45.3	49.3	62.4	65.6	44.4	49.3	60.1	65.5
BZ	23.1	23.9	36.5	37.3	16.0	17.9	29.5	30.9	15.8	17.6	30.4	30.9	16.8	17.6	29.1	30.9
PORH	110.6*	167.3	138.5*	198.6	93.5*	134.8	113.5*	160.9	92.8*	133.2	112.4*	159.2	92.5*	132.4	111.7 *	158.5

Table 4.10 – Same as Table 4.8, but for $\boldsymbol{\rho = 0.8}$.

ROI (pixels)	1×1				3×3				5×5				7×7			
Type of Profile	Lorentzian		Gaussian		Lorentzian		Gaussian		Lorentzian		Gaussian		Lorentzian		Gaussian	
Group	young	elderly	young	elderly	young	elderly	young	elderly	young	elderly	young	elderly	young	elderly	young	elderly
Rest	65.1	72.6	79.8	87.7	55.5	60.7	69.7	75.5	53.7	60.1	70.9	74.4	53.7	59.9	67.8	74.2
BZ	27.4	28.4	40.3	41.3	18.6	20.7	32.0	33.6	18.4	20.5	33.1	33.5	19.4	20.4	31.5	33.5
PORH	156.1*	281.3	180.2*	308.5	122.1*	185.9	137.4*	206.3	120.8*	182.4	135.6*	202.8	120.2*	181.1	135.6*	202.8

Table 4.11 – Same as Table 4.8, but for $\boldsymbol{\rho = 0.7}$.

ROI (pixels)	1×1				3×3				5×5				7×7			
Type of Profile	Lorentzian		Gaussian		Lorentzian		Gaussian		Lorentzian		Gaussian		Lorentzian		Gaussian	
Group	young	elderly	young	elderly	young	elderly	young	elderly	young	elderly	young	elderly	young	elderly	young	elderly
Rest	92.3	110.6	104.4	123.0	71.6	79.0	83.6	91.4	70.5	77.8	85.7	89.6	68.8	77.5	80.7	89.3
BZ	34.4	35.6	46.5	47.7	22.1	24.7	35.5	37.2	21.8	24.3	36.8	37.1	23.2	24.3	34.8	37.1
PORH	312.9*	942.3	336.8*	970.3	187.7*	344.3	196.5*	358.0	183.5*	323.6	190.9*	337.5	181.7*	317.9	188.6 *	335.5

4.6 Results of aging effect on micro- and macrocirculation parameters when static scatterers influence is computed experimentally

4.6.1 Experimental value of ρ

In order to improve the quantitative reliability of LSCI, the effect of static scatterers on the optical signal has to be considered. Therefore, a refined speckle contrast formulation was introduced that takes into account the scattering light from rigid contributions (i.e., the formula shown in Eqs. 4.4 and 4.5). In such formula, the static contribution ρ is calculated in an additional step of data processing (Zakharov et al., 2009), as discussed below.

Traditional LSCI uses an exposure time T longer than the dynamic scatterers correlation time τ_c, and the time between two successive frames (Δt) is longer than T ($\Delta t > T >> \tau_c$). This means that between successive frames, no correlations of the dynamic speckles are present on a time scale of Δt and thus $g_{1d}(\Delta t) \approx 0$. Therefore, the correlation between two successive speckle patterns appears only due to the presence of static scatterers. Therefore, Eq. 3.16 can be written as (Vaz et al., 2016)

$$g_2(\Delta t) = 1 + \beta\rho^2 \ , \tag{4.7}$$

where $g_2(\Delta t)$ is equivalent to the 2D-correlation coefficient between two successive frames. Since the static scatterers distribution is not homogeneous in the tissue, the ρ value should be computed locally in a region of interest smaller than the image. An experimental value of ρ – corresponding to the contribution of the non-fluctuating component to the total intensity – could therefore be computed by a comparison of successive frames and making use of a multi-speckle averaging scheme (Zakharov et al., 2006)

$$\rho = 1 - \beta^{-1/2}\left[\frac{\langle I_1 I_2\rangle}{\langle I_1\rangle\langle I_2\rangle} - 1\right]^{1/2} , \tag{4.8}$$

where I_1 and I_2 are two successive intensity images, $\langle I\rangle$ denotes the spatial averaging of the intensity over a selected area containing N pixels, and $\langle I_1 I_2\rangle = \frac{1}{N}\sum_{i=1}^{N} I_1(x_i)I_2(x_i)$. In this manuscript, the value of ρ was computed from a ROI size of 5×5 pixels.

In this study, 16 healthy subjects without known disease were studied. These 16 subjects were subdivided into two groups. The first group included 8 young subjects (3 women and 5 men) who were younger than 30 years old (aged between 20 and 30 years). The second group included 8 elderly subjects (8 women) who were older than 50 years old (aged between 50 and 62 years). Perfusion and MBCV computed from

LSCI are studied in three physiological states: rest, biological zero, and post-reactive reactive hyperaemia. MBCV values computed for each subject in two cases: $\rho = 1$ and ρ computed from Eq. (4.8).

In what follows, two cases of ρ are considered: 1) $\rho = 1$, which corresponds to the case where static scatterers are not taken into account; 2) $\rho \neq 1$: the ρ value for each subject was determined from Eq. (4.8). Afterwards, Eq. (4.4) led to the determination of the moving blood cells velocity values for the two cases.

Results and discussion The experimental ρ values computed from Eq. 4.8 for the 16 subjects, and for the three physiological states, are shown in Fig. 4.2. From this figure we can observe that ρ values vary from 0.94 to 0.99. Moreover, we note that the ρ values obtained during biological zero are lower than those obtained at rest, and ρ values obtained at rest are lower than those obtained during post-occlusive reactive hyperaemia. This is in accordance with what could be expected. Indeed, during a vascular occlusion there is no flow and therefore the effect of static scatterers is relatively higher than at rest or during post-occlusive reactive hyperaemia. Because ρ corresponds to the fraction of total light that interacts with moving scatteres, ρ is naturally lower during biological zero than at rest or during post-occlusive reactive hyperaemia. However, we note that these variations are very low (ρ values vary from 0.94 to 0.99). As a result and because ρ values do not change much during the three physiological states (biological zero, rest and post-occlusive reactive hyperaemia), we used an average value of ρ, for each subject, to compute the expression value of speckle contrast K (Khalil et al., 2015).

The mean velocity values obtained for a Lorentzian and for a Gaussian profile for $\rho = 1$, and for ρ values computed from Eq. 4.8 are shown in Tables 4.12 and 4.13, respectively. Our results show (Tables 4.12 and 4.13) that the velocity of moving scatterers at rest, during biological zero, and post-occlusive reactive hyperaemia differs with ρ values for *both* profiles of moving scatterers (Lorentzian and Gaussian): velocity values of moving scatterers increase when the experimental static scatterers effect is taken into account (in this case $\rho < 1$; e.g., increasing thickness of skin). Therefore, our experimental results confirm an effect of static scatterers (like skin) over the velocity of moving scatterers for the Lorentzian and the Gaussian profiles. However, these differences when the static scatterers effect is taken into account and when it is not, are not statistically significant (see Tables 4.12 and 4.13).

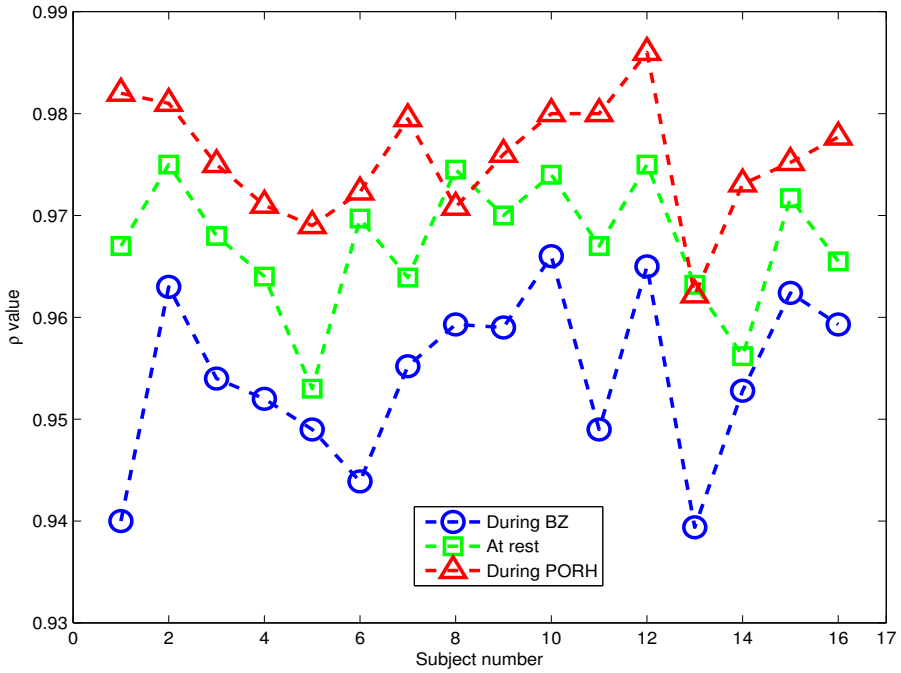

Figure 4.2 – Experimental ρ values computed from Eq. 4.8 for the 16 subjects, during the three physiological states: rest, BZ, and PORH. The eight first subjects correspond to the young group, whereas the eight last subjects correspond to the elderly group.

Table 4.12 – Mean velocity results (μm/s) of moving scatterers computed from LSCI data over different ROI sizes and for $\rho = 1$. Three physiological states are analyzed: 1 min at rest, 1 min during BZ, and 3 s during PORH peak. The results are obtained from two groups (young and elderly) of eight subjects in each group, when Lorentzian and Gaussian velocity profiles are assumed for moving scatterers. *means statistically significant with results obtained from the elderly group for the same ROI size.

ROI (pixels)	1×1				3×3				5×5				7×7			
Profile	Lorentzian		Gaussian		Lorentzian		Gaussian		Lorentzian		Gaussian		Lorentzian		Gaussian	
Group	young	elderly	young	elderly	young	elderly	young	elderly	young	elderly	young	elderly	young	elderly	young	elderly
Rest	41.3	47.3	59.6	66.6	35.6	41.4	52.3	59.2	35.6	40.5	52.1	59.4	34.3	40.2	50.7	57.8
BZ	19.2	21.0	32.7	34.8	13.9	15.9	26.4	29.1	12.8	15.6	23.5	29.2	13.1	15.5	25.5	28.7
PORH	80.9*	135.3	108.4*	175.3	74.0*	110.9	99.1.6*	144.6	66.6*	109.3	89.1*	145.8	71.6*	108.4	96.1*	141.5

Table 4.13 – Mean velocity results (μm/s) of moving scatterers computed from LSCI data over different ROI sizes and for ρ computed from Eq. 4.8 where static scatterers effect is considered. Three physiological states are analyzed: 1 min at rest, 1 min during BZ, and 3 s during PORH peak. The results are obtained from two groups (young and elderly) of eight subjects in each group, when Lorentzian and Gaussian velocity profiles are assumed for moving scatterers. *means statistically significant with results obtained from the elderly group for the same ROI size.

ROI (pixels)	1×1				3×3				5×5				7×7			
Profile	Lorentzian		Gaussian		Lorentzian		Gaussian		Lorentzian		Gaussian		Lorentzian		Gaussian	
Group	young	elderly	young	elderly	young	elderly	young	elderly	young	elderly	young	elderly	young	elderly	young	elderly
Rest	44.0	50.5	62.8	69.0	37.8	44.0	54.0	61.2	38.9	42.9	57.3	64.9	36.3	42.7	52.4	59.7
BZ	20.3	22.2	34.2	35.9	14.6	16.8	27.1	29.9	13.7	16.3	25.1	31.1	13.7	19.5	26.1	29.5
PORH	87.1*	147.0	116.3*	183.2	79.4*	119.7	102.7*	150.4	73.2*	117.9	99.4*	166.4	76.8*	117.0	99.7 *	147.2

4.6.2 Impact of aging on micro- and macrovascular parameters

The arterial network of the cardiovascular system is composed of two subsystems – macro- and microcirculation – which interact to enable an optimal adaptation to various physiologic disturbances. With age and/or risk factors such as hypertension and pathologies such as diabetes, modifications appear in both the macro- and microcirculation subsystems (see e.g., Feihl et al., 2009). The monitoring and analyses of large vessels characteristics (such as the arteries) provide a good vital biomarker to assess the status of macrocirculation. Thus, pulse wave velocity (PWV) is a measure of arterial stiffness. The latter is considered as an important predictor of cardiovascular events (Pereira et al., 2014). On the other hand, assessment of microvascular blood flow has been recognized as important for the follow-up of pathologies such as diabetes or Raynaud's phenomenon, but also to analyze the effect of aging (Li et al., 2006b; Tsuda et al., 2014). Thus, it has been shown that age changes the morphology and quantification of the cutaneous microvasculature(Li et al., 2006b,a). Moreover, age is a primary risk factor for cardiovascular disease (Najjar et al., 2005).

Studying the relationship between macro- and microcirculation may lead to an early estimation of many disorders in the cardiovascular system. Several authors emphasized that the two subsystems, macrocirculation and microcirculation, must be taken into account simultaneously (Feihl et al., 2009).

In this section, we propose to analyze the impact of age on data recorded simultaneously from the macrocirculation (PWV) and the microcirculation (LSCI) in healthy subjects. The analysis in healthy subjects is important as it is the first step before an analysis in pathological subjects. Our goals are therefore the following: study the evolution with age of 1) the possible correlation between PWV and LSCI microvascular perfusion; 2) the possible correlation between PWV and microvascular MBCV extracted from LSCI data; 3) the possible correlation between microvascular perfusion and microvascular red blood cells velocity extracted from LSCI data. Furthermore, for the three above mentioned items, three physiological states are analyzed: rest, vascular occlusion, and post-occlusive reactive hyperaemia peak.

The same two age groups as mentioned previously in Sec. 4.6 were included in this study: the younger group ($n = 8$, 20–30 years old) and the older group ($n = 8$, 50–62 years old).

This study was conducted under the same general procedure as mentioned above in Sec. 4.3, where a model of Lorentzian velocity distribution and a ROI of 5×5 pixels were used to compute MBCV. Contrast and perfusion were computed from Eqs. 4.4 and 4.6, respectively. For the recordings of the PWV signals, a Mobil-O-Graph (Ambulatory

Table 4.14 – Average values of ρ computed from Eq. (4.8) in two groups (young and elderly) of eight subjects in each group.

young	elderly
0.94 ± 0.04	0.94 ± 0.06

Blood Pressure and 24h PWA monitor, Germany) was used. The PWV was recorded for each subject, at rest, at the forearm level.

Results and discussion When using Eq. (4.8), the values of ρ obtained for each population are mentioned in Table 4.14. We observe that the average value of ρ for the younger group does not differ significantly from the one obtained with the elderly subjects. With these ρ values and during post-occlusive reactive hyperaemia, we observe a strong correlation between perfusion and age and between velocity and age, as well as between PWV and age at rest (R^2 equal to 0.67, 0.63, 0.91 respectively). For $\rho = 1$ in the computation of the velocity values, we also obtain a strong correlation between velocity and age (R^2 equal to 0.72). Our first findings are therefore that the studied parameters of microcirculation and macrocirculation are correlated with age.

Moreover, Fig. 4.3 shows the evolution of microvascular blood cells velocity with perfusion for the three physiological states (rest, vascular occlusion, and post-occlusive reactive hyperaemia), and for all the subjects, when the static scatterers effect is neglected ($\rho = 1$). From this figure, we observe that moving blood cell velocity values increase with perfusion values. We also note a strong correlation between them ($Velocity = 0.21 \times Perfusion^{1.27}, R^2 = 0.98$). Moreover, we note that the highest moving blood cells velocity values (and therefore the highest perfusion values) are obtained for the aged subjects during post-occlusive reactive hyperaemia. When $\rho = 1$, strong correlations are also obtained between perfusion values obtained during post-occlusive reactive hyperaemia and PWV values (see Fig. 4.4), as well as between moving blood cells velocity obtained during post-occlusive reactive hyperaemia and PWV values (see Fig. 4.5): for perfusion values recorded during post-occlusive reactive hyperaemia and PWV we have: $Perfusion = -2.4 \times PWV^2 + 46.3 \times PWV - 74.9, R^2 = 0.76$; for moving blood cells velocity recorded during post-occlusive reactive hyperaemia and PWV we have: $Velocity = -4.4 \times PWV^2 + 72.3 \times PWV - 184.7, R^2 = 0.77$. For the other physiological states (rest and biological zero), the correlation is much lower ($R^2 < 0.3$).

PWV is a measure of arterial stiffness (Wilkinson et al., 1998) and it is recognized that it increases with age. Our results regarding PWV are therefore in accordance with

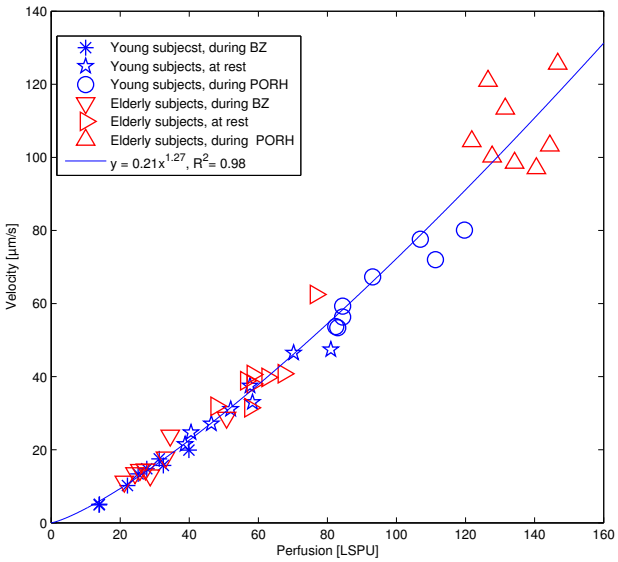

Figure 4.3 – Moving blood cells velocity values and perfusion values computed from LSCI data for 16 subjects, at rest, during vascular occlusion, and post-occlusive reactive hyperaemia. Curve shows line of best fit by least squares.

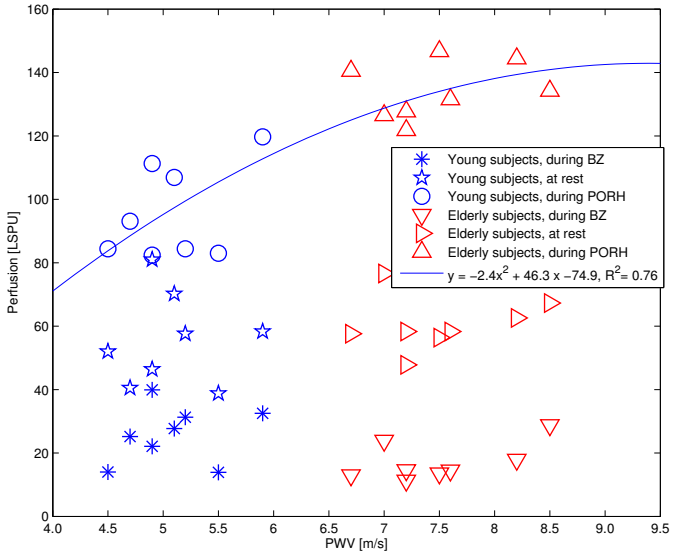

Figure 4.4 – LSCI perfusion values, at rest, during vascular occlusion, and post-occlusive reactive hyperaemia and PWV values, for 16 subjects. Curve shows line of best fit by least squares for data recorded during post-occlusive reactive hyperaemia.

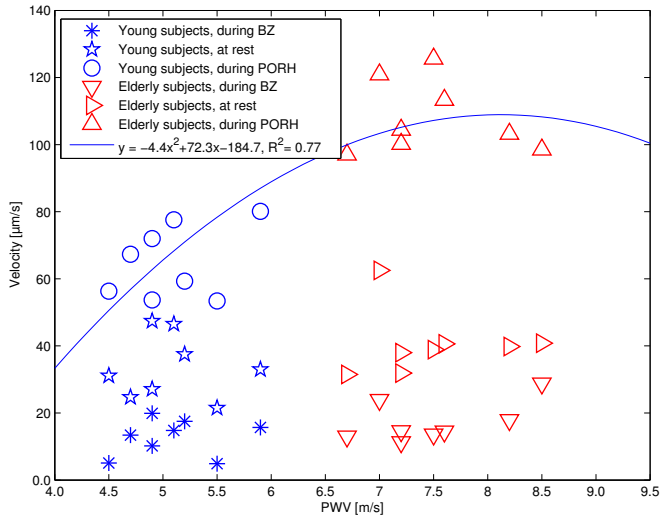

Figure 4.5 – Moving blood cells velocity values computed from LSCI data, at rest, during vascular occlusion, and post-occlusive reactive hyperaemia and PWV values, for 16 subjects. Curve shows line of best fit by least squares for data recorded during post-occlusive reactive hyperaemia. The value of ρ has been set to 1.

Table 4.15 – Correlation values computed between velocity and PWV when LSCI data are recorded at rest, vascular occlusion, and during reactive hyperaemia. PWV is recorded at rest.

ρ	$\rho = 1$			ρ computed from Eq. (4.8)		
Biological state	Rest	BZ	PORH	Rest	BZ	PORH
Correlation between velocity and PWV	0.13	0.29	0.77	0.11	0.32	0.71

what was expected. Stiffness being higher for aged people, the revascularization of vessels after the vascular occlusion (PORH) may lead to higher moving blood cells velocity values. The effect of static scatterers on the correlation R^2 values between moving scatterers velocity and PWV is shown in Table 4.15. From this table we observe that the correlation values do not vary much in the presence or absence of static scatterers.

Studies have reported an attenuated vasodilator response of skin microcirculation to a variety of stimuli, with age (Hagisawa et al., 1991; Minson et al., 2002; Holowatz et al., 2003; James et al., 2006). This attenuation is thought to be the result of endothelial dysfunction (Gates et al., 2009). Thus, Tikhonova *et al.* recently reported a higher increase of perfusion in young people compared to aged subjects after an occlusion removal (Tikhonova et al., 2013). Hagisawa *et al.* reported the same conclusion some years before (Hagisawa et al., 1991). These findings are different from ours: during post-occlusive reactive hyperaemia we found the highest perfusion values for the aged subjects. The discrepancy may be explained by differences in at least three parameters: 1) to monitor microvascular blood flow Tikhonova *et al.*, as well as Hagisawa *et al.*, employed a different technique from the one used in our work: they used laser Doppler flowmetry while we used LSCI. These two techniques do not probe the same volume of tissue (laser Doppler flowmetry probes deeper than LSCI) (O'Doherty et al., 2009); 2) the age ranges studied are different: Tikhonova *et al.* studied a group composed of people between 19-30 years old and another group composed of people between 30-60 years old (Tikhonova et al., 2013). Hagisawa *et al.* studied a group composed of people between 22-27 years old and another group composed of people between 62-68 years old (Hagisawa et al., 1991). In our younger group, people were between 20 and 30 years old whereas in our older group people were between 50 and 62 years old; 3) the effect of fitness. It has been reported that effect of fitness has an influence on the peak of post-occlusive reactive hyperaemia: Tew *et al.* found a higher post-occlusive reactive hyperaemia peak in aged fit participants than in active young subjects, and post-occlusive reactive hyperaemia peak in active subjects was higher than for seden-

tary aged subjects (Tew et al., 2010). The latter study was conducted through laser Doppler flowmetry signals. Moreover, microvessel function is worse in older sedentary compared with older active or younger men, and this is attributable to impaired nitric oxide signalling (Black et al., 2008). Other factors may also explain the differences between our results and the ones of Tikhonova *et al.*, as medical drugs (e.g., at age-specific and hormone replacement therapy) and other vasoactive substances. Furthermore, it has previously been reported that gender has an impact on microcirculation (Hodges et al., 2010), which was not studied in this work.

4.7 Conclusion

The process of *in vivo* LSCI data acquired on the forearm skin demonstrates the following essential points:

— the analysis of the effect of static scatterers on moving blood cells velocity from LSCI data shows that the static scatterers (such as skin) play an important role in the determination of moving blood cells velocity values. The more the static scatterers, the higher the value of moving scatterers velocity.

— the impact of age on the velocity of red blood cells can be studied from LSCI data. Our results show that elderly subjects have statistically significant higher red blood cells velocity values during post-occlusive reactive hyperaemia compared to young subjects.

— in healthy subjects, perfusion and moving blood cells' velocity, two correlated and age-related parameters of microcirculation, are correlated with PWV, a marker of arterial stiffness at the macrovascular level.

Finally, in our work Eq. 4.4 was used to determine moving blood cells velocity values when a Lorentzian velocity profile is assumed, whereas Eq. 4.5 was used to determine moving blood cells velocity values when a Gaussian velocity profile is assumed. It could now be interesting to compare our results with the ones given by the other models presented in Sec. 3.4.1. Moreover, our velocity values could be compared with those given by other acquisition techniques. Alternatively, further works should be performed in diseased patients. It might be of interest to study the relationship between macro- and microcirculation in diseased patients, to show whether the correlation between these two subsystems still exists and to try to define new criteria for different diseased states. The latter could lead to modifications in patients treatment. For example, it has been shown in diabetic patients that PWV is predictive of cardiovascular mortality (Djaberi et al., 2008). It could be of interest to study if microcirculation parameters can also predict this

risk and to assess the time-course of the modifications of microcirculation parameters. Do these modifications appear earlier than PWV modifications? Do microcirculation markers (perfusion or moving blood cells velocity or both) assessed by optical laser devices predict better the cardiovascular mortality? Do clinicians have interest to perform both methods to characterize patients risk?

5

Impact of aging on microvascular perfusion through a nonlinear analysis of LSCI data

By applying entropy-based complexity measures to LSCI time series, the objective of this chapter is to present our work to study the impact of aging on the microcirculation by measuring the complexity of microvascular signals over multiple time scales. For this purpose, forearm skin microvascular blood flow was studied with LSCI in two age groups (younger and older). To estimate age-dependent changes in microvascular blood flow, we applied three entropy-based complexity algorithms to LSCI time series. The results show that the method used for measuring the complexity of LSCI time series can differentiate younger from older groups: the data fluctuations in the younger group have a significantly higher complexity than those obtained from the older group.

Contents

5.1 Introduction

To assess the microcirculation function, a critical task is to obtain relevant physiological information from medical images. Therefore, the application of information theory analysis such as the concept of entropy (a measure of the disorder, see below) has been introduced as a useful tool for the the investigation of physiological signals (see Blokh and Stambler, 2016, for review). Consequently, many signal and image processing methods have been proposed in order to allow a better understanding of the underlying physiological characteristics. Among these methods, the sample entropy computation has become of great interest in the biomedical field (Richman and Moorman, 2000). It has been used to measure the regularity of physiological time series (Chen et al., 2009; Humeau et al., 2008; Hornero et al., 2006). However, sample entropy is a single scale analysis, whereas the cardiovascular system manifests in multiple temporal scales to increase its adaptive capacity in an evolving environment. Hence, the complexity of the cardiovascular system operates in multiple temporal scales. Therefore, single scale entropy analyses do not provide multiple level information on the behavior of the complex physiological system. To overcome this drawback, multiscale entropy (MSE, see Sec. 5.3) has been introduced as a useful tool to process physiological signals in multiple time scales (Costa et al., 2005, 2002). MSE relies on the same principles as sample entropy statistics. MSE analyses are widely used on data recorded from the macrocirculation for the diagnosis of different kinds of pathologies, but also to analyze

the impact of aging (Costa et al., 2005, 2008; Trunkvalterova et al., 2008; Escudero et al., 2006). The MSE algorithm has also been applied by Humeau-Heurtier *et al.* (Humeau-Heurtier et al., 2013b, 2014b) to LSCI data obtained from the microvascular system. In their studies, the efforts were made to better understand the perfusion time series given by LSCI. However, no study related to aging was performed. The aging processes are multiparametric with nonlinear relations between these parameters (Blokh and Stambler, 2016). Thus, the application of nonlinear analyses to LSCI data might be reasonable for the investigation of aging process. In addition, in chapter three, we analyzed the aging effect over microvascular parameters (perfusion and moving blood cells velocity from LSCI data) and macro-circulation parameters (pulse-wave velocity), and the relationship between these parameters. The signal processing tools used were different from the ones proposed in this chapter. The impact of aging on the microcirculation has not been studied yet by using entropy-based complexity algorithms on LSCI data. The latter having good temporal and spatial resolutions, they could be of interest in the follow-up of age-dependent microvascular alterations. Other laser-based studies have been conducted to study the influence of age (Knight et al., 2010). Therefore, by processing laser speckle contrast images, our purpose is to determine if alterations of microcirculation caused by aging can be studied through complexity measures. For this purpose, we applied MSE and its refined versions, composite MSE (CMSE), and refined CMSE (RCMSE) to LSCI time series. Furthermore, a comparison of the results given by MSE, CMSE, and RCMSE algorithms is proposed.

In what follows, the measurement procedure and theoretical background are introduced in Sections 5.2 and 5.3, respectively. The experimental results are presented in Section 5.4. Then, a discussion is proposed in Section 5.5. Finally, conclusions are given in Section 4.7.

5.2 Materials

5.2.1 Subjects

Eighteen healthy subjects without known history of disease were included in this study. The subjects were divided into two age groups: younger and older. The younger group included nine subjects (five women and four men), ranging from 20 to 30 years. The older group included nine subjects (five women and four men), ranging from 50 to 68 years. Prior to participation, all subjects gave their written, informed consent, and the study was conducted in accordance with the Declaration of Helsinki.

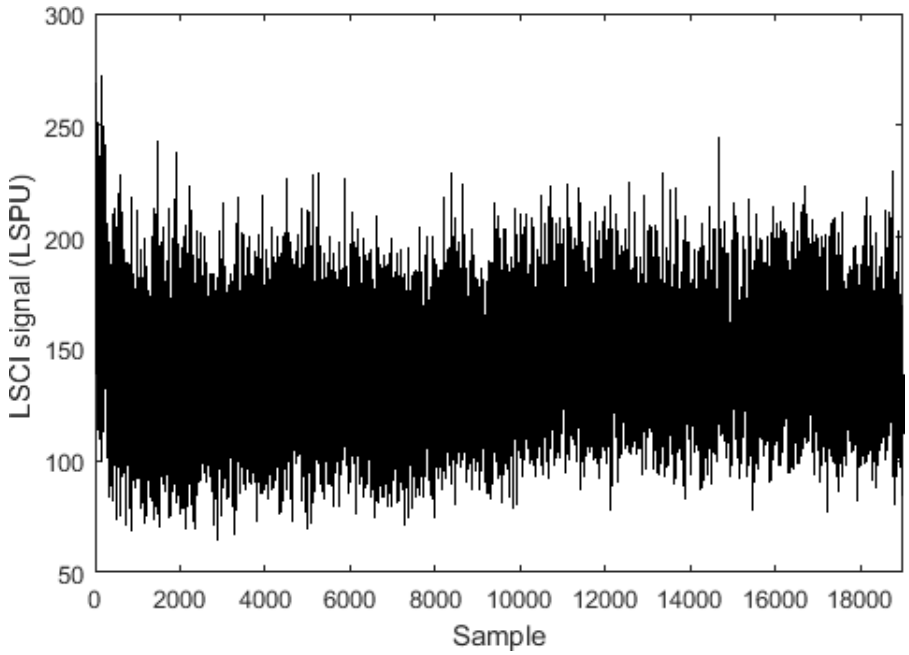

Figure 5.1 – Relative blood flow time course computed from LSCI data during 20 min at rest. LSCI signal computed from a region of interest of 31×31 pixels.

5.2.2 Experimental protocol

For the application of MSE, CMSE, and RCMSE to LSCI time series, all the perfusion images were acquired from the ventral face of the forearm using a PeriCam PSI System (Perimed, Sweden). The imager has a laser wavelength of 785 nm and an exposure time of 6 ms. In this imager, the speckle pattern in the illuminated area is monitored using a 1388×1038 pixels CCD camera (Perimed, Sweden), and the contrast is thereafter computed spatially. Perfusion (computed from the inverse of the contrast K as shown previously in Eq. 4.6) is processed in this work.

The laser speckle contrast imaging technique is, by definition, very sensitive to movements. Therefore, the subjects were asked to be supine and avoid moving during the data acquisition. Before processing the LSCI data with the entropy-based measures, no pre-processing was performed to remove the possible presence of outliers (we took care to check that outliers, if present, were very few and of low amplitude, see Fig. 5.1).

The superficial blood flow was recorded in laser speckle perfusion units (LSPU) with a sampling frequency of 16 Hz. A temperature-controlled room (Abraham et al., 2013) without any airstream (Mahé et al., 2011a) was used for this purpose. Moreover, the distance between the laser head and the forearm skin was adjusted to 15 ± 1 cm (Mahé

et al., 2011b) which provided images with a resolution of around 0.45 mm. Perfusion images were stored on a computer for an off-line analysis.

In this work, 19000 perfusion images (around 20 minutes) for each subject were processed. This length has been chosen to have access to low frequency oscillations already found in other microvascular data (Stefanovska et al., 1999; Bracic and Stefanovska, 1999; Kvandal et al., 2006).

5.3 Methods

5.3.1 Image processing procedure

In order to analyze the complexity of LSCI time series, the following image processing steps were used:

1. On the first perfusion image of each subject, one pixel was chosen arbitrarily, and its perfusion was followed in time for all the 19000 successive perfusion images

2. An average perfusion value was computed inside a ROI around each of the pixels chosen in step 1 in order to get a reasonable signal and reduce the spatial variability of blood flow (Rousseau et al., 2011b). This resulted in a new time evolution signal. For this purpose, ROI of different sizes were analyzed as suggested by (Humeau-Heurtier et al., 2013b): 1×1 pixel, 3×3 pixels, 9×9 pixels, 15×15 pixels, 23×23 pixels, and 31×31 pixels. A previous work (Humeau-Heurtier et al., 2013b) has reported that MSE values for ROI sizes larger than 23×23 pixels are close to the ones obtained with an ROI of size 23×23 pixels. This is why the largest ROI size chosen in our work was not larger than 31×31 pixels

3. For each ROI size (1×1, 3×3, 9×9, 15×15, 23×23, and 31×31 pixels), MSE, CMSE, RCMSE values were estimated and presented as a function of scale factor, τ

5.3.2 What is entropy?

The entropy is the main concept of information theory. It is a measure of the *"disorder"* of the energy of a collection of particles. For a given discrete random variable Y with possible values $\{y_1, y_2, \therefore, y_M\}$ and with probabilities $\{p_1, p_2, \therefore, p_M\}$, entropy is defined as (Shannon, 1949)

$$H(Y) = \sum_{i=1}^{M} p_i \log_2(\frac{1}{p_i}) \ , \tag{5.1}$$

where P_i is the probability of outcome y_i occurring in the set of possible outcomes M.

The entropy values range is $0 \leq H(X) \leq \log_2 M$. Therefore, $H(Y)$ is equal to zero if and only if the random variable Y has only a single outcome. This case is so-called a certain event. In contrast, the greatest entropy value occurs when the random variable Y has the outcomes of equal probability. In other words, the probability of all the possible outcomes equals $1/M$. This means, with increasing the outcomes of Y, the uncertainty to predict a particular event increases.

In this way, the entropy is the information theoretical measure of uncertainty of a random variable. The uncertainty can likewise be described as "variability" or "irregularity".

The measure of entropy serves for the description of the state of particular system at any particular point in time using "time series" methodology. The use of time series for prediction of dynamic behavior of system in time will be detailed in the next section.

5.3.3 Multiscale entropy

The MSE approach aims at evaluating the underlying complexity of the dynamic system across multiple time scales. In this study, MSE was computed as initially introduced (Costa et al., 2002). For a given one dimensional vector of data, $\{x_1, ..., x_i, ...x_N\}$, groups of successive points are time-binned to create a coarse-grained time series, $\{y^{(\tau)}\}$. For this purpose, the original times series are subdivided into nonoverlapping groups of length τ. Then, an average of the data points inside each group is performed (see Fig. 5.2). The steps mentioned above to generate a coarse-grained time series are accomplished using the equation

$$y_j^{(\tau)} = \frac{1}{\tau} \sum_{i=(j-1)\tau+1}^{j\tau} x_i, \qquad 1 \leq j \leq N/\tau. \tag{5.2}$$

Finally, each coarse-grained time series is evaluated by computing an entropy measure (sample entropy, SampEn) (Richman and Moorman, 2000). The result is displayed versus the scale factor, τ.

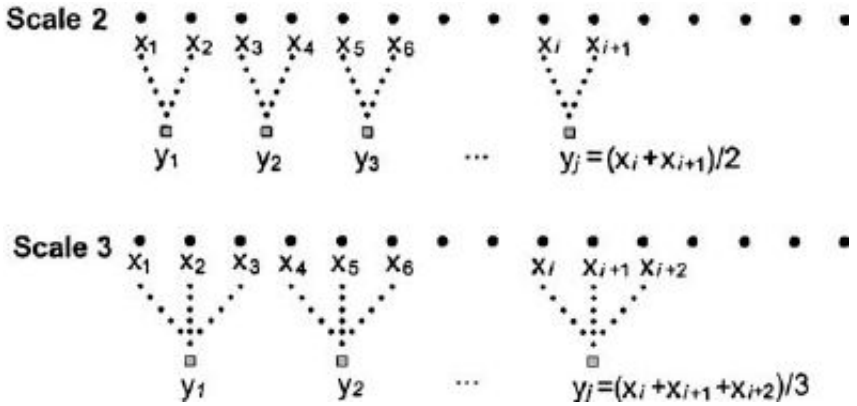

Figure 5.2 – Schematic illustration of the coarse-graining procedure of MSE for scale factors 2 and 3 (Costa et al., 2003).

The sample entropy reflects the conditional probability that two embedded subsets that are close to each other for m successive points, within a given tolerance r, will also remain close to each other if one more point is embedded to each subset. For data of N samples, $N-m$ vectors $x_m(i)$ are constructed for $\{i|1 \leq i \leq N-m\}$ as $x_m(i) = \{x(i+k) : 0 \leq k \leq m-1\}$. The distance d between two vectors $x_m(i)$ and $x_m(j)$ is defined as $d\left[x_m(i), x_m(j)\right] = max\{|x(i+k) - x(j+k)| : 0 \leq k \leq m-1\}$. Then, $B_i^m(r)$ is computed as $(N-m-1)^{-1}$ times the number of vectors $x_m(j)$ within r of $x_m(i)$ where j ranges from 1 to $N-m$ and $j \neq i$ (self-matches are excluded). $B^m(r)$ is thus determined as

$$B^m(r) = (N-m)^{-1} \sum_{i=1}^{N-m} B_i^m(r), \tag{5.3}$$

where

$$B_i^m(r) = \frac{n_i^m(r)}{(N-m-1)}, \tag{5.4}$$

$B^m(r)$ is the probability that two sequences will match for m points, and $n_i^m(r)$ represents the number of vectors $x_m(j)$, such that $d\left[x_m(i), x_m(j)\right] \leq r$. $B^{m+1}(r)$ is the probability that two sequences will match for $m+1$ points, and is computed in the same way as in Eq. 5.3. The sample entropy $(SampEn(m,r))$ is then defined as

$$SampEn(m,r) = \lim_{N \to +\infty} \left\{ -\ln \left[\frac{B^{m+1}(r)}{B^m(r)} \right] \right\}. \tag{5.5}$$

For finite N, it is estimated by the statistics as (Richman and Moorman, 2000)

$$SampEn(m, r, N) = -\ln\left[\frac{B^{m+1}(r)}{B^{m}(r)}\right]. \tag{5.6}$$

The SampEn algorithm has proved to be useful for relatively short and noisy datasets (Richman and Moorman, 2000). Thus, for the coarse-grained time series mentioned in Eq. 5.2,

$$MSE(x, \tau, m, r) = -\ln\left(\frac{n_{\tau}^{m+1}}{n_{\tau}^{m}}\right), \tag{5.7}$$

where n_{τ}^{m} represents the total number of m-dimensional matched vector pairs and is constructed from the coarse-grained time series at a scale factor of τ.

In the MSE algorithm, estimated values of SampEn are plotted *versus* the scale factors, τ. These entropy values are used for assessing the complexity degree of normalized time series. An increasing or consistent behavior of the entropy values *versus* an increase in scale factors indicates that the original time series is highly complex, containing information over multiple time scales. In contrast, a decrease in entropy values with scale factors shows that the original time series carries information only on the smallest scales.

Two important parameters have to be considered during the estimation of SampEn values: the tolerance degree r, and the pattern length m. Previous studies have shown that $m = 1$ or 2, and $r = [0.1, 0.25]$ of the standard deviation of the original signal are adequate to obtain good statistical validity for SampEn (Richman and Moorman, 2000). As used previously for microvascular data studies (Humeau et al., 2011, 2010), $m = 2$, and $r = 0.15 \times$ standard deviation of the signal were chosen herein. Furthermore, in order to reveal microvascular physiological activities, acting in a time scale interval τT of 6.625–105.25 s (Stefanovska et al., 1999; Bracic and Stefanovska, 1999; Kvandal et al., 2006), a wide range of scale factors was analyzed: scale factors τ ranging from 106 to 1684.

Finally, it has recently been reported that SampEn depends on the relation between the frequency of the studied dynamics and sampling rate (Liao and Jan, 2016). A modified SampEn has been proposed to reflect the degree of regularity of time series regardless of sampling rate. It has been shown that the modified SampEn yields more consistent results than SampEn (Liao and Jan, 2016).

5.3.4 Composite multiscale entropy

CMSE was introduced to reduce the variance of estimated entropy values of MSE at large scale factors τ (Wu et al., 2013b). Unlike MSE, CMSE generates k-child coarse-grained time series for each scale factor τ (see Fig. 5.3). So, for a given discrete time series $\{x_1, ..., x_i, ...x_N\}$, the kth-child coarse-grained time series for scale factor τ is produced as (Wu et al., 2013b) $y_k^{(\tau)} = \{y_{k,1}^{(\tau)} \ y_{k,2}^{(\tau)} ... y_{k,p}^{(\tau)}\}$ where

$$y_{k,j}^{(\tau)} = \frac{1}{\tau} \sum_{i=(j-1)\tau+k}^{j\tau+k-1} x_i, \qquad 1 \leq j \leq N/\tau, 1 \leq k \leq \tau. \tag{5.8}$$

Then, for each scale factor τ, sample entropy values are estimated for all k-child coarse-grained groups. The mean value of the τ entropy values corresponds to CMSE (Wu et al., 2013b).

$$CMSE(x, \tau, m, r) = \frac{1}{\tau} \sum_{k=1}^{\tau} \left(-\ln \frac{n_{k,\tau}^{m+1}}{n_{k,\tau}^{m}} \right), \tag{5.9}$$

where $n_{k,\tau}^{m}$ is the total number of m-dimensional matched vector pairs and is computed from the kth-child coarse-grained time series at a scale factor τ. Different from MSE, the CMSE algorithm provides higher entropy reliability on both synthetic and real data (Wu et al., 2013b).

5.3.5 Refined composite multiscale entropy

Although CMSE provides higher reliability in entropy estimation than traditional MSE, the probability that CMSE fails to produce an estimate of the entropy becomes higher when the complexity measure is applied to short time series. To overcome this drawback, RCMSE was proposed (Wu et al., 2014). From Eq. (5.9), we can observe that when CMSE is computed, undefined entropy is obtained when either $n_{k,\tau}^{m+1}$ or $n_{k,\tau}^{m}$ is zero. Thus, the shorter the time series, the more the probability of having an undefined entropy. Consequently, CMSE has better accuracy estimation than traditional MSE, but at the expense of entropy estimation ability. Therefore, RCMSE addresses this drawback based on the following equation (Wu et al., 2014)

$$RCMSE(x, \tau, m, r) = -\ln \left(\frac{\sum_{k=1}^{\tau} n_{k,\tau}^{m+1}}{\sum_{k=1}^{\tau} n_{k,\tau}^{m}} \right). \tag{5.10}$$

From Eq. (5.10), it is obvious that RCMSE gives rise to undefined entropy only when all $n_{k,\tau}^{m+1}$ or $n_{k,\tau}^{m}$ are zero. Accordingly, RCMSE increases the ability to estimate

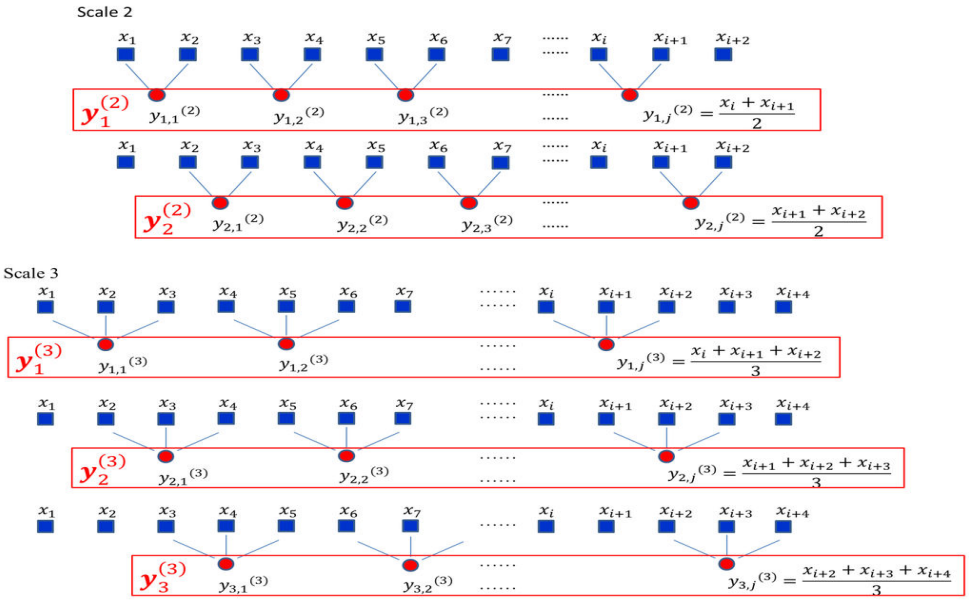

Figure 5.3 – Schematic illustration of the coarse-graining procedure of CMSE for scale factors 2 and 3 (Wu et al., 2013b).

entropy values compared to CMSE. RCMSE shows a lower variability and data-length dependence than either the MSE or CMSE algorithms when applied to white and and $1/f$ noises (Wu et al., 2014).

5.3.6 Statistical analysis

For the two populations (young subjects and old subjects) the sum of RCMSE values over the scales studied (106 to 1684; see below) was computed, and this for all the ROI sizes studied: 1×1 pixel, 3×3 pixels, 9×9 pixels, 15×15 pixels, 23×23 pixels, and 31×31 pixels. This gave an index for the two populations, and for each ROI size. A statistical analysis was performed on this index to compare the results between the young subjects and the older ones, for each ROI size.

Because of the small size of the sample (only 9 subjects in each group), the normality of the distribution (RCMSE index) for each ROI was checked using Shapiro-Wilk test. The results showed normal distribution for younger and older groups, and for all ROI sizes. Therefore, statistical analyses were performed using a t-test analysis (unpaired, two-tailed) to compare the complexity index of the young group with the one of the old group after checking for the equality of variances (F-test).

For all statistical analyses, a two-tailed p value < 0.05 was considered significant.

5.4 Results

Figure 5.4a shows the mean experimental results for MSE, CMSE, and RCMSE, for the two groups of subjects, when the value of a LSCI single pixel time series is analyzed. From this figure we can observe that the entropy values obtained from the younger group (blue) and from the aged group (red) are close to each other for all time scales (binning time interval τT = [6.6–105.2] s). This is true for MSE, CMSE, and RCMSE. Furthermore, a monotonic decrease in entropy values versus time scale is observed for the two groups. The reduction in entropy values at large time scales, τT, shows that the analyzed signal is an independent random variable, containing information only at the smallest time scales. This behavior is close to the one of a Gaussian white noise realization (Costa et al., 2002). For the analysis of Gaussian white noise data, as the length of the windows used to build coarse-graining time series signal increases, the average value inside each window converges to a fixed value, because no new pattern arises on large scales. Hence, the standard deviation dramatically diminishes with scale factor. The same is found for MSE, CMSE, and RCMSE of LSCI single pixel time series. This reflects that the LSCI single pixel time series have information only at the shortest scales. However, it is worth mentioning that the application of MSE to LSCI data shows small and rapid variations in entropy values when time scales large enough are analyzed. This behavior can be observed when either single pixel or ROI are analyzed (see Figs. 5.4a to 5.4f). In contrast, CMSE and RCMSE manifest a relatively stable decrease during the increase of time scales.

A markedly loss of complexity is observed with aging when a ROI large enough is chosen (see Fig. 5.4f). The difference is hardly visible with a ROI size of 3×3 pixels (see Fig. 5.4b) and increases when ROI size increases (see Fig. 5.4f). There were no significant differences between the younger and older groups on the entropy index values obtained from RCMSE of LSCI single pixel and 3×3 pixels ($p = 0.649$, and $p = 0.259$, respectively). In contrast, the entropy index values of RCMSE LSCI 9×9 pixels, 15×15 pixels, 23×23 pixels, and 31×31 pixels for the younger group are significantly different from the ones obtained from older group ($p = 0.02, p = 0.008, p = 0.007$, and $p = 0.008$, respectively).

From Fig. 5.4a, we observe that when MSE and CMSE are applied to experimental LSCI single pixel time series, the probability of undefined entropy was zero. This was not the case after a spatial averaging over neighboring pixels (see Figs. 5.4b to 5.4f). It is obvious from these figures that the validity of both MSE and CMSE is worse when larger scale factors are used. Therefore, the probability that the entropy estimate will be undefined increases as the scale factor increases. It has been shown that the probability that the estimate of MSE and CMSE is undefined increases as the entropy of the time series increases (Wu et al., 2014). In MSE, when large scale factors are used

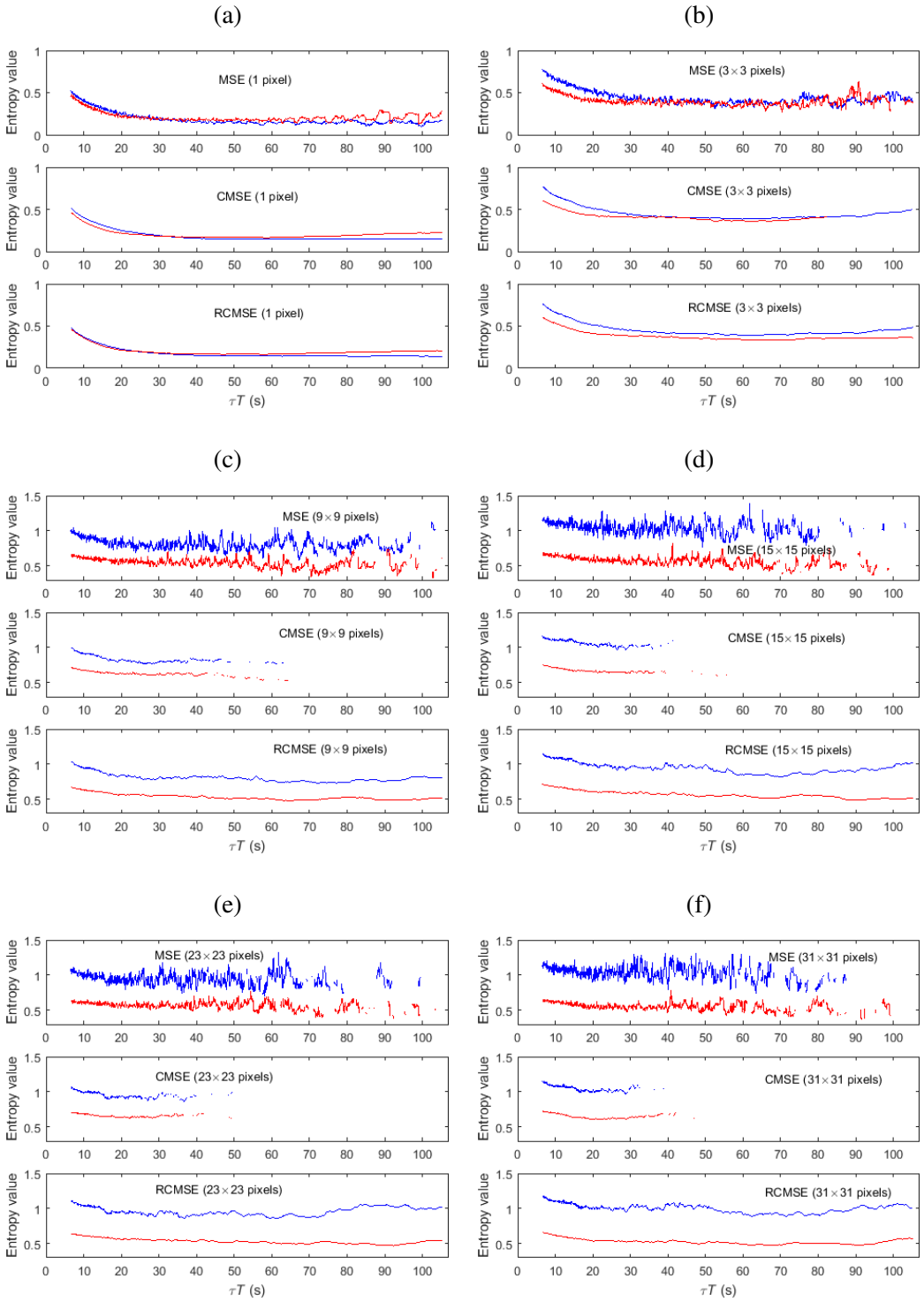

Figure 5.4 – Mean experimental entropy values for the two healthy groups of subjects: younger group (blue) and older group (red) with 9 subjects in each group. For each subfigure, three methods are shown: MSE (top), CMSE (middle), and RCMSE (bottom). Results for LSCI times series are obtained from (a): 1×1 pixel; (b): 3×3 pixels; (c): 9×9 pixels; (d): 15×15 pixels; (e): 23×23 pixels; (f): 31×31 pixels. A scale factor interval from $\tau = 106$ to $\tau = 1684$ is analyzed, which provides a binning time interval from $\tau T = 6.625$ s to $\tau T = 105.25$ s.

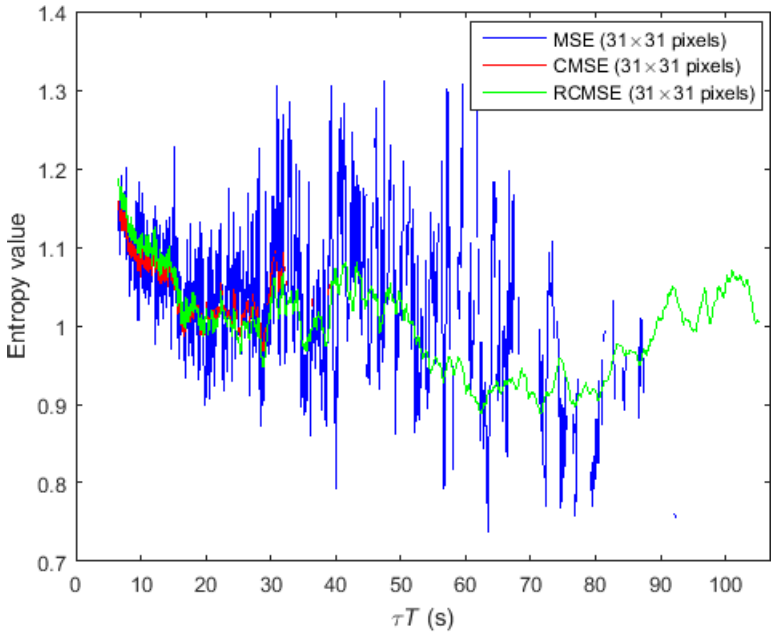

Figure 5.5 – Average values for MSE, CMSE, and RCMSE of LSCI time series (ROI of size 31×31 pixels) recorded on 9 healthy young subjects. A scale factor interval from $\tau = 106$ to $\tau = 1684$ is analyzed, which provides a binning time interval from $\tau T = 6.625$ s to $\tau T = 105.25$ s.

to build the coarse-grained time series, the variance increases very fast that may lead to underestimation of entropy (i.e., spike increases observed in entropy values over all the patterns of the MSE), or even undefined entropy values—no template vectors are matched to one another. In contrast, CMSE reduces the variance. This leads to more accurate estimation of entropy values (Wu et al., 2013b). As it is obvious from Figs. 5.4b to 5.4f that CMSE gradually provides higher entropy reliability, and better separability between younger and older groups than MSE. However, CMSE increases the probability of undefined entropy due to the reasons mentioned in Sec. 5.3, in particular for large time scales (Wu et al., 2014). By opposition, and as shown in Fig. 5.5, RCMSE shows better validity than MSE and CMSE. Therefore, in what follows, RCMSE will be used to present the remaining findings due to its better validity compared to MSE and CMSE.

Within the range of time scales analyzed, one can hypothesize that the strong rhythmic behavior of the peripheral cardiovascular activities may lead to low entropy values. Therefore, peripheral cardiovascular activities could be identified according to their regularities and time-related values. In this respect, we can distinguish two physiologically-linked areas over the pattern of RCMSE, extending between 6.625 s and 105.25 s for the younger subjects (see Fig. 5.6). First, the entropy values reach a local minimum for bin-

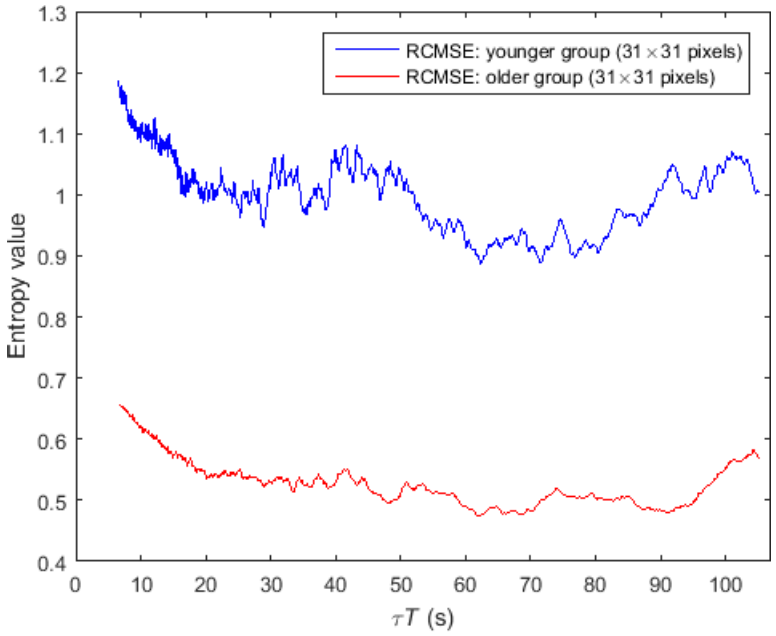

Figure 5.6 – RCMSE of LSCI 31×31 pixels time series recorded on healthy subjects. Results are the mean entropy values of two groups; younger group (blue) and older group (red) of 9 subjects each. A scale factor interval from $\tau = 106$ to $\tau = 1684$ is analyzed, which provides a binning time interval from $\tau T = 6.625$ s to $\tau T = 105.25$ s. This is an enlarged version of the RCMSE plot in Fig. 5.4f.

ning time interval τT around 31–42 s. The temporal fluctuations around this interval are considered as the first area that has high regularity. The second physiologically-related area is observed around binning time interval of 60–80 s. From Fig. 5.6 we observe that for the younger group, the processes acting around this interval of 60–80 s have a high regularity. In contrast, the physiologically-linked areas over the pattern of RCMSE for older group have weaker features. From Fig. 5.6, the first local minimum for the older group can be observed around 48 s, whereas a second global area is between 60–70 s, and another close to 90 s.

5.5 Discussion

From Figs. 5.4a to 5.4f, we have observed that the application of MSE to LSCI data shows small and rapid variations in entropy values when time scales large enough are analyzed. The same behavior of small and rapid variations in entropy values at large scale factors has been observed by the application of MSE to successive signals of a pulse wave velocity (Chang et al., 2014). In MSE, the variance increases as large scale

factors are used to build the coarse-grained time series, that may lead to underestimation of entropy. Furthermore, from Figs. 5.4b to 5.4f, we observe that choosing larger ROI sizes modifies the behavior of MSE, CMSE, and RCMSE. The modifications of MSE, CMSE, and RCMSE trends with ROI show that LSCI ROIs do not behave as Gaussian white noise. The signal-to-noise ratio increases as the ROI increases (Humeau-Heurtier et al., 2013b).

It has been mentioned above from Figs. 5.4b to 5.4f that the validity of both MSE and CMSE is worse when large scale factors are used. This experimental finding is in agreement with the theoretical study of Wu *et al.* (Wu et al., 2014), where correlated and uncorrelated noises were analyzed. They found that the validity degree of the MSE and CMSE depends on the time series length, and entropy values of the time series: the larger the scale factors, the shorter the coarse-grained time series. Our signals contain 19000 data points, and therefore, the shortest coarse-grained time series contain 11 points. As a result to all mentioned above, MSE, CMSE, and RCMSE are able to estimate the underlying complexity of LSCI signals. However, RCMSE provides better validity for short time series.

This study demonstrates that the application of MSE, CMSE, and RCMSE to microvascular data (LSCI time series) can remarkably differentiate between younger and older groups: the fluctuations of the younger group show higher complexity than those obtained from the older group. The loss of complexity within the microvascular blood flow signal may be explained as a consequence of changes occurring within the cardiovascular system. It was previously found that macro- and microcirculation are correlated systems (Khalil et al., 2015). Furthermore, it has been reported that the cardiac fluctuations of healthy young subjects are highly complex, but this complexity decreases with aging (Lin et al., 2014; Beckers et al., 2006; Goldberger et al., 2002; Voss et al., 2009).

A living organism system is a highly complex system. This complexity comes from a wide range of adaptive reactions to different physiological variables within the external environment. Therefore, physiological complexity of the living system reflects its ability to adapt to the ever-changing circumstances, that will be needed to merge multiscale processes. Alternatively, under baseline condition, a continuous decrease in complexity reflects damaged physiological responses of the living organism to changes in the external environment (Costa et al., 2005). By the application of MSE to macrovascular data, a loss of the complexity in cardiac signal has been observed due to aging (Costa et al., 2005). A reduction in signal complexity with aging has also been reported when nonlinear measures are applied to successive signals of a pulse wave velocity (Wu et al., 2011). Furthermore, it has been shown that aging has a crucial role on the interconnection network of the cardiovascular system (Vaillancourt and Newell, 2002; Kaplan et al.,

1991). For example, several modifications in cardiac electrophysiology, including an increase in sympathetic nervous system activity (Seals and Esler, 2000), or alterations in the muscular tissue of the heart, appear with aging (Lakatta and Levy, 2003). Wu *et al.* (Wu et al., 2013a) demonstrated a reduction of complexity with age of both the heart and blood vessels signals. Diminished functional responses to stimuli have been reported by many authors as a distinctive attribute of age-related pathology (Manor and Lipsitz, 2013; Kyriazis, 2003; Lipsitz and Goldberger, 1992). Other authors have recently mentioned that the relation between QT and RR interval variability derived from the heart deteriorates with aging (Baumert et al., 2013). The first finding confirms a general complexity loss with aging on LSCI data (microvascular blood flow). Furthermore, this study demonstrates that the entropy-based complexity measures when applied to microvascular signal (LSCI time series) can differentiate between younger and older groups.

Alterations in microvascular activities with aging have been reported in many previous studies (Tikhonova et al., 2013; Yvonne-Tee et al., 2008). A reduction in the amount of oxygen reaching the tissues, and unbalance in constructive and destructive metabolism processes may occur with aging (Harris and Rumbaut, 2001; Konstantinova et al., 2004; Ogrin et al., 2005). Furthermore, a reduction in functioning capillary numbers, and a defect in their basic functions may appear with aging due to phenomena such as vascular rarefaction, regularity loss, vascular destruction, irregular calibration, and attenuation of angiogenesis processes (Ryan, 2004; Kelly et al., 1995; Noon et al., 1997; Tikhonova et al., 2013; Sadoun and Reed, 2003). It has been pointed out that vascular destruction and oxidant stress contribute to capillary rarefaction (Gates et al., 2009). Aging is associated with inhibition of endothelial function and cellular chemical processes, deterioration of the sympathetic innervation (Bari et al., 2005; Kenney and Munce, 2003). Moreover, aging leads to a deterioration in nitric oxide, prostanoid, endothelium derived hyperpolarizing factor(s) and endothelin-1 pathways (Gates et al., 2009). It has also been shown that collagen and elastic fibers are damaged with aging (El-Domyati et al., 2002; Gilchrest, 1989). Furthermore, one might hypothesize that the reduced complexity of the older group may be connected with age-related structural changes in the skin. It has been reported that a number of physiological features vary with age, including collagen structure, water accumulation, and the thickness of the epidermis, dermis, and the skin as a whole (see Ref. Waller and Maibach, 2005, for review).

It is worth mentioning that, from Fig. 5.6, the profiles of RCMSE of the younger group are slightly different from the ones of the older group. These differences could be due to the following reasons: 1) the movement artifacts. LSCI is highly sensitive to movements. Therefore, it is difficult to have long acquisitions without any movement artifacts. However, it has been shown that a signal contaminated by a small percentage

of outliers may remarkably change the standard deviation but not substantially alter the temporal structure of the time series (Costa et al., 2005). Another algorithm dedicated to signals with outliers could also be used to process LSCI data (Lo et al., 2015); 2) the average entropy values computed from the seven subjects. Each microvascular activity does not fluctuate at exactly the same period time for each subject. These fluctuations may lead to different patterns in entropy values.

In this work, two physiologically-linked areas were identified according to their regularities and time-related values. The first area is related to binning time interval between 31 s and 42 s for younger group, and around 48 s for older group. It has been shown that the neurogenic activities are linked to this time interval of 31–48 s (Söderström et al., 2003; Kvernmo et al., 1999). The second area that has a high regularity is observed around the binning time interval of 60–80 s for younger group, and around 60–70 s, and another close to 90 s for the older group. The interval between 60–90 s has been previously observed in blood flow signals using time-frequency analyses (Stefanovska et al., 1999), and as well as in HRV signals (Bracic and Stefanovska, 1999). The periodic process around this interval is considered as a marker of endothelial activity (Stefanovska et al., 1999).

5.6 Conclusion

This chapter presented the major study of our efforts to analyze the effect of aging on microcirculation of healthy subjects by applying entropy-based complexity measures to LSCI time series. The RCMSE algorithm is able to differentiate the younger group from the older group. RCMSE is a simple method for evaluating the complexity of physiological signals through short time series. It could be interesting now to conduct a similar study on data recorded from another body site (such as the leg or the contralateral forearm). Furthermore, it may be of utility in the clinical research to analyze RCMSE values of LSCI data recorded in pathological subjects.

6

Summary and outlook

In this chapter a summary will be presented on the utility of LSCI data in order to study the impact of aging on the microcirculation as described in this PhD work. An outlook to future improvements and applications of LSCI will also be given.

Contents

6.1 Summary

In this thesis, LSCI were acquired from the forearm skin of healthy subjects in order to study the impact of aging on the microcirculation. Image and signal processing algorithms were used in two different ways to achieve this goal: 1) the study and analysis of microvascular parameters (perfusion and red blood cells velocity) when assumptions on moving scatterers velocity are made; 2) the processing of LSCI data with nonlinear analyses.

In Chap. 4, we addressed two main points:

— the possible impact of static scatterers on moving blood cells velocity computed from the speckle contrast K. For this purpose, two ways were followed. The first way is by simulating the expression of speckle contrast K mathematically. The second way is by computing an experimental value of the fraction of statically scattered light to be used in the speckle contrast K. For these two ways, moving blood cells velocity was computed from speckle contrast K and compared, when the static scatterers effect is taken into account and when it is not. The analysis of the effect of static scatterers on moving blood cells velocity from LSCI data shows that the static scatterers (such as skin) play an important role in the determination of moving blood cells velocity values. The more the quantity of static scatterers, the higher the value of moving scatterers velocity.

— the impact of aging on LSCI data acquired from microcirculation. For this purpose, we analyzed the microvascular parameters (perfusion and velocity) and macrocirculation parameter (PWV) in healthy subjects, subdivided into two age groups (younger and older). The possible relationship between these parameters were also studied. Our results show that the impact of age on the velocity of red blood cells can be studied from LSCI data. The elderly subjects have statistically significant higher red blood cells velocity values during post-occlusive reactive hyperaemia compared to young subjects. This may be due to stiffness of vessels that increases with age. PWV is a measure of arterial stiffness (Wilkinson et al., 1998) and it is recognized that it increases with age. Stiffness being higher for aged people, the revascularization of vessels after the vascular occlusion (post-

occlusive reactive hyperaemia) may lead to higher moving blood cells velocity values.

On the other hand, perfusion and moving blood cells velocity, two correlated and age-related parameters of microcirculation, are correlated with PWV, a marker of arterial stiffness at the macrovascular level.

In Chap. 5 three entropy-based complexity measures were applied to LSCI time series: MSE, CMSE, and RCMSE. The RCMSE algorithm is able to differentiate the younger group from the older group. RCMSE is a simple method for evaluating the complexity of physiological signals through short time series. We found that the data fluctuations in the younger group have a significantly higher complexity than those obtained from the older group. The loss of complexity with age within the microvascular blood flow signal may be explained as a consequence of changes occurring within the cardiovascular system. We have previously mentioned that macro- and microcirculation are correlated systems (Khalil et al., 2015). It has been reported that the cardiac fluctuations of healthy young subjects are highly complex, but this complexity decreases with aging (Lin et al., 2014; Beckers et al., 2006; Goldberger et al., 2002; Voss et al., 2009).

From the clinical point of view, our findings are important because we have shown in healthy subjects that: 1) it is possible to reveal the influence of aging on microvascular blood flow through a signal processing approach performed on laser speckle contrast data; 2) micro- and macrocirculation are correlated systems.

From the scientific point of view, our work is important as we: 1) studied, theoretically and experimentally, the possible impact of static scatterers on the estimation of MBCV from the speckle contrast K; 2) compared the accuracy of three entropy-based algorithms.

The study in healthy subjects allowed us to reveal the utility of LSCI data for assessing the impact of aging on the microcirculation. Age-related changes in skin microcirculation can be attributed to alterations in the circulatory system as a whole. Understanding these changes in microcirculatory system with age may give new insights for prevention and treatment.

6.2 Outlook

In our work Eq. 4.4 was used to determine moving blood cells velocity values when a Lorentzian velocity profile is assumed, whereas Eq. 4.5 was used to determine moving blood cells velocity values when a Gaussian velocity profile is assumed. It could now

be interesting to compare our results with the ones given by other models presented in Sec. 3.4.1. Alternatively, a modified equation of contrast has recently been given by Khaksari and Kirkpatrick (Khaksari and Kirkpatrick, 2016). They demonstrated that the calculated speckle contrast is sensitive to both concentration and the velocity of the scattering particles. Their equation draws a mathematical and physical linkage between random (Lorentzian) and ordered motion (Gaussian) of particles. They claimed that a weighted linear combination of these two models is likely the most appropriate model for relating speckle contrast to particle motion (Khaksari and Kirkpatrick, 2016). It might be preferable to apply such an equation to LSCI data and to compare the results with the ones presented in this manuscript.

In this PhD study, the possible impact of the static scatterers on MBCV values was investigated numerically and experimentally. A more detailed analysis of this issue is needed, in particular, the relationship between the scattering particles concentration and the influence of the static scatterers. For instance, it has recently been shown that the scattering particles concentration seems to be inversely related to the influence of the static scatterers (Khaksari and Kirkpatrick, 2016).

It is worth mentioning that the sample size was different for each study presented in this PhD work. This can be explained as a result of the number of recordings available at the time of each experiment. This PhD work was carried out in parallel with LSCI data acquisition.

Further work should be performed in diseased patients. It might be of interest to study the relationship between macro- and microcirculation in diseased patients, to show whether the correlation between these two subsystems still exists and to try to define new criteria for different diseased states. The latter could lead to modifications in patients treatment. For example, it has been shown in diabetic patients that PWV is predictive of cardiovascular mortality (Djaberi et al., 2008). It could be of interest to study if microcirculation parameters can also predict this risk and to assess the time-course of the modifications of microcirculation parameters. Do these modifications appear earlier than PWV modifications? Do microcirculation markers (perfusion or moving blood cells velocity or both) assessed by optical laser devices predict better the cardiovascular mortality? Do clinicians have interest to perform both methods to characterize patients risk?

In this thesis, entropy-based complexity measures, including MSE, CMSE, and RCMSE were applied to LSCI data to measure the complexity of microcirculation. These methods were performed based on SampEn presented in Sec. 5.3.3. A modified SampEn has recently been proposed (Liao and Jan, 2016). It has been shown that it

yields more consistent results than SampEn (Liao and Jan, 2016). It could be interesting to use the modified SampEn instead of SampEn and to compare the results given by the two entropy algorithms.

On the other hand, it could be interesting now to apply entropy-based complexity measures to data recorded from another body site (such as the leg or the contra-lateral forearm). Furthermore, it may be of utility in the clinical research to analyze RCMSE values of LSCI data recorded in pathological subjects.

The use of nonlinear analyses permits not only to establish the nonlinear correlations between diagnostic parameters of interest, but may also provide a theoretical insight into the nature of aging processes by establishing the measures of variability, adaptation, regulation or homeostasis, within a system of interest (Blokh and Stambler, 2016). Therefore, it might be helpful to increase the use of such measures in research that may considerably increase diagnostic capabilities and the fundamental theoretical mathematical understanding of aging processes.

On the other hand, it has been shown that nonlinear analyses can be applied to study a variety of aging-related diseases such as neurodegeneration and heart diseases (see Blokh and Stambler, 2016, for review). It could be interesting now to apply entropy-based complexity measures to LSCI data in order to study the aging processes under those diseases, and in addition to explore potential anti-aging intervention. It might also be of special importance to use nonlinear analyses methods for the study of aging processes, this facilitate the early diagnosis of diabetes. It has been shown that the diagnostic parameters relevant to diabetes, as well as underlying biological mechanisms, have a great similarity with normal aging processes (Blokh and Stambler, 2014).

The measures of entropy are included in major common analytics software packages such as SPSS and can be used routinely and conveniently. However, most biomedical studies have traditionally relied on linear statistics, without much use of the non-linear, information-theory statistics. It may be hoped that their increased use in research may considerably increase diagnostic and therapeutic capabilities as well as the fundamental theoretical mathematical understanding of aging processes (Blokh and Stambler, 2014).

One of the limitations of our study is the absence of direct comparison with other laser-based techniques such as LDPI. Recently, it has been shown that the perfusion values determined by LDPI are comparable to those from LSCI (Chen et al., 2016). However, it is still suggested that the perfusion range and characteristics of the measured skin should be carefully considered if LDPI and LSCI measures are compared (Chen et al., 2016). Another group found that these two techniques can be related through a

linear relationship if the static speckle effect and exposure time duration are considered (Sun et al., 2016). Therefore, further research is needed to improve the interpretations of these issues before doing a comparison study between LSCI and LDPI.

The essential challenge in LSCI is to model the link between the speckle contrast measure and the perfusion. Therefore, in order to improve the reliability of LSCI, some authors recommended to integrate it with other optical-based techniques such as SDF imaging (Nadort et al., 2016). Furthermore, as recently pointed out by Khaksari and Kirkpatrick (Khaksari and Kirkpatrick, 2016), change in scattering particles concentration may lead to underestimation of moving scatterers velocity when using LSCI. Such a change may emerge from a change in hematocrit level. Typically, a change in hematocrit can be precluded physiologically. However, one could imagine LSCI being utilized as a part of time-course studies where a change in hematocrit is conceivable or when comparing LSCI results between individuals, who may have different hematocrit. In these cases, the results shown by Khaksari and Kirkpatrick (Khaksari and Kirkpatrick, 2016) demonstrated that the scattering particles concentration must be considered in the elucidation of those results.

Finally, several measurement improvements could be made to LSCI to make it more accurate as mentioned earlier in the thesis. Nevertheless, our process on LSCI data provided relevant results and useful elements for the understanding of the impact of aging on microcirculation, and the interactions between micro- and macrocirculation systems.

Bibliography

Abdurashitov, A. S. et al. (2015). Histogram analysis of laser speckle contrast image for cerebral blood flow monitoring. *Front. Optoelectron*, 15:1–8.

Abraham, P., Bourgeau, M., Camo, M., Humeau-Heurtier, A., Durand, S., Rousseau, P., and Mahe, G. (2013). Effect of skin temperature on skin endothelial function assessment. *Microvasc. Res.*, 88:56–60.

Abularrage, C. J., Sidawy, A. N., Aidinian, G., Singh, N., Weiswasser, J. M., and Arora, S. (2005). Evaluation of the microcirculation in vascular disease. *J. Vasc. Surg.*, 42(3):574–581.

Acharya, S., Gurung, D. B., and Saxena, V. P. (2014). Human males and females body thermoregulation: Perfusion effect analysis. *J. Therm. Biol.*, 45:30–36.

Ajmani, R. S. and Rifkind, J. M. (1998). Hemorheological changes during human aging. *Gerontology*, 44(2):111–120.

Aliverdiev, A., Caponero, M., and Moriconi, C. (2002). Speckle velocimeter for a self-powered vehicle. *Tech. Phys.*, 47(8):1044–1048.

Allen, J. and Howell, K. (2014). Microvascular imaging: techniques and opportunities for clinical physiological measurements. *Physiol. Meas.*, 35(7):R91–R141.

Anderson, M. E. et al. (2004). Digital iontophoresis of vasoactive substances as measured by laser Doppler imaging: a non-invasive technique by which to measure microvascular dysfunction in Raynaud's phenomenon. *Rheumatology*, 43(8):986–991.

Armitage, G. A., Todd, K. G., Shuaib, A., and Winship, I. R. (2010). Laser speckle contrast imaging of collateral blood flow during acute ischemic stroke. *J. Cereb. Blood Flow Metab.*, 30(8):1432–1436.

Ayata, C., Dunn, A. K., Gursoy-Özdemir, Y., Huang, Z., Boas, D. A., and Moskowitz, M. A. (2004). Laser speckle flowmetry for the study of cerebrovascular physiology in normal and ischemic mouse cortex. *J. Cereb. Blood Flow Metab.*, 24(7):744–755.

Balaji, G. N. et al. (2014). An efficient view classification of echocardiogram using morphological operations. *J. Theor. Appl. Inform. Tech.*, 67(3).

Bandyopadhyay, R., Gittings, A. S., Suh, S. S., Dixon, P. K., and Durian, D. J. (2005). Speckle-visibility spectroscopy: a tool to study time-varying dynamics. *Rev. Sci. Instrum.*, 76(9):093–110.

Bari, F. et al. (2005). Flow motion pattern differences in the forehead and forearm skin: age-dependent alterations are not specific for Alzheimer's disease. *Microvasc. Res.*, 70(3):121–128.

Basak, K., Manjunatha, M., and Dutta, P. K. (2012). Review of laser speckle-based analysis in medical imaging. *Med. Biol. Eng. Comput.*, 50(6):547–558.

Baumert, M., Czippelova, B., Porta, A., and Javorka, M. (2013). Decoupling of qt interval variability from heart rate variability with ageing. *Physiol. Meas.*, 34(11):1435.

Beckers, F., Verheyden, B., and Aubert, A. E. (2006). Aging and nonlinear heart rate control in a healthy population. *Am. J. Physiol. Heart. Circ. Physiol.*, 290(6):H2560–H2570.

Bentov, I. and Reed, M. J. (2015). The effect of aging on the cutaneous microvasculature. *Microvasc. Res.*, 100:25–31.

Berne, R. M. and Levy, M. N. (1998). The arterial system. *Physiology*, 3:462–463.

Bezemer, R., Legrand, M., Klijn, E., Heger, M., Post, I. C., et al. (2010). Real-time assessment of renal cortical microvascular perfusion heterogeneities using near-infrared laser speckle imaging. *Opt. Express*, 18(14):15054–15061.

Bi, R., Dong, J., and Lee, K. (2013). Deep tissue flowmetry based on diffuse speckle contrast analysis. *Opt. Letters*, 38(9):1401–1403.

Bi, R. et al. (2015). Optical methods for blood perfusion measurementtheoretical comparison among four different modalities. *J. Opt. Soc. Am. A*, 32(5):860–866.

Biniek, K. et al. (2015). Understanding age-induced alterations to the biomechanical barrier function of human stratum corneum. *J. Dermatol. Sci.*, 80(2):94–101.

Binzoni, T., Humeau-Heurtier, A., Abraham, P., and Mahe, G. (2013). Blood perfusion values of laser speckle contrast imaging and laser Doppler flowmetry: is a direct comparison possible? *IEEE Trans. Biomed. Eng.*, 60(5):1259–1265.

Black, M. A., Green, D. J., and Cable, N. T. (2008). Exercise prevents age-related decline in nitric-oxide-mediated vasodilator function in cutaneous microvessels. *J. Physiol.*, 586(14):3511–3524.

Blokh, D. and Stambler, I. (2014). Estimation of heterogeneity in diagnostic parameters of age-related diseases. *Aging Dis.*, 5(4):218–225.

Blokh, D. and Stambler, I. (2016). The application of information theory for the research of aging and aging-related diseases. *Prog. Neurobiol.*

Boas, D. A. and Dunn, A. K. (2010). Laser speckle contrast imaging in biomedical optics. *J. Biomed. Opt.*, 15(1):011109– 011109–12.

Bolay, H., Reuter, U., Dunn, A. K., Huang, Z., Boas, D. A., and Moskowitz, M. A. (2002). Intrinsic brain activity triggers trigeminal meningeal afferents in a migraine model. *Nat. Med.*, 8(2):136–142.

Bollinger, A. and Fagrell, B. (1990). *Clinical capillaroscopy: a guide to its use in clinical research and practice*. Hogrefe & Huber Toronto/Lewiston/New York/Bern/Göttingen/Stuttgart.

Bonner, R. and Nossal, R. (1981). Model for laser Doppler measurements of blood flow in tissue. *Appl. Opt.*, 20(12):2097–2107.

Bos, J. D. and Kapsenberg, M. L. (1993). The skin immune system: progress in cutaneous biology. *Immunol. Today*, 14(2):75–78.

Bracic, M. and Stefanovska, A. (1999). Wavelet analysis in studying the dynamics of blood circulation. *Nonlinear Phenom. Complex Syst.*, 2:68–77.

Brandes, R. P. et al. (2005). Endothelial aging. *Cardiovasc. Res.*, 66(2):286–294.

Bratz, I. N. and Kanagy, N. L. (2004). Nitric oxide synthase-inhibition hypertension is associated with altered endothelial cyclooxygenase function. *Am. J. Physiol. Heart Circ. Physiol.*, 287(6):H2394–H2401.

Braverman, I. M. (1989). Ultrastructure and organization of the cutaneous microvasculature in normal and pathologic states. *J. Invest. Dermatol.*, 93:2S–9S.

Braverman, I. M. (2000). The cutaneous microcirculation. *J. Investig. Dermatol. Symp. Proc.*, 5(1):3–9.

Brent, R. (1973). *Algorithms for minimization without derivatives*. Prentice-Hall.

Bricq, S., Mahé, G., Rousseau, D., Humeau-Heurtier, A., Chapeau-Blondeau, F., Varela, J. R., and Abraham, P. (2012). Assessing spatial resolution versus sensitivity from laser speckle contrast imaging: application to frequency analysis. *Med. Biol. Eng. Comput.*, 50(10):1017–1023.

Briers, D., Duncan, D. D., Hirst, E., Kirkpatrick, S. J., Larsson, M., et al. (2013). Laser speckle contrast imaging: theoretical and practical limitations. *J. Biomed. Opt.*, 18(6):066018–066018.

Briers, J. D. (1975). Wavelength dependence of intensity fluctuations in laser speckle patterns from biological specimens. *Opt. Commun.*, 13(3):324–326.

Briers, J. D. (2001). Laser Doppler, speckle and related techniques for blood perfusion mapping and imaging. *Physiol. Meas.*, 22(4):R35–36.

Briers, J. D. (2007). Laser speckle contrast imaging for measuring blood flow. *Optica Applicata*, 37(1/2):139–152.

Briers, J. D. and Fercher, A. F. (1982). Retinal blood-flow visualization by means of laser speckle photography. *Invest. Ophthalmol. Vis. Sci.*, 22(2):255–259.

Briers, J. D., Richards, G., and He, X. W. (1999). Capillary blood flow monitoring using laser speckle contrast analysis (LASCA). *J. Biomed. Optic.*, 4(1):164–175.

Briers, J. D. and Webster, S. (1995). Quasi real-time digital version of single-exposure speckle photography for full-field monitoring of velocity or flow fields. *Opt. Commun.*, 116(1):36–42.

Briers, J. D. and Webster, S. (1996). Laser speckle contrast analysis (LASCA): a non-scanning, full-field technique for monitoring capillary. *J. Biomed. Opt.*, 1(2):174–179.

Broderick, P. A. and Kolodny, E. H. (2010). Biosensors for brain trauma and dual laser Doppler flowmetry: Enoxaparin simultaneously reduces stroke-induced dopamine and blood flow while enhancing serotonin and blood flow in motor neurons of brain, in vivo. *Sensors*, 11(1):138–161.

Brown, W. R. and Thore, C. R. (2011). Review: Cerebral microvascular pathology in ageing and neurodegeneration. *Neuropathol. Appl. Neurobiol.*, 37(1):56–74.

Bruning, R. S., Kenney, W. L., and Alexander, L. M. (2015). Altered skin flowmotion in hypertensive humans. *Microvasc. Res.*, 97:81–87.

Buckley, E. M., Cook, N. M., Durduran, T., Kim, M. N., Zhou, C., et al. (2009). Cerebral hemodynamics in preterm infants during positional intervention measured with diffuse correlation spectroscopy and transcranial Doppler ultrasound. *Opt. Express*, 17(15):12571–12581.

Calleja-Agius, J., Brincat, M., and Borg, M. (2013). Skin connective tissue and ageing. *Best Pract. Res. Cl. Ob.*, 27(5):727–740.

Cernadas, M. R., Sanchez de Miguel, L., and Garcia-Duran, M. (1998). Expression of constitutive and inducible nitric oxide synthases in the vascular wall of young and aging rats. *Circ. Res.*, 83(3):279–286.

Chang, Y., Wu, H. T., Chen, H. R., Liu, A., Yeh, J., Lo, M., et al. (2014). Application of a modified entropy computational method in assessing the complexity of pulse wave velocity signals in healthy and diabetic subjects. *Entropy*, 16(7):4032–4043.

Chen, D., Ren, J., Wang, Y., Zhao, H., Li, B., and Gu, Y. (2016). Relationship between the blood perfusion values determined by laser speckle imaging and laser Doppler imaging in normal skin and port wine stains. *Photodiagnosis Photodyn. Ther.*, 13:1–9.

Chen, W., Zhuang, J., Yu, W., and Wang, Z. (2009). Measuring complexity using fuzzyen, apen, and sampen. *Med. Eng. Phys.*, 31(1):61–68.

Cheng, H., Luo, Q., Zeng, S., Chen, S., Cen, J., and Gong, H. (2003). Modified laser speckle imaging method with improved spatial resolution. *J. Biomed. Opt.*, 8(3):559–564.

Cheng, H., Yan, Y., and Duong, T. Q. (2008). Temporal statistical analysis of laser speckle images and its application to retinal blood-flow imaging. *Opt. Express*, 16(14):10214–10219.

Conover, W. (1999). *Practical nonparametric statistics, 3rd edn Wiley*. New York: John Wiley & Sons.

Cordovil, I., Huguenin, G., Rosa, G., Bello, A., Köhler, O., de Moraes, R., and Tibiriçá, E. (2012). Evaluation of systemic microvascular endothelial function using laser speckle contrast imaging. *Microvasc. Res.*, 83(3):376–379.

Costa, M., Ghiran, I., Peng, C. K., Nicholson-Weller, A., and Goldberger, A. L. (2008). Complex dynamics of human red blood cell flickering: alterations with in vivo aging. *Phys. Rev. E*, 78(2):020901.

Costa, M., Goldberger, A. L., and Peng, C. K. (2002). Multiscale entropy analysis of complex physiologic time series. *Phys. Rev. Lett.*, 89(6):068102–1–068102–4.

Costa, M., Goldberger, A. L., and Peng, C. K. (2005). Multiscale entropy analysis of biological signals. *Phys. Rev. E*, 71(2):021906.

Costa, M., Peng, C.-K., Goldberger, A. L., and Hausdorff, J. M. (2003). Multiscale entropy analysis of human gait dynamics. *Physica A*, 330(1-2):53–60.

Cowen, T. (1993). Ageing in the autonomic nervous system: a result of nerve-target interactions? a review. *Mech. Ageing Dev.*, 68(1):163–173.

Cracowski, J. L., Gaillard-Bigot, F., Cracowski, C., Roustit, M., and Millet, C. (2011). Skin microdialysis coupled with laser speckle contrast imaging to assess microvascular reactivity. *Microvasc. Res.*, 82(3):333–338.

Cracowski, J. L., Gaillard-Bigot, F., Cracowski, C., Sors, C., Roustit, M., and Millet, C. (2013). Involvement of cytochrome epoxygenase metabolites in cutaneous postocclusive hyperemia in humans. *J. Appl.Physiol.*, 114(2):245–251.

Dahan, M. L. (2008). *L'effet du vieillissement sur la microcirculation cutanée*. PhD thesis, Université Claude Bernard-Lyon I. CrossRef.

Davis, M. A. and Dunn, A. K. (2015). Dynamic light scattering Monte Carlo: a method for simulating time-varying dynamics for ordered motion in heterogeneous media. *Opt. Express*, 23(13):17145–17155.

Davis, M. A. et al. (2014). Imaging depth and multiple scattering in laser speckle contrast imaging. *J. Biomed. Opt.*, 19(8):086001–1–10.

De Backer, D., Creteur, J., Preiser, J., Dubois, M., and Vincent, J. (2002). Microvascular blood flow is altered in patients with sepsis. *Am. J. Respir. Crit. Care Med.*, 166(1):98–104.

De Ciuceis, C., Porteri, E., Rizzoni, D., Rizzardi, N., Paiardi, S., Boari, G., Miclini, M., Zani, F., Muiesan, M. L., and Donato, F. (2007). Structural alterations of subcutaneous small-resistance arteries may predict major cardiovascular events in patients with hypertension. *Am. J. Hypertens.*, 20(8):846–852.

Djaberi, R., Beishuizen, E. D., Pereira, A. M., Rabelink, T. J., Smit, J. W., Tamsma, J. T., Huisman, M. V., and Jukema, J. W. (2008). Non-invasive cardiac imaging techniques and vascular tools for the assessment of cardiovascular disease in type 2 diabetes mellitus. *Diabetologia*, 51(9):1581–1593.

Domoki, F., Zölei, D., Oláh, O., Tóth-Szuki, V., Hopp, B., Bari, F., and Smausz, T. (2012). Evaluation of laser-speckle contrast image analysis techniques in the cortical microcirculation of piglets. *Microvasc. Res.*, 83:311–317.

Dragojević, T., Bronzi, D., Varma, H. M., Valdes, C. P., Castellvi, C., et al. (2015). High-speed multi-exposure laser speckle contrast imaging with a single-photon counting camera. *Biomed. Opt. Express*, 6(8):2865–2876.

Draijer, M., Hondebrink, E., van Leeuwen, T., and Steenbergen, W. (2009). Review of laser speckle contrast techniques for visualizing tissue perfusion. *Lasers Med. Sci.*, 24(4):639–651.

Draijer, M. J. (2010). *High speed perfusion imaging based on laser speckle fluctuations*. PhD thesis, University of Twente, Enschede. CrossRef.

Draijer, M. J., Hondebrink, E., van Leeuwen, T. G., and Steenbergen, W. (2008). Connecting laser Doppler perfusion imaging and laser speckle. In *Biomedical Optics (BiOS) 2008*, pages 68630C–68630C–8.

Duncan, D. D. and Kirkpatrick, S. J. (2008a). Can laser speckle flowmetry be made a quantitative tool? *J. Opt. Soc. Am. A Opt. Image Sci.*, 25(8):2088–2094.

Duncan, D. D. and Kirkpatrick, S. J. (2008b). Spatio-temporal algorithms for processing laser speckle imaging data. In *Biomedical Optics (BiOS) 2008*, volume 6858, pages 685802–685802.

Duncan, D. D., Kirkpatrick, S. J., and Gladish, J. C. (2008a). What is the proper statistical model for laser speckle flowmetry? In *Biomedical Optics (BiOS) 2008*, pages 685502–685502–7.

Duncan, D. D., Kirkpatrick, S. J., and Wang, R. K. (2008b). Statistics of local speckle contrast. *J. Opt. Soc. Am. A Opt. Image Sci. Vis*, 25(1):9–15.

Dunn, A. K. (2012). Laser speckle contrast imaging of cerebral blood flow. *Ann. Biomed. Eng.*, 40(2):367–377.

Dunn, A. K., Bolay, H., Moskowitz, M. A., and Boas, D. A. (2001). Dynamic imaging of cerebral blood flow using laser speckle. *Cereb. Blood Flow Metab.*, 21:195–201.

Dunn, A. K., Devor, A., Bolay, H., Andermann, M. L., Moskowitz, M. A., et al. (2003). Simultaneous imaging of total cerebral hemoglobin concentration, oxygenation, and blood flow during functional activation. *Opt. Lett.*, 28(1):28–30.

El-Domyati, M., Attia, S., Saleh, F., Brown, D., Birk, D. E., Gasparro, F., Ahmad, H., and Uitto, J. (2002). Intrinsic aging vs. photoaging: a comparative histopathological, immunohistochemical, and ultrastructural study of skin. *Exp. Dermatol.*, 11(5):398–405.

Eriksson, S., Nilsson, J., and Sturesson, C. (2014). Non-invasive imaging of microcirculation: a technology review. *Med. Device Diagn. Ind.*, 7:445–452.

Escudero, J., Abásolo, D., Hornero, R., Espino, P., and López, M. (2006). Analysis of electroencephalograms in alzheimer's disease patients with multiscale entropy. *Physiol. Meas.*, 27(11):1091.

Essex, T. J. and Byrne, P. O. (1991). A laser Doppler scanner for imaging blood flow in skin. *J. Biomed. Eng.*, 13(3):189–194.

Evans, E., Rendell, M., Bartek, J., Connor, S., Bamisedun, O., Dovgan, D., and Giitter, M. (1993). Thermally-induced cutaneous vasodilatation in aging. *J. Gerontol.*, 48(2):M53–M57.

Feher, A., Broskova, Z., and Bagi, Z. (2014). Age-related impairment of conducted dilation in human coronary arterioles. *Am. J. Physiol. Heart Circ. Physiol.*, 306(12):H1595–H1601.

Feihl, F., Liaudet, L., and Waeber, B. (2009). The macrocirculation and microcirculation of hypertension. *Curr. Hypertens. Rep.*, 11(3):182–9.

Fenske, N. A. and Conard, C. B. (1988). Aging skin. *Am. Fam. Physician.*, 37(2):219–230.

Fercher, A. F. and Briers, J. D. (1981). Flow visualization by means of single exposure speckle photography. *Opt. Comm.*, 37(5):326–330.

Fercher, A. F., Peukert, M., and Roth, E. (1986). Visualization and measurement of retinal blood flow by means of laser speckle photography. *Opt. Eng.*, 6(25):731–735.

Ferraro, B., Cruz, Y. L., Baldwin, M., Coppola, D., and Heller, R. (2010). Increased perfusion and angiogenesis in a hindlimb ischemia model with plasmid FGF-2 delivered by noninvasive electroporation. *Gene. Ther.*, 17(6):763–769.

Fishman, A. P. and Richards, D. W. (2013). *Circulation of the blood: men and ideas*. Springer. CrossRef.

Flammer, J., Orgül, S., Costa, V. P., Orzalesi, N., Krieglstein, G. K., Serra, L. M., et al. (2002). The impact of ocular blood flow in glaucoma. *Prog. Retin. Eye Res.*, 21(4):359–393.

Forrester, K. R., Stewart, C., Tulip, J., Leonard, C., and Bray, R. C. (2002). Comparison of laser speckle and laser Doppler perfusion imaging: measurement in human skin and rabbit articular tissue. *Med. Biol. Eng. Comput.*, 40(6):687–697.

Forrester, K. R., Tulip, J., Leonard, C., Stewart, C., and Bray, R. C. (2004). A laser speckle imaging technique for measuring tissue perfusion. *IEEE Trans. Biomed. Eng.*, 51(11):2074–2084.

Forsythe, G. E., Malcolm, M. A., and Moler, C. B. (1976). *Computer methods for mathematical computations*. Prentice-Hall. CrossRef.

Frank, O. (1990). The basic shape of the arterial pulse. first treatise: mathematical analysis. *J. Mol. Cell. Cardiol.*, 22(3):255–277.

Fujimoto, J. G. (2003). Optical coherence tomography for ultrahigh resolution in vivo imaging. *Nat. Biotechnol.*, 21(11):1361–1367.

Fujimoto, J. G., Pitris, C., Boppart, S. A., and Brezinski, M. E. (2000). Optical coherence tomography: an emerging technology for biomedical imaging and optical biopsy. *Neoplasia*, 2(1):9–25.

Fukuoka, S., Hotokebuchi, T., Jingushi, S., Fujii, H., Sugioka, Y., and Iwamoto, Y. (1999). Evaluation of blood flow within the subchondral bone of the femoral head: use of the laser speckle method at surgery for osteonecrosis. *J. Orthop. Res.*, 17(1):80–87.

Ganong, W. F. and Barrett, K. E. (2005). *Review of medical physiology*, volume 21. McGraw-Hill Medical ˆ eNew York New York.

Gates, P. E., Strain, W. D., and Shore, A. C. (2009). Human endothelial function and microvascular ageing. *Exp. Physiol.*, 94(3):311–316.

Gilchrest, B. A. (1989). Skin aging and photoaging: an overview. *J. Am. Acad. Dermatol.*, 21(3):610–613.

Goldberger, A. L., Peng, C. K., and Lipsitz, L. A. (2002). What is physiologic complexity and how does it change with aging and disease? *Neurobiol. aging*, 23(1):23–26.

Goodman, J. W. (1975). Statistical properties of laser speckle patterns. In *Laser Speckle and Related Phenomena*, volume 9, chapter 2, pages 9–75. Springer-Verlage. CrossRef.

Goodman, J. W. (1985). *Statistical Optics*. Wiley & Sons, New York.

Gowen, A. A., Taghizadeh, M., and ODonnell, C. P. (2009). Identification of mushrooms subjected to freeze damage using hyperspectral imaging. *J. Food Eng.*, 93(1):7–12.

Groner, W., Winkelman, J. W., Harris, A. G., Ince, C., Bouma, G. J., Messmer, K., and Nadeau, R. G. (1999). Orthogonal polarization spectral imaging: a new method for study of the microcirculation. *Nat. Med.*, 5(10):1209–1212.

Grothusen, J. R. and Schwartzman, R. J. (2011). Laser Doppler imaging: usefulness in chronic pain medicine. *Pain Physician*, 14:491–498.

Hadgraft, J. (2001). Skin, the final frontier. *Int. J. Pharm.*, 224(1):1–18.

Hagisawa, S., Barbenel, J. C., and Kenedi, R. M. (1991). Influence of age on postischaemic reactive hyperaemia. *Clin. Phys. Physiol. Meas.*, 12(3):227.

Hahn, P., Migacz, J., O'Connell, R., Maldonado, R. S., Izatt, J. A., and Toth, C. A. (2011). The use of optical coherence tomography in intraoperative ophthalmic imaging. *Ophthalmic Surg. Lasers Imaging*, 42:S85–92.

Harris, N. R. and Rumbaut, R. E. (2001). Age-related responses of the microcirculation to ischemia-reperfusion and inflammation. *Pathophysiology*, 8(1):1–10.

Hellmann, M., Roustit, M., and Cracowski, J. L. (2015). Skin microvascular endothelial function as a biomarker in cardiovascular diseases? *Pharmacol. Rep.*, 67(4):803–810.

Herrera, A. M., Martinez, E. C., and Seow, C. Y. (2004). Electron microscopic study of actin polymerization in airway smooth muscle. *Am. J. Physiol-lung C.*, 286(6):L1161–L1168.

Heymes, C., Habib, A., Yang, D., Mathieu, E., Marotte, F., Samuel, J., and Boulanger, C. M. (2000). Cyclo-oxygenase-1 and- 2 contribution to endothelial dysfunction in ageing. *Br. J. Pharmacol.*, 131(4):804–810.

Hodges, G. J., Sharp, L., Clements, R. E., Goldspink, D. F., George, K. P., and Cable, N. T. (2010). Influence of age, sex, and aerobic capacity on forearm and skin blood flow and vascular conductance. *Eur. J. Appl. Physiol.*, 109(6):1009–1015.

Holick, M. F. (2003). Vitamin d: A millenium perspective. *J. Cell. Biochem.*, 88(2):296–307.

Holick, M. F. (2007). Vitamin d deficiency. *New Engl. J. Med.*, 357(3):266–281.

Holowatz, L. A., Houghton, B. L., Wong, B. J., Wilkins, B. W., Harding, A. W., Kenney, W. L., and Minson, C. T. (2003). Nitric oxide and attenuated reflex cutaneous vasodilation in aged skin. *Am. J. Physiol.*, 284(5):H1662–H1667.

Holowatz, L. A., Thompson, C. S., Minson, C. T., and Kenney, W. L. (2005). Mechanisms of acetylcholine-mediated vasodilatation in young and aged human skin. *J. Physiol.*, 563(3):965–973.

Holowatz, L. A., Thompson-Torgerson, C. S., and Kenney, W. L. (2008). The human cutaneous circulation as a model of generalized microvascular function. *J. Appl. Physiol.*, 105(1):370–372.

Hornero, R., Espino, P., Poza, J., et al. (2006). Entropy analysis of the eeg background activity in alzheimer's disease patients. *Physiol. Meas.*, 27(3):241.

Humeau, A., Buard, B., Mahé, G., Rousseau, D., Chapeau-Blondeau, F., and Abraham, P. (2010). Multiscale entropy of laser Doppler flowmetry signals in healthy human subjects. *Med. phys.*, 37(12):6142–6146.

Humeau, A., Chapeau-Blondeau, F., Rousseau, D., Rousseau, P., Trzepizur, W., and Abraham, P. (2008). Multifractality, sample entropy, and wavelet analyses for age-related changes in the peripheral cardiovascular system: preliminary results. *Med. Phys.*, 35(2):717–723.

Humeau, A., Mahé, G., Chapeau-Blondeau, F., Rousseau, D., and Abraham, P. (2011). Multiscale analysis of microvascular blood flow: a multiscale entropy study of laser Doppler flowmetry time series. *IEEE Trans. Biomed. Eng.*, 58(10):2970–2973.

Humeau-Heurtier, A., Abraham, P., Durand, S., and Mahé, G. (2014a). Excellent inter- and intra-observer reproducibility of microvascular tests using laser speckle contrast imaging. *Clin. Hemorheol. Microcirc.*, 58(3):439–446.

Humeau-Heurtier, A., Abraham, P., and Mahe, G. (2015a). Analysis of laser speckle contrast images variability using a novel empirical mode decomposition: Comparison of results with laser Doppler flowmetry signals variability. *IEEE Trans. Med. Imaging*, 34(2):618–627.

Humeau-Heurtier, A., Baumert, M., Mahé, G., and Abraham, P. (2014b). Multiscale compression entropy of microvascular blood flowsignals: Comparison of results from laser speckle contrastand laser Doppler flowmetry data in healthy subjects. *Entropy*, 16(11):5777–5795.

Humeau-Heurtier, A., Guerreschi, E., Abraham, P., and Mahe, G. (2013a). Relevance of laser Doppler and laser speckle techniques for assessing vascular function: state of the art and future trends. *IEEE Trans. Biomed. Eng.*, 60(3):659–666.

Humeau-Heurtier, A., Mahé, G., and Abraham, P. (2015b). Microvascular blood flow monitoring with laser speckle contrast imaging using the generalized differences algorithm. *Microvas. Res.*, 98:54–61.

Humeau-Heurtier, A., Mahe, G., and Abraham, P. (2015c). Multi-dimensional complete ensemble empirical mode decomposition with adaptive noise applied to laser speckle contrast images. *IEEE Trans. Med. Imaging*, 34(99):2103–2117.

Humeau-Heurtier, A., Mahe, G., Durand, S., and Abraham, P. (2013b). Multiscale entropy study of medical laser speckle contrast images. *IEEE Trans. Biomed. Eng.*, 60(3):872–879.

Humeau-Heurtier, A., Mahe, G., Durand, S., and Abraham, P. (2013c). Skin perfusion evaluation between laser speckle contrast imaging and laser Doppler flowmetry. *Opt. Commun.*, 291:482–487.

Humeau-Heurtier, A., Mahe, G., Durand, S., Henrion, D., and Abraham, P. (2012). Laser speckle contrast imaging: multifractal analysis of data recorded in healthy subjects. *Med. Phys.*, 39:5849–5856.

Isono, H., Kishi, S., Kimura, Y., Hagiwara, N., Konishi, N., and Fujii, H. (2003). Observation of choroidal circulation using index of erythrocytic velocity. *Arch. Ophthalmol.*, 121(2):225–231.

Jakovels, D., Saknite, I., Krievina, G., Zaharans, J., and Spigulis, J. (2014). Mobile phone based laser speckle contrast imager for assessment of skin blood flow. In *Eigth International Conference on Advanced Optical Materials and Devices*, pages 94210J–94210J. CrossRef.

James, M. A., Tullett, J., Hemsley, A. G., and Shore, A. C. (2006). Effects of aging and hypertension on the microcirculation. *Hypertension*, 47(5):968–974.

James, W. D., Berger, T., and Elston, D. (2015). *Andrews' diseases of the skin: clinical dermatology*. Elsevier Health Sciences.

Jones, P. B., Kyoung, S. H., Boas, D. A., Hyman, B. T., Moskowitz, M. A., Ayata, C., and Dunn, A. K. (2004). Simultaneous multispectral reflectance imaging and laser speckle flowmetry of cerebral blood flow and oxygen metabolism in focal cerebral ischemia. *J. Biomed. Opt.*, 13(4):044007–044007.

Jung, W. and Boppart, S. A. (2012). Modern trends in imaging v: Optical coherence tomography for rapid tissue screening and directed histological sectioning. *Anal. Cell. Pathol.*, 35(3):129–143.

Kalka, C., Masuda, H., Takahashi, T., Kalka-Moll, W. M., Silver, M., Kearney, M., Li, T., Isner, J. M., and Asahara, T. (2000). Transplantation of ex vivo expanded endothelial progenitor cells for therapeutic neovascularization. *Proc. Natl Acad. Sci.*, 97(7):3422–3427.

Kang, D.-H. et al. (2001). Impaired angiogenesis in the aging kidney: Vascular endothelial growth factor and thrombospondin-1 in renal disease. *Am. J. Kidney Dis.*, 37(3):601–611.

Kanitakis, J. (2001). Anatomy, histology and immunohistochemistry of normal human skin. *Eur. J. Dermatol.*, 12(4):390–9.

Kaplan, D. T., Furman, M. I., Pincus, S. M., Ryan, S. M., Lipsitz, L. A., and Goldberger, A. L. (1991). Aging and the complexity of cardiovascular dynamics. *Biophys. J.*, 59(4):945.

Kazmi, S. M., Balial, S., and Dunn, A. K. (2014). Optimization of camera exposure durations for multi-exposure speckle imaging of the microcirculation. *Biomed. Opt. Express*, 5(7):2157–2171.

Kazmi, S. M., Richards, L. M., Schrandt, C. J., Davis, M. A., and Dunn, A. K. (2015a). Expanding applications, accuracy, and interpretation of laser speckle contrast imaging of cerebral blood flow. *J. Cerebr. Blood F. Met.*, 35:10761084.

Kazmi, S. M., Wu, R. K., and Dunn, A. K. (2015b). Evaluating multi-exposure speckle imaging estimates of absolute autocorrelation times. *Opt. Lett.*, 40(15):3643–3646.

Kazmi, S. M. S., Parthasarthy, A. B., Song, N. E., Jones, T. A., and Dunn, A. K. (2013). Chronic imaging of cortical blood flow using Multi-Exposure Speckle Imaging. *J. Cereb. Blood Flow Metab.*, 33(6):798–808.

Kellogg, D. L., Zhao, J. L., Coey, U., and Green, J. V. (2005). Acetylcholine-induced vasodilation is mediated by nitric oxide and prostaglandins in human skin. *J. Appl. Physiol.*, 98(2):629–632.

Kelly, R. I., Pearse, R., Bull, R. H., Leveque, J. L., de Rigal, J., and Mortimer, P. S. (1995). The effects of aging on the cutaneous microvasculature. *J. Am. Acad. Dermatol.*, 33(5):749–756.

Kelm, M., Feelisch, M., Spahr, R., Piper, H., Noack, E., and Schrader, J. (1988). Quantitative and kinetic characterization of nitric oxide and EDRF released from cultured endothelial cells. *Biochem. Biophs. Res. Commun.*, 154(1):236–244.

Kempen, J. H., O'Colmain, B. J., Leske, M. C., Haffner, S. M., Klein, R., Moss, S. E., Taylor, H. R., and Hamman, R. F. (2004). The prevalence of diabetic retinopathy among adults in the United States. *Arch. Ophthalmol.*, 122(4):552–563.

Kenney, W. L. and Munce, T. A. (2003). Invited review: aging and human temperature regulation. *J. Appl. Physiol.*, 95(6):2598–2603.

Khaksari, K. and Kirkpatrick, S. J. (2016). Laser speckle contrast imaging is sensitive to advective flux. *J. Biomed. Opt*, 21(7):076001.

Khalil, A., Humeau-Heurtier, A., Abraham, P., and Mahe, G. (2014a). Comparative study to analyze the effect of aging on microvascular blood flow by processing laser speckle contrast images when lorentzian and gaussian velocity profiles are assumed

for moving scatterers. In *4th International Conference on Image Processing Theory, Tools and Applications (IPTA)*, Paris, France. CrossRef.

Khalil, A., Humeau-Heurtier, A., Abraham, P., and Mahé, G. (2014b). Processing of laser speckle contrast images to analyze the impact of aging on moving blood cells when a Lorentzian velocity profile is assumed. In *Proc. 22nd European Signal Processing Conference (EUSIPCO-2014)*, pages 2035–2039, Lisbon, Portugal.

Khalil, A., Humeau-Heurtier, A., Mahé, G., and Abraham, P. (2015). Laser speckle contrast imaging: age-related changes in microvascular blood flow and correlation with pulse-wave velocity in healthy subjects. *J. Biomed. Opt.*, 20(5):051010–051010–7.

Kheong, M. K. and Cheng, H. M. (2015). *Learning and Teaching Tools for Basic and Clinical Respiratory Physiology*. Springer. CrossRef.

Kirby, M. A., Khaksari, K., and Kirkpatrick, S. J. (2015). Nematic liquid crystal spatial light modulator for mimicking laser speckle contrast imaging. In *SPIE BiOS*, pages 932203–932203. CrossRef.

Kirkpatrick, K. and Khaksariand, S. J. (2015). Effects of combined scattering and absorption coefficients on laser speckle contrast imaging. In *Proc. of SPIE*, volume 9322, pages 93220U–1. CrossRef.

Kirkpatrick, S. J., Duncan, D. D., and Wells-Gray, E. M. (2008). Detrimental effects of speckle-pixel size matching in laser speckle contrast imaging. *Opt. Lett.*, 33(24):2886–2888.

Klabunde, R. (2011). *Cardiovascular physiology concepts*. Lippincott Williams & Wilkins.

Knight, J. A., Blackmore, K. M., Wong, J., Tharmalingam, S., and Lilge, L. (2010). Optical spectroscopy of the breast in premenopausal women reveals tissue variation with changes in age and parity. *Med. Phys.*, 37(2):419–426.

Konishi, N., Tokimoto, Y., Kohra, K., and Fujii, H. (2002). New laser speckle flowgraphy system using CCD camera. *Opt. Rev.*, 9(4):163–169.

Konstantinova, E., Tolstaya, T., Prishchep, S., Milutin, A., Mironova, E., and Ivanova, L. (2004). Plasma lipid levels, blood rheology, platelet aggregation, microcirculation state and oxygen transfer to tissues in young and middle-aged healthy people. *Clin. Hemorheol. Microcirc.*, 30(3):443–448.

Krstic, R. V. (1991). *Human microscopic anatomy: an atlas for students of medicine and biology*. Springer.

Kvandal, P., Landsverk, S. A., Bernjak, A., Stefanovska, A., Kvernmo, H. D., and Kirkeboen, K. A. (2006). Low-frequency oscillations of the laser Doppler perfusion signal in human skin. *Microvasc. Res.*, 72(3):120–127.

Kvernmo, H., Stefanovska, A., Kirkebøen, K. A., and Kvernebo, K. (1999). Oscillations in the human cutaneous blood perfusion signal modified by endothelium-dependent and endothelium-independent vasodilators. *Microvas. Res.*, 57(3):298–309.

Kyriazis, M. (2003). Practical applications of chaos theory to the modulation of human ageing: nature prefers chaos to regularity. *Biogerontology*, 4(2):75–90.

Lakatta, E. G. and Levy, D. (2003). Arterial and cardiac aging: major shareholders in cardiovascular disease enterprises part ii: the aging heart in health: links to heart disease. *Circulation*, 107(2):346–354.

Lal, C., Banerjee, A., and Sujatha, N. U. (2013). Role of contrast and fractality of laser speckle image in assessing flow velocity and scatterer concentration in phantom body fluids. *J. Biomed. Opt.*, 11(8):111419–111419–7.

Le, T. M., Paul, J. S., Al-Nashash, H., Tan, A., Luft, A. R., et al. (2007). New insights into image processing of cortical blood flow monitors using laser speckle imaging. *IEEE Trans. Med. Imaging*, 26(6):833–842.

Leutenegger, M., Martin-Williams, E., Harbi, P., Thacher, T., Raffoul, W., et al. (2011). Real-time full field laser Doppler imaging. *Biomed. Opt. Exp.*, 2(6):1470–1477.

Levy, H., Ringuette, D., and Levi, O. (2012). Rapid monitoring of cerebral ischemia dynamics using laser-based optical imaging of blood oxygenation and flow. *Biomed. Opt. Express*, 3(4):777–791.

Li, H., Liu, Q., Lu, H., Li, Y., Zhang, H. F., and Tong, S. (2014). Directly measuring absolute flow speed by frequency–domain laser speckle imaging. *Opt. express*, 22(17):21079–21087.

Li, L., Mac-Mary, S., Marsaut, D., Sainthillier, J. M., Nouveau, S., et al. (2006a). Age-related changes in skin topography and microcirculation. *Arch. Dermatol. Res.*, 297(9):412–416.

Li, L., Mac-Mary, S., Sainthillier, J. M., Nouveau, S., de Lacharriere, O., and Humbert, P. (2006b). Age-related changes of the cutaneous microcirculation in vivo. *Gerontology*, 52(3):142–153.

Li, P., Ni, S., Zhang, L., Zeng, S., and Luo, Q. (2006c). Imaging cerebral blood flow through the intact rat skull with temporal laser speckle imaging. *Opt. Lett.*, 31(12):1824–1826.

Li, P., Ni, S., Zhang, L., Zeng, S., and Luo, Q. (2006d). Imaging cerebral blood flow through the intact rat skull with temporal laser speckle imaging. *Opt. Lett.*, 31:1824–1826.

Liao, F. and Jan, Y.-K. (2016). Using modified sample entropy to characterize aging-associated microvascular dysfunction. *Front. Physiol.*, 7:1–11.

Lin, P., Lo, M., Tsao, J., Chang, Y., Lin, C., and Ho, Y. (2014). Correlations between the signal complexity of cerebral and cardiac electrical activity: A multiscale entropy analysis. *PLoS ONE*, 9:87798.

Lindahl, F., Tesselaar, E., and Sjöberg, F. (2013). Assessing paediatric scald injuries using laser speckle contrast imaging. *Burns*, 39(4):662–666.

Lindeboom, J. A., Mathura, K. R., Harkisoen, S., Akker, H. P., and Ince, C. (2005). Effect of smoking on the gingival capillary density: assessment of gingival capillary density with orthogonal polarization spectral imaging. *J. Clin. Periodontol.*, 32(12):1208–1212.

Lipsitz, L. A. and Goldberger, A. L. (1992). Loss of'complexity'and aging: potential applications of fractals and chaos theory to senescence. *JAMA*, 267(13):1806–1809.

Liu, S., Li, P., and Luo, Q. (2008). Fast blood flow visualization of highresolution laser speckle imaging data using graphics processing unit. *Opt. Express*, 16(19):14321–14329.

Lo, M.-T., Chang, Y.-C., Lin, C., Young, H.-W. V., Lin, Y.-H., Ho, Y.-L., Peng, C.-K., and Hu, K. (2015). Outlier-resilient complexity analysis of heartbeat dynamics. *Sci. Rep.*, 5:8836.

Lotrič, M. B. (1999). *Couplings among subsystems that regulate blood flow*. PhD thesis, University of Ljubljana, Ljubljana.

Lu, G. and Fei, B. (2014). Medical hyperspectral imaging: a review. *J. Biomed. Opt.*, 19(1):010901.

Lu, H., Li, Y., Li, H., Yuan, L., Liu, Q., et al. (2015). Single-trial estimation of the cerebral metabolic rate of oxygen with imaging photoplethysmography and laser speckle contrast imaging. *Opt. Lett.*, 40(7):1193–1196.

Luo, Z., Yuan, Z., Pan, Y., and Du, C. (2009). Simultaneous imaging of cortical hemodynamics and blood oxygenation change during cerebral ischemia using dual-wavelength laser speckle contrast imaging. *Opt. Lett.*, 34:1480–1482.

Lupi, O., Semenovitch, I., Treu, C., and Bouskela, E. (2008). Orthogonal polarization technique in the assessment of human skin microcirculation. *Int. J. Dermatol.*, 47(5):425–431.

Lüscher, T. F. and Noll, G. (1996). Endothelial function as an end-point in interventional trials: concepts, methods and current data. *J. Hypertens. Suppl.*, 14:S111–S121.

Madsen, S. J. (2013). *Optical Methods and Instrumentation in Brain Imaging and Therapy*. Springer.

Mahe, G., Abraham, P., Faucheur, A. L., Bruneau, A., Humeau-Heurtier, A., and Durand, S. (2013). Cutaneous microvascular functional assessment during exercise: A novel approach using laser speckle contrast imaging. *Pflugers Arch.*, 465(4):451–458.

Mahé, G., Durand, S., Humeau, A., Leftheriotis, G., Rousseau, P., and Abraham, P. (2011a). Air movements interfere with laser speckle contrast imaging recordings. *Lasers Med. Sci.*, 27(5):1073–1076.

Mahe, G., Durand, S., Humeau-Heurtier, A., Leftheriotis, G., and Abraham, P. (2012). Impact of experimental conditions on noncontact laser recordings in microvascular studies. *Microcirculation*, 19(8):669–675.

Mahé, G., Haj-Yassin, F., Rousseau, P., Humeau, A., Durand, S., Leftheriotis, G., and Abraham, P. (2011b). Distance between laser head and skin does not influence skin blood flow values recorded by laser speckle maging. *Microvasc. Res.*, 82(3):439–442.

Mahe, G., Rousseau, P., Durand, S., Bricq, S., Leftheriotis, G., and Abraham, P. (2011). Laser speckle contrast imaging accurately measures blood flow overmoving skin surfaces. *Microvasc. Res.*, 81(2):183–188.

Mahmud, M. S., Cadotte, D. W., Vuong, B., Sun, C., Luk, T. W., Mariampillai, A., and Yang, V. X. (2013). Review of speckle and phase variance optical coherence tomography to visualize microvascular networks. *J. Biomed. Opt.*, 18(5):050901–050901.

Makrantonaki, E. and Zouboulis, C. C. (2007). Characteristics and pathomechanisms of endogenously aged skin. *Dermatology*, 214(4):352–360.

Manor, B. and Lipsitz, L. A. (2013). Physiologic complexity and aging: Implications for physical function and rehabilitation. *Prog. Neuro-Psychoph.*, 45:287–293.

Marín, J. (1995). Age-related changes in vascular responses: a review. *Mech. Ageing Dev.*, 79(2):71–114.

Martin, H. L., Loomis, J. L., and Kenney, W. L. (1995). Maximal skin vascular conductance in subjects aged 5-85 yr. *J. Appl. Physiol.*, 79(1).

Maton, A. (1997). *Human biology and health*. Prentice Hall.

Matsumoto, M., Suzuma, K., Fukazawa, Y., Yamada, Y., Tsuiki, E., Fujikawa, A., et al. (2014). Retinal blood flow levels measured by laser speckle flowgraphy in patients who received intravitreal bevacizumab injection for macular edema secondary to central retinal vein occlusion. *Retin. Cases Brief. Rep.*, 8(1):60–66.

Matz, R. L. and Andriantsitohaina, R. (2003). Age-related endothelial dysfunction. *Drugs & aging*, 20(7):527–550.

Matz, R. L., Schott, C., Stoclet, J. C., and Andriantsitohaina, R. (2000). Age-related endothelial dysfunction with respect to nitric oxide, endothelium-derived hyperpolarizing factor and cyclo-oxygenase products. *Physiol. Res.*, 49(1):11–18.

Miao, P., Chao, Z., Feng, S., Yu, H., Ji, Y., et al. (2015). Local scattering property scales flow speed estimation in laser speckle contrast imaging. *Laser Phys. Lett.*, 12(7):075601.

Miao, P., Rege, A., Li, N., Thakor, N. V., and Tong, S. (2010). High resolution cerebral blood flow imaging by registered laser speckle contrast analysis. *IEEE Trans. Biomed. Eng.*, 57(5):1152–1157.

Millet, C., Roustit, M., Blaise, S., and Cracowski, J. L. (2011). Comparison between laser speckle contrast imaging and laser Doppler imaging to assess skin blood flow in humans. *Microvasc. Res.*, 82(2):147–151.

Minson, C. T. (2010). Thermal provocation to evaluate microvascular reactivity in human skin. *J. Appl. Physiol.*, 109(4):1239–1246.

Minson, C. T., Holowatz, L. A., Wong, B. J., Kenney, W. L., and Wilkins, B. W. (2002). Decreased nitric oxide-and axon reflex-mediated cutaneous vasodilation with age during local heating. *J. Appl. Physiol.*, 93(5):1644–1649.

Mizukoshi, K., Yonekura, K., Futagawa, M., Nakamura, T., Hirayama, K., and Takahashi, K. (2015). Changes in dermal papilla structures due to aging in the facial cheek region. *Skin Res. Technol.*, 21(2):224–231.

Monstrey, S. M., Hoeksema, H., Baker, R. D., Jeng, J., Spence, R. S., Wilson, D., and Pape, S. A. (2011). Burn wound healing time assessed by laser Doppler imaging. part 2: validation of a dedicated colour code for image interpretation. *Burns*, 37(2):249–256.

Muris, D. M., Houben, A. J., Schram, M. T., and Stehouwer, C. D. (2013). Microvascular dysfunction: an emerging pathway in the pathogenesis of obesity-related insulin resistance. *Rev. Endocrinol. Metab. Disord.*, 14(1):29–38.

Nadort, A., Kalkman, K., van Leeuwen, T. G., and Faber, D. J. (2016). Quantitative blood flow velocity imaging using laser speckle flowmetry. *Sci. Rep.*, 6:25258–1–10.

Nadort, A., Woolthuis, R. G., van Leeuwen, T. G., and Faber, D. J. (2013). Quantitative laser speckle flowmetry of the in vivo microcirculation using sidestream dark field microscopy. *Biomed. Opt. Express*, 4(11):2347–2361.

Nagahara, M., Tamaki, Y., Araie, M., and Umeyama, T. (2001). The acute effects of stellate ganglion block on circulation in human ocular fundus. *Acta Ophthalmol. Scand.*, 79(1):45–48.

Najjar, S. S., Scuteri, A., and Lakatta, E. G. (2005). Arterial aging is it an immutable cardiovascular risk factor? *Hypertension*, 46(3):454–462.

Nammas, W., Ligthart, J. M., Karanasos, A., Witberg, K. T., and Regar, E. (2013). Optical coherence tomography for evaluation of coronary stents in vivo. *Expert Rev. Cardiovasc. Ther.*, 11(5):577–588.

Nishino, K., Fujiyama, T., Hashizume, H., and Nakauchi, S. (2013). Detection and visualization of intracutaneous allergic type-specific elements using long-wavelength near-infrared hyperspectral imaging. *Skin Res. Technol.*, 19(1):e157–e166.

Noon, J. P., Walker, B. R., Webb, D. J., Shore, A. C., Holton, D. W., Edwards, H. V., and Watt, G. C. (1997). Impaired microvascular dilatation and capillary rarefaction in young adults with a predisposition to high blood pressure. *J. Clin. Invest.*, 99(8):1873.

Obradovic, B., Carrier, R. L., Vunjak-Novakovic, G., and Freed, L. E. (1999). Gas exchange is essential for bioreactor cultivation of tissue engineered cartilage. *Biotechnol. Bioeng.*, 63(2):197–205.

Obrenovitch, T. P., Chen, S., and Farkas, E. (2009). Simultaneous, live imaging of cortical spreading depression and associated cerebral blood flow changes, by combining voltage-sensitive dye and laser speckle contrast methods. *Neuroimage*, 45(1):68–74.

Odland, G. and Ross, R. (1968). Human wound repair i. epidermal regeneration. *J. Cell Biol.*, 39(1):135–151.

O'Doherty, J., McNamara, P., Clancy, N. T., Enfield, J. G., and Leahy, M. J. (2009). Comparison of instruments for investigation of microcirculatory blood flow and red blood cell concentration. *J. Biomed. Opt.*, 14(3):034025–034025.

Ogrin, R., Darzins, P., and Khalil, Z. (2005). Age-related changes in microvascular blood flow and transcutaneous oxygen tension under basal and stimulated conditions. *J. Gerontol. Ser. A-Biol. Sci. Med. Sci.*, 60(2):200–206.

Okamoto, M., Matsuura, T., and Ogata, N. (2014). Ocular blood flow before, during, and after vitrectomy determined by laser speckle flowgraphy. *Ophthalmic Surg. Lasers Imaging Retin*, 45(2):118–124.

Olausson, J. (2015). *Studies on microcirculation in insulin resistance*. PhD thesis, University of Gothenburg, Gothenburg, Sweden. CrossRef.

Omarjee, L., Signolet, I., Humeau-Heutier, A., Martin, L., Henrion, D., and Abraham, P. (2015). Optimisation of movement detection and artifact removal during laser speckle contrast imaging. *Microvasc. Res.*, 97:75–80.

Parthasarathy, A. B., Kazmi, S. M., and Dunn, A. K. (2010). Quantitative imaging of ischemic stroke through thinned skull in mice with Multi Exposure Speckle Imaging. *Biomed. Opt. Express*, 1(1):246–259.

Parthasarathy, A. B., Tom, W. J., Gopal, A., Zhang, X., and Dunn, A. K. (2008). Robust flow measurement with multi-exposure speckle imaging. *Opt. Express*, 16(3):1975–1989.

Pauling, J. D., Shipley, J. A., Raper, S., Watson, M. L., Ward, S. G., Harris, N. D., and McHugh, N. J. (2012). Comparison of infrared thermography and laser speckle contrast imaging for the dynamic assessment of digital microvascular function. *Microvasc. Res.*, 83(2):162–167.

Payette, J. R., Kohlenberg, E., Leonardi, L., Pabbies, A., Kerr, P., Liu, K., and Sowa, M. G. (2005). Assessment of skin flaps using optically based methods for measuring blood flow and oxygenation. *Reconstr. Surg.*, 115(2):539–546.

Pecora, R. (1972). Quasi-elastic light scattering from macromolecules. *Annu. Rev. Biophys. Bioeng.*, 1(1):257–276.

Pennings, F. A., Ince, C., and Bouma, G. J. (2006). Continuous real-time visualization of the human cerebral microcirculation during arteriovenous malformation surgery using orthogonal polarization spectral imaging. *Neurosurgery*, 59(1):167–71.

Pereira, T., Maldonado, J., Polónia, J., Silva, J. A., Morais, J., Rodrigues, T., and Marques, M. (2014). Aortic pulse wave velocity and HeartSCORE: Improving cardiovascular risk stratification. A sub-analysis of the EDIVA (Estudo de DIstensibilidade VAscular. *project. Blood pressure*, 23(2):109–115.

Ponticorvo, A., Cardenas, D., Dunn, A. K., Ts'o, D., and Duong, T. Q. (2013). Laser speckle contrast imaging of blood flow in rat retinas using an endoscope. *J. Biomed. Opt.*, 9(18):090501–090501–3.

Porth, C. (2011). *Essentials of pathophysiology: concepts of altered health states*. Lippincott Williams & Wilkins. CrossRef.

Potts, R. (1997). Skin barrier: principles of percutaneous absorption. *Arch. Derm.*, 133(7):924–924.

Puhl, G., Schaser, K. D., Vollmar, B., Menger, M. D., and Settmacher, U. (2003). Noninvasive in vivo analysis of the human hepatic microcirculation using orthogonal polorization spectral imaging. *Transplantation*, 75(6):756–761.

Puissant, C., Abraham, P., Durand, S., Humeau-Heurtier, A., Faure, S., et al. (2013). Reproducibility of non-invasive assessment of skin endothelial function using laser Doppler flowmetry and laser speckle contrast imaging. *PloS one*, 8(4):e61320.

Puschmann, S., Rahn, C. D., Wenck, H., Gallinat, S., and Fischer, F. (2012). Approach to quantify human dermal skin aging using multiphoton laser scanning microscopy. *J. Biomed. Opt.*, 17(3):0360051–0360056.

Qiu, H., Zhou, Y., Gu, Y., Ang, Q., Zhao, S., et al. (2012). Monitoring microcirculation changes in port wine stains during vascular targeted photodynamic therapy by laser speckle imaging. *Photobiol.*, 88(4):978–984.

Qiu, J., Li, Y., Huang, Q., Wang, Y., and Li, P. (2013). Correcting speckle contrast at small speckle size to enhance signal to noise ratio for laser speckle contrast imaging. *Opt. Express*, 21(23):28902.

Ragol, S., Remer, I., Shoham, Y., Hazan, S., Willenz, U., et al. (2015). Static laser speckle contrast analysis for noninvasive burn diagnosis using a camera-phone imager. *J. Biomed. Opt.*, 20(8):086009–086009.

Ramirez-San-Juan, J. C., Mendez-Aguilar, E., Salazar-Hermenegildo, N., Fuentes-Garcia, A., Ramos-Garcia, R., and Choi, B. (2013). Effects of speckle/pixel size ratio on temporal and spatial speckle-contrast analysis of dynamic scattering systems: Implications for measurements of blood-flow dynamics. *Biomed. Opt. Express*, 4(10):1883–1889.

Ramirez-San-Juan, J. C., Ramos-Garcia, R., Guizar-Iturbide, I., Martinez-Niconoff, G., and Choi, B. (2008). Impact of velocity distribution assumption on simplified laser speckle imaging equation. *Opt. Express*, 16(5):3197–3203.

Ramirez-San-Juan, J. C., Ramos-Garcia, R., Martinez-Niconoff, G., and Choi., B. (2014a). Simple correction factor for laser speckle imaging of flow dynamics. *Opt. Lett.*, 39(3):678–681.

Ramirez-San-Juan, J. C., Regan, C., Coyotl-Ocelotl, B., and Choi, B. (2014b). Spatial versus temporal laser speckle contrast analyses in the presence of static optical scatterers. *J. Biomed. Opt.*, 19(10):106009.

Rege, A., Seifert, A. C., Schlattman, D., Ouyang, Y., Li, K. W., et al. (2012a). Longitudinal in vivo monitoring of rodent glioma models through thinned skull using laser speckle contrast imaging. *J. Biomed. Opt.*, 17(12):126017–126017.

Rege, A., Senarathna, J., Nan, L., and Thakor, N. V. (2012b). Anisotropic processing of laser speckle images improves spatiotemporal resolution. *IEEE Trans. Biomed. Eng.*, 59(5):1272–1280.

Remer, I. and Bilenca, A. (2015). Laser speckle spatiotemporal variance analysis for noninvasive widefield measurements of blood pulsation and pulse rate on a camera-phone. *J. Biophotonics*, pages 1–6.

Ren, J., Li, P., Zhao, H., Chen, D., Zhen, J., Wang, Y., et al. (2014). Assessment of tissue perfusion changes in port wine stains after vascular targeted photodynamic therapy: a short-term follow-up study. *Lasers Med. Sci.*, 29(2):781–788.

Rhodin, J. A. (1967). The ultrastructure of mammalian arterioles and precapillary sphincters. *J. Ultrastruct. Res.*, 18(1):181–223.

Rice, T. B. et al. (2013). Quantitative, depth-resolved determination of particle motion using multi-exposure, spatial frequency domain laser speckle imaging. *Biomed. Opt. Express*, 4(12):2880.

Richards, L. M., Kazmi, S. M. S., Davis, J. L., Olin, K. E., and Dunn, A. K. (2013). Low-cost laser speckle contrast imaging of blood flow using a webcam. *Biomed. Opt. Express*, 4(10):2269–2283.

Richardson, D. (1989). Effects of age on cutaneous circulatory response to direct heat on the forearm. *J. Gerontol.*, 44(6):M189–M194.

Richman, J. S. and Moorman, J. R. (2000). Physiological time-series analysis using approximate entropy and sample entropy. *Am. J. Physiol.*, 278(6):H2039–H2049.

Ring, E. F., Porto, L. O., and Bacon, P. A. (1981). Quantitative thermal imaging to assess inositol nicotinate treatment for raynaud's syndrome. *J. Int. Med. Res.*, 9(6):393–400.

Rodmell, P. I. (2005). *Novel pulse oximeter*. PhD thesis, University of Nottingham, UK.

Romero, G. G. Alanis, E. E. and Rabal, H. J. (2000). Statistics of the dynamic speckle produced by a rotating diffuser and its application to the assessment of paint drying. *Opt. Eng.*, 39(6):1652–1658.

Rooke, G. A.and Savage, M. V. and Brengelmann, G. L. (1994). Maximal skin blood flow is decreased in elderly men. *J. Appl. Physiol.*, 77(1):11–14.

Rosenfeld, P. J., Moshfeghi, A. A., and Puliafito, C. A. (2005). Optical coherence tomography findings after an intravitreal injection of bevacizumab (avastin) for neovascular age–related macular degeneration. *Ophthalmic Surg. Lasers Imaging*, 36(4):331–335.

Rousseau, P., Mahé, G., Haj-Yassin, F., Durand, S., Humeau, A., Leftheriotis, G., and Abraham, P. (2011a). Increasing the "region of interest" and "time of interest", both reduce the variability of blood flow measurements using laser speckle contrast imaging. *Microvas. Res.*, 82(1):88–91.

Rousseau, P., Mahé, G., Haj-Yassin, F., Durand, S., Humeau, A., Leftheriotis, G., and Abraham, P. (2011b). Increasing the "region of interest" and "time of interest", both reduce the variability of blood flow measurements using laser speckle contrast imaging. *Microvas. Res.*, 82(1):88–91.

Roustit, M. and Cracowski, J. L. (2012). Non-invasive assessment of skin microvascular function in humans: an insight into methods. *Microcirculation*, 19(1):47–64.

Roustit, M. and Cracowski, J. L. (2013). Assessment of endothelial and neurovascular function in human skin microcirculation. *Trends Pharmacol. Sci.*, 34(7):373–384.

Roustit, M., Millet, C., Blaise, S., Dufournet, B., and Cracowski, J. L. (2010). Excellent reproducibility of laser speckle contrast imaging to assess skin microvascular reactivity. *Microvasc. Res.*, 80(3):505–511.

Royl, G., Leithner, C., Sellien, H., Müller, J. P., Megow, D., Offenhauser, N., et al. (2006). Functional imaging with laser speckle contrast analysis: vascular compartment analysis and correlation with laser Doppler flowmetry and somatosensory evoked potentials. *Brain Res.*, 1121(1):95–103.

Ruaro, B., Sulli, A., Alessandri, E., Pizzorni, C., Ferrari, G., and Cutolo, M. (2015). Laser speckle contrast analysis: a new method to evaluate peripheral blood perfusion in systemic sclerosis patients. *Ann. Rheum. Dis.*, 73(6):1181–1185.

Ryan, T. (2004). The ageing of the blood supply and the lymphatic drainage of the skin. *Micron.*, 35:161–171.

Sadoun, E. and Reed, M. Y. (2003). Impaired angiogenesis in aging is associated with alterations in vessel density, matrix composition, inflammatory response, and growth factor expression. *J. Histochem Cytochem*, 51(9):1119–1130.

Salgado, M. A., Salgado-Filho, M. F., Reis-Brito, J. O., Lessa, M. A., and Tibirica, E. (2014). Effectiveness of laser Doppler perfusion monitoring in the assessment of microvascular function in patients undergoing on-pump coronary artery bypass grafting. *J. Cardiothor. Vasc. An.*, 28(5):1211–1216.

Sandberg, M., Zhang, Q., Styf, J., Gerdle, B., and Lindberg, L. G. (2005). Non-invasive monitoring of muscle blood perfusion by photoplethysmography: evaluation of a new application. *Acta. Physiol. Scand.*, 183(4):335–343.

Scardina, G. A., Carini, F., Noto, F., and Messina, P. (2013). Microcirculation in the healing of surgical wounds in the oral cavity. *Int. J. Oral. Maxillofac. Surg.*, 42(1):31–35.

Schmidt, R. F., Thews, G., and Biederman-Thorson, M. A. (1989). *Human physiology*. Springer-Verlag Berlin.

Schrandt, C. J., Kazmi, S. M., Jones, T. A., and Dunn, A. K. (2015). Chronic monitoring of vascular progression after ischemic stroke using multiexposure speckle imaging and two-photon fluorescence microscopy. *J. Cerebr. Blood F. Met.*, 35(35):933–942.

Seals, D. R. and Esler, M. D. (2000). Human ageing and the sympathoadrenal system. *J. Physiol.*, 528(3):407–417.

Seifalian, A. M., Stansby, G., Jackson, A., Howell, K., and Hamilton, G. (1994). Comparison of laser Doppler perfusion imaging, laser Doppler flowmetry, and thermographic imaging for assessment of blood flow in human skin. *Eur. J. Vasc. Surg.*, 8(1):65–69.

Senarathna, J., Rege, A., Li, N., and Thakor, N. V. (2013). Laser speckle contrast imaging: theory, instrumentation and applications. *IEEE Rev. Biomed. Eng.*, 6:99–110.

Serov, A. and Lasser, T. (2005). High-speed laser Doppler perfusion imaging using an integrating CMOS image sensor. *Opt. Express*, 13:6416–6428.

Serov, A. and Lasser, T. (2006). Combined laser Doppler and laser speckle imaging for real-time blood flow measurements. In *Biomedical Optics (BiOS) 2006*, volume 6094, pages 609406–609406–8.

Serov, A., Steinacher, B., and Lasser, T. (2005). Full-field laser Doppler perfusion imaging and monitoring with an intelligent cmos camera. *Opt. Express*, 13(10):3681–3689.

Serov, A. N., Steenbergen, W., De Mul, F., and Lasser, T. (2003). Quasi-parallel laser-Doppler perfusion imaging using a CMOS image sensor. In *Saratov Fall Meeting 2002 Laser Physics and Photonics, Spectroscopy, and Molecular Modeling III; Coherent Optics of Ordered and Random Media III*, pages 73–84. International Society for Optics and Photonics.

Shahidi, A. M., Patel, S. R., Flanagan, J. G., and Hudson, C. (2013). Regional variation in human retinal vessel oxygen saturation. *Exp. Eye Res.*, 113:143–147.

Shannon, C. E. (1949). Communication theory of secrecy systems. *Bell Syst. Tech. J.*, 28(4):656–715.

Sharma, K., Kohli, P., and Gulati, M. (2012). An update on exercise stress testing. *Curr. Probl. Cardiol.*, 37(5):177–202.

Shiga, Y., Asano, T., Kunikata, H., Nitta, F., Sato, H., Nakazawa, T., et al. (2014). Relative flow volume, a novel blood flow index in the human retina derived from laser speckle flowgraphy. *Invest. Ophthalmol. Vis. Sci.*, 55(6):3899–3904.

Shih, B. B., Allan, D., de Gruijl, F. R., and Rhodes, L. E. (2014). Robust detection of minimal sunburn in pigmented skin by 785 nm laser speckle contrast imaging of blood flux. *J. Invest. Dermatol.*

Shin, H. K., Dunn, A. K., Jones, P. B., Boas, D. A., Lo, E. H., et al. (2007). Normobaric hyperoxia improves cerebral blood flow and oxygenation, and inhibits peri-infarct depolarizations in experimental focal ischaemia. *Brain*, 130(6):1631–1642.

Shin, H. K., Dunn, A. K., Jones, P. B., Boas, D. A., Moskowitz, M. A., and Ayata, C. (2005). Vasoconstrictive neurovascular coupling during focal ischemic depolarizations. *J. Cereb. Blood Flow Metab.*, 8(26):1018–1030.

Shore, A. C. (2000). Capillaroscopy and the measurement of capillary pressure. *Br. J. Clin. Pharmacol.*, 50(6):501–513.

Shuster, S., Black, M. M., and McVitie, E. (1975). The influence of age and sex on skin thickness, skin collagen and density. *Br. J. Dermatol.*, 93(6):639–643.

Singh, N., Prasad, S., Singer, D. R., and MacAllister, R. J. (2002). Ageing is associated with impairment of nitric oxide and prostanoid dilator pathways in the human forearm. *Clin. Sci.*, 102(5):595–600.

Smausz, T., Zölei, D., and Hopp, B. (2009). Real correlation time measurement in laser speckle contrast analysis using wide exposure time range images. *Appl. Opt.*, 48:1425–1429.

Söderström, T., Stefanovska, A., Veber, M., and Svensson, H. (2003). Involvement of sympathetic nerve activity in skin blood flow oscillations in humans. *Am. J. Physiol, Heart Circ. Physiol.*, 284(5):H1638–H1646.

Son, T., Lee, J., and Jung, B. (2013). Contrast enhancement of laser speckle contrast image in deep vasculature by reduction of tissue scattering. *J. Opt. Soc. Korea*, 17(1):86–90.

Souza, E. G., De Lorenzo, A., Huguenin, G., Oliveira, G. M., and Tibiriçá, E. (2014). Impairment of systemic microvascular endothelial and smooth muscle function in individuals with early-onset coronary artery disease: studies with laser speckle contrast imaging. *Coronary Arter. Disease*, 25(1):23–28.

Srienc, A. I., Kurth-Nelson, Z. L., and Newman, E. A. (2010). Imaging retinal blood flow with laser speckle flowmetry. *Front Neuroenerg.*, 2:128.

Stanhewicz, A. E., Ferguson, S. B., Bruning, R. S., and Alexander, L. M. (2014). Laser-speckle contrast imaging: A novel method for assessment of cutaneous blood flow in perniosis. *JAMA Dermatol.*, 150(6):658–660.

Stefanovska, A., Bracic, M., and Kvernmo, H. (1999). Wavelet analysis of oscillations in the peripheral blood circulation measured by laser Doppler technique. *IEEE Trans. Biomed. Eng.*, 46(10):1230–1239.

Stelton, S. et al. (2015). Practice implications for peristomal skin assessment and care from the 2014 world council of enterostomal therapists international ostomy guideline. *Adv. Skin. Wound Care*, 28(6):275–284.

Stern, M. D. (1975). In vivo evaluation of microcirculation by coherent light scattering. *Nature (London)*, 254:56–58.

Stewart, C. J., Frank, R., Forrester, K. R., Tulip, J., Lindsay, R., and Bray, R. C. (2005). A comparison of two laser-based methods for determination of burn scar perfusion: laser Doppler versus laser speckle imaging. *Burns*, 31(6):744–752.

Stoianovici, C., Wilder-Smith, P., and Choi, B. (2011). Assessment of pulpal vitality using laser speckle imaging. *Lasers Surg. Med.*, 43(8):833–837.

Strong, A., Bezzina, E., Anderson, P., Boutelle, M., Hopwood, S., and Dunn, A. (2005). Evaluation of laser speckle flowmetry for imaging cortical perfusion in experimental

stroke studies: quantitation of perfusion and detection of periinfarct depolarisations. *J. Cereb. Blood Flow Metab.*, 26(5):645–53.

Sugiyama, T., Araie, M., Riva, C. E., Schmetterer, L., and Orgul, S. (2010). Use of laser speckle flowgraphy in ocular blood flow research. *Acta Ophthalmol.*, 88(7):723–729.

Sujatha, N. and Banerjee, A. (2015). An experimental model for minimizing errors in laser speckle contrast imaging for microcirculation analysis. In *International Conference on Experimental Mechanics 2014*, pages 93021R–93021R.CrossRef.

Sun, S., Hayes-Gill, B. R., He, D., Zhu, Y., Huynh, N. T., and Morgan, S. P. (2016). Comparison of laser Doppler and laser speckle contrast imaging using a concurrent processing system. *Opt. Lasers Eng.*, 83:1–9.

Szabó, Z., Berg, S., Sjökvist, S., Gustafsson, T., Carleberg, P., Uppsäll, M., Wren, J., Ahn, H., and Smedby, Ö. (2013). Real-time intraoperative visualization of myocardial circulation using augmented reality temperature display. *Int. J. Cardiovasc. Imaging*, 29(2):521–528.

Taddei, S., Virdis, A., Ghiadoni, L., Salvetti, G., Bernini, G., Magagna, A., and Salvetti, A. (2001). Age-related reduction of NO availability and oxidative stress in humans. *Hypertension*, 38(2):274–279.

Takeshima, Y., Miyake, H., Nakagawa, I., Motoyama, Y., Park, Y. S., et al. (2015). Visualization of regional cerebral blood flow dynamics during cortical venous occlusion using laser speckle contrast imaging in a rat model. *J. Stroke Cerebrovasc.*, pages 1–7.

Tamaki, Y., Araie, M., Kawamoto, E., Eguchi, S., and Fujii, H. (1994). Noncontact, two-dimensional measurement of retinal microcirculation using laser speckle phenomenon. *Invest. Ophthalmol. Visual Sci.*, 35(11):3825–3834.

Tanaka, H., Dinenno, F. A., Monahan, K. D., Clevenger, C. M., DeSouza, C. A., and Seals, D. R. (2000). Aging, habitual exercise, and dynamic arterial compliance. *Circulation*, 102(11):1270–1275.

Tee, G. B., Rasool, A. H., Halim, A. S., and Rahman, A. R. (2004). Dependence of human forearm skin postocclusive reactive hyperemia on occlusion time. *J. Pharmacol. Toxicol. Methods*, 50(1):73–78.

Tew, G. A., Klonizakis, M., Crank, H., Briers, J. D., and Hodges, G. J. (2011). Comparison of laser speckle contrast imaging with laser Doppler for assessing microvascular function. *Microvasc. Res.*, 82(3):326–332.

Tew, G. A., Klonizakis, M., and Saxton, J. M. (2010). Effects of ageing and fitness on skin-microvessel vasodilator function in humans. *Eur. J. Appl. Physiol.*, 109(2):173–181.

Thompson, O., Andrews, M., and Hirst, E. (2011). Correction for spatial averaging in laser speckle contrast analysis. *Biomed. Opt. Express*, 2(4):1021–1029.

Thompson, O., Bakker, J., Kloeze, C., Hondebrink, E., and Steenbergen, W. (2012). Experimental comparison of perfusion imaging systems using multi-exposure laser speckle, single exposure laser speckle and full-field laser Doppler. *Proc. SPIE*, 8222:822204–1–822204–8.

Thompson, O. B. and Andrews, K. (2010). Tissue perfusion measurements: multiple-exposure laser speckle analysis generates laser Doppler–like spectra. *J. Biomed. Opt.*, 15(2):027015–027015.

Thompson, O. B. and Andrews, M. K. (2008). Spectral density and tissue perfusion from speckle contrast measurements. In *Biomedical Optics (BiOS) 2008*, pages 68472D–68472D–7.

Tikhonova, I. V., Tankanag, A. V., and Chemeris, N. K. (2013). Time–amplitude analysis of skin blood flow oscillations during the post-occlusive reactive hyperemia in human. *Skin Res. Technol.*, 19(1):e174–e181.

Timoshina, P. A., Shi, R., Zhang, Y., Zhu, D., Semyachkina-Glushkovskaya, O. V., et al. (2015). Comparison of cerebral microcirculation of alloxan diabetes and healthy mice using laser speckle contrast imaging. In *Saratov Fall Meeting 2014*, pages 94480B–94480B.

Tobin, D. J. (2017). Introduction to skin aging. *J. Tissue Viability*, 26(1):37–46.

Tom, W. J., Ponticorvo, A., and Dunn, A. K. (2008). Efficient processing of laser speckle contrast images. *IEEE Trans. Med. Imaging*, 27(12):1728–1738.

Tomiyama, H. and Yamashina, A. (2010). Non-invasive vascular function tests:. *Cir. J.*, 74(1):24–33.

Tortora, G. J. and Derrickson, B. H. (2008). *Principles of anatomy and physiology*. John Wiley & Sons.

Trunkvalterova, Z., Javorka, M., Tonhajzerova, I., Javorkova, J., Lazarova, Z., Javorka, K., and Baumert, M. (2008). Reduced short-term complexity of heart rate and blood pressure dynamics in patients with diabetes mellitus type 1: multiscale entropy analysis. *Physiol. Meas.*, 29(7):817.

Tsuchida, Y. (1993). The effect of aging and arteriosclerosis on human skin blood flow. *J. Dermatol. Sci.*, 5(3):175–181.

Tsuda, S., Kunikata, H., Shimura, M., Aizawa, N., Omodaka, K., Shiga, Y., Yasuda, M., Yokoyama, Y., and Nakazaw, T. (2014). Pulse-waveform analysis of normal population using laser speckle flowgraphy. *Curr. Eye Res.*, 0(0):1–9.

Tuchin, V. and Tuchin, V. (2007). *Tissue optics: light scattering methods and instruments for medical diagnosis*, volume 642. SPIE press Bellingham.

Tuma, R. F., Durán, W. N., and Ley, K. (2011). *Microcirculation*. Academic Press.

Turek, Z., Cerny, V., and Parizkova, R. (2008). Noninvasive in vivo assessment of the skeletal muscle and small intestine serous surface microcirculation in rat: sidestream dark-field (SDF) imaging. *Physiol. Res.*, 57(3):365–371.

Vaillancourt, D. E. and Newell, K. M. (2002). Changing complexity in human behavior and physiology through aging and disease. *Neurobiol. Aging*, 23(1):1–11.

Valdes, C. P., Varma, H. M., Kristoffersen, A. K., Dragojevic, T., Culver, J. P., and Durduran, T. (2014). Speckle contrast optical spectroscopy, a non-invasive, diffuse optical method for measuring microvascular blood flow in tissue. *Biomed. Opt. Express*, 5(8):2769.

Vaz, P., Humeau-Heurtier, A., Figueiras, E., Correia, C., and Cardoso, J. (2016). Laser speckle imaging to monitor microvascular blood flow: a review. *IEEE Rev. Biomed. Eng.*, pages 1–15.

Venus, M., Waterman, J., and McNab, I. (2011). Basic physiology of the skin. *Surgery (Oxford)*, 29(10):471–474.

Vionnet, J., Calero-Romero, I., Heim, A., Rotaru, C., Engelberger, R. P., Dischl, B., et al. (2014). No major impact of skin aging on the response of skin blood flow to a submaximal local thermal stimulus. *Microcirculation*, 21(8):730–737.

Vo-Dinh, T. (2014). *Biomedical photonics handbook: biomedical diagnostics*, volume 2. CRC press.

Voss, A., Schulz, S., Schroeder, R., Baumert, M., and Caminal, P. (2009). Methods derived from nonlinear dynamics for analysing heart rate variability. *Philos. T. Roy. Soc. A.*, 367(1887):277–296.

Waller, J. M. and Maibach, H. I. (2005). Age and skin structure and function, a quantitative approach (I): blood flow, pH, thickness, and ultrasound echogenicity. *Skin Res. Technol.*, 11(4):221–235.

Wardell, K., Jakobsson, A., and Nilsson, G. E. (1993). Laser Doppler perfusion imaging by dynamic light scattering. *IEEE Trans. Biomed. Eng.*, 40(4):309–316.

Watanabe, G., Fujii, H., and Kishi, S. (2008). Imaging of choroidal hemodynamics in eyes with polypoidal choroidal vasculopathy using laser speckle phenomenon. *Ophthalmol.*, 52(3):175–181.

Webster, S. and Briers, J. D. (1994). Time-integrated speckle for the examination of movement in biological systems. In *OE/LASE'94*, pages 444–452.

Weiss, M., Milman, B., Rosen, B., Eisenstein, Z., and Zimlichman, R. (1992). Analysis of the diminished skin perfusion in elderly people by laser Doppler flowmetry. *Age Ageing*, 21(4):237–241.

Whittemore, S. (2009). *The circulatory system*. Infobase Publishing. CrossRef.

Wilkinson, I. B., Cockcroft, J. R., and Webb, D. J. (1998). Pulse wave analysis and arterial stiffness. *J. Cardiovasc. Pharmacol.*, 32(Suppl 3):S33–7.

World Health Organization (2015). World report on ageing and health. 2015. *Luxembourg*, pages 1–260.

Wu, H., Hsu, P., Lin, C., Wang, H., Sun, C., Liu, A., et al. (2011). Multiscale entropy analysis of pulse wave velocity for assessing atherosclerosis in the aged and diabetic. *IEEE Trans. Biomed. Eng.*, 58(10):2978–2981.

Wu, H., Liu, C., Lo, M., Hsu, P., Liu, A., Chang, K., and Tang, C. (2013a). Multiscale cross-approximate entropy analysis as a measure of complexity among the aged and diabetic. *Comput. Math. method M.*, 2013.

Wu, S. D., Wu, C. W., Lin, S. G., Lee, K. Y., and Peng, C. K. (2014). Analysis of complex time series using refined composite multiscale entropy. *Phys. Lett. A*, 378(20):1369–1374.

Wu, S. D., Wu, C. W., Lin, S. G., Wang, C. C., and Lee, K. Y. (2013b). Time series analysis using composite multiscale entropy. *Entropy*, 15(3):1069–1084.

Yang, O. and Choi, B. (2012). Laser speckle imaging using a consumer–grade color camera. *Opt. Lett.*, 37(19):3957–3959.

Yen, A. and Braverman, I. M. (1976). Ultrastructure of the human dermal microcirculation: the horizontal plexus of the papillary dermis. *J. Invest. Dermatol.*, 66(30):131–142.

Yokoi, N. and Aizu, Y. (2015). Depth measurement of a blood flow region based on speckle decorrelation. *Opt. Rev.*, 22(2):365–373.

Yuan, S. (2008). *Sensitivity, noise and quantitative model of laser speckle contrast imaging*. PhD thesis, Tufts University, Medford.

Yuan, S., Devor, A., Boas, D. A., and Dunn, A. K. (2005). Determination of optimal exposure time for imaging of blood flow changes with laser speckle contrast imaging. *Appl. Opt.*, 44(10):1823–1830.

Yudovsky, D., Nouvong, A., Schomacker, K., and Pilon, L. (2011). Monitoring temporal development and healing of diabetic foot ulceration using hyperspectral imaging. *J. Biophotonics*, 4(4):565–576.

Yvonne-Tee, G. B., Rasool, A. H., Halim, A. S., Wong, A. R., and Rahman, A. R. (2008). Method optimization on the use of postocclusive hyperemia model to assess microvascular function. *Clin. Hemorheol. Micro.*, 38(2):119–133.

Zakharov, P., Volker, A., Buck, A., Weber, B., and Scheffold, F. (2006). Quantitative modeling of laser speckle imaging. *Opt. Lett.*, 31(23):3465–3467.

Zakharov, P., Völker, A. C., Wyss, M. T., Haiss, F., Calcinaghi, N., Zunzunegui, C., et al. (2009). Dynamic laser speckle imaging of cerebral blood flow. *Optics Express*, 17(16):13904–13917.

Zaproudina, N., Varmavuo, V., Airaksinen, O., and Närhi, M. (2008). Reproducibility of infrared thermography measurements in healthy individuals. *Physiol. Meas.*, 29(4):515–524.

Zölei-Szénási, D., Czimmer, S., Smausz, T., Domoki, F., Hopp, B., et al. (2015). Enhancements on multi-exposure LASCA to reveal information of speed distribution. *J. Eur. Opt. Soc. Rapid Publ.*, 10:15033–15033–7.

Zysk, A. M., Nguyen, F. T., Oldenburg, A. L., Marks, D. L., and Boppart, S. A. (2007). Optical coherence tomography: a review of clinical development from bench to bedside. *J. Biomed. Opt.*, 12(5):051403–051403.

UNIVERSITE BRETAGNE LOIRE

université angers

Thèse de Doctorat

Adil I. KHALIL

Traitement d'images de speckle laser :
Étude à partir de modèles mathématiques et utilisation d'analyses non linéaires pour appréhender l'effet de l'âge sur la microcirculation sanguine

Processing of laser speckle contrast images:
Study from mathematical models and use of nonlinear analyses to investigate the impact of aging on microvascular blood flow

Résumé
Le vieillissement est un facteur de risque des maladies cardiovasculaires. Il est associé à des altérations fonctionnelles et structurelles du système vasculaire. Une étude approfondie du processus de vieillissement et le développement de systèmes d'imagerie et des traitements de données associés deviennent donc une priorité. Par l'analyse d'images de contraste par speckle laser (LSCI), l'objectif de cette thèse est d'étudier l'influence de l'âge sur la microcirculation. Pour ce faire, des données de LSCI ont été acquises sur l'avant-bras de sujets sains jeunes et âgés. A partir de modèles mathématiques, nous avons déterminé la vitesse des érythrocytes de la microcirculation chez les deux groupes de sujets. Par ailleurs, nous avons également mené une étude de la complexité de séries temporelles d'LSCI s'appuyant sur des mesures d'entropie multiéchelle. Nos résultats montrent que : 1) le groupe de sujets plus âgés présente des valeurs de vitesse des globules rouges significativement plus élevées que celles des sujets jeunes à l'hyperémie réactive post-occlusive ; 2) les fluctuations des séries temporelles de LSCI dans le groupe des sujets jeunes ont une complexité supérieure à celles du groupe de sujets âgés. Ces modifications observées sur la microcirculation pourraient être attribuées à des modifications du système vasculaire dans son ensemble. La compréhension de ces altérations pourrait conduire à de nouvelles perspectives en matière de prévention et de traitement des pathologies liées à l'âge.

Mots clés
Image de contraste par speckle laser, microcirculation, traitement d'image, analyse non linéaire, complexité, entropie.

Abstract
Aging is a primary risk factor for cardiovascular diseases. It is associated with functional and structural alterations in the vascular system. Therefore, a deep study of the aging process and the development of imaging systems and associated processing become of the utmost importance. By processing laser speckle contrast images (LSCI), this PhD work aims at studying the influence of age on microcirculation. In our work, LSCI data were acquired from the skin forearm of healthy subjects, subdivided into two age groups (younger and older). From mathematical models, we determined red blood cells velocity in microcirculation in the two groups of subjects. Moreover, we applied multiscale entropy-based algorithms to LSCI time series in order to study the complexity of microvascular signals. Our main findings are: 1) the older group has significantly higher velocity values than the younger group at post-occlusive reactive hyperaemia; 2) LSCI fluctuations in the younger group have significantly higher complexity than those of the older group. Age-related changes in skin microcirculation can be attributed to alterations in the vascular system as a whole. Understanding these changes in the microcirculatory system may give new insights for prevention and treatment of age-related diseases.

Key Words
Laser speckle contrast imaging, microcirculation, image processing, nonlinear analysis, complexity, entropy.